UNIVERSITY OF OKLAHOMA

GRADUATE COLLEGE

CHARACTERIZATION OF CHEMICALLY MODIFIED HUMAN AMNIOTIC MEMBRANES FOR TISSUE ENGINEERING APPLICATIONS

A DISSERTATION

SUBMITTED TO THE GRADUATE FACULTY

in partial fulfillment of the requirements for the

Degree of

DOCTOR OF PHILOSOPHY

By

JULIEN ARRIZABALAGA
Norman, Oklahoma
2018

CHARACTERIZATION OF CHEMICALLY MODIFIED HUMAN AMNIOTIC MEMBRANES FOR TISSUE ENGINEERING APPLICATIONS

A DISSERTATION APPROVED FOR THE
STEPHENSON SCHOOL OF BIOMEDICAL ENGINEERING

BY

_____
Dr. Matthias U. Nollert, Chair

_____
Dr. Roger G. Harrison, Jr.

_____
Dr. Edgar A. O'Rear, III

_____
Dr. Vassilios I. Sikavitsas

_____
Dr. James D. Baldwin

To my parents,

Acknowledgements

In 2011, Dr. Nollert welcomed me in his laboratory for a master exchange program. Six years later I am completing my Ph.D. with him. I would like to thank him for the opportunity he gave me to work for him and also for his mentorship and guidance over the years. I also would like to acknowledge my committee members for their support and their time, Dr. Harrison, Dr. O'Rear, Dr. Sikavitsas and Dr. Baldwin.

I would also like to thank Dr. Jeffrey Gimble from Tulane University in Baton Rouge, LA, for providing us human adipose-derived stem cells.

I would like to thank all members of Dr. Nollert's laboratory that I have seen coming and leaving over the years. I have a special thank though to Jaclyn, Mathilde, and Jin who had a large input in my work and life of the lab. They were always ready to help and to share knowledge.

I would like to thank all the students in the department who assisted with numerous experiments over the years and instilled a daily sense of excitement. They helped me become a better researcher and always made working in Sarkeys entertaining.

Leaving my family, my friends and my country to study in the United States was not easy but I found a home in Oklahoma not only in the Biomedical Engineering

department but also in my host family. Breck and Theresa thank you so much for your friendship and your time.

Six years ago, I did not arrive in Norman alone. Camille came along with me and I would like to thank her for her presence, her support and her help.

Finally, I would like to thank my parents, for allowing me the freedom in my studies and for supporting my choices.

Table of Contents

List of Tables

List of Figures

Abstract

The human amniotic membrane (hAM) is a collagen-based extracellular matrix derived from the human placenta. It is a readily-available, inexpensive, and naturally biocompatible material. Despite its attractive biological and biochemical properties, the hAM has been restricted for some tissue engineering or regenerative medicine applications by its moderate mechanical properties and rapid biodegradation. In this work, the use of riboflavin, a water-soluble vitamin, is investigated to crosslink and strengthen the human amniotic membrane under UVA light. The effect of riboflavin-UVA crosslinking on hAM properties were determined via infrared spectroscopy, uniaxial tensile testing, proteolytic degradation, permeability testing, SEM, and quantification of free (un-crosslinked) amine groups. Improved hAM mechanical properties must not come at the expense of reduced cellular proliferation and induction capabilities. In this study were assessed the viability, proliferation, immunophenotype, and multilineage differentiation ability of human adipose-derived stem cells seeded on riboflavin-UVA crosslinked membranes. Overall, hAM crosslinked with riboflavin-UVA benefited from a stable 2.5-fold increase in mechanical properties and improved biodegradation, all while retaining their biocompatibility and abilities to support the cultivation and differentiation of adipose-derived stem cells. Together, these results suggest that riboflavin-UVA crosslinking is an effective strategy to enhance the hAM for potential cardiovascular and tendon tissue engineering applications. Additionally, porcine adipose-derived stem cells (pASCs) were identified as a reliable stem cell source thanks to their abundance, straightforward isolation, and broad differentiation

abilities. Knowledge of the properties of pASCs is critical for the success of therapeutic studies in preclinical pig models. Finally, the construction of a simple mechanical testing apparatus using off-the-shelf materials and open-source software for a total cost of less than $100 is reported.

Chapter 1: General Introduction

The hAM is a collagen-based extracellular matrix derived from the human placenta. It is a readily-available, inexpensive, and naturally biocompatible material. Over the past decade, the development of tissue engineering and regenerative medicine, along with new decellularization protocols, has recast this simple biomaterial as a tunable matrix for cellularized tissue engineered constructs. Thanks to its anti-inflammatory properties and low immunogenicity, the hAM is now commonly used in a broad range of medical fields. New preparation techniques and composite scaffold strategies have also emerged as ways to tune the properties of the hAM. The current state of understanding about the human amniotic membrane (hAM) as a biomaterial is summarized in Chapter 2.

In Chapter 2, the processing techniques available for the hAM are also examined, along with their effect on the mechanical properties, biodegradation, and cellular response of processed scaffolds. The latest *in vitro* applications, *in vivo* studies, clinical trials, and commercially-available products based on the hAM are reported, organized by medical field. The possible alterations to the hAM to tune its properties, either through composite materials incorporating hAM, chemical crosslinking, or innovative layering and tissue preparation strategies are also examined. Overall, Chapter 2 compiles the current literature about the myriad capabilities of the human amniotic membrane, providing a much-needed update on this biomaterial.

Despite its attractive biological and biochemical properties, the hAM has been restricted for some tissue engineering or regenerative medicine applications by its moderate mechanical properties and rapid biodegradation. To overcome these limitations, alterations to the hAM have been made to tune its properties, either through incorporating composite materials, chemical crosslinking, or innovative layering and tissue preparation strategies into the hAM.

Chapter 3 describes the use of riboflavin, a water-soluble vitamin, to crosslink and strengthen the human amniotic membrane under UVA light. The effect of riboflavin-UVA crosslinking on hAM properties were determined via infrared spectroscopy, uniaxial tensile testing, proteolytic degradation, permeability testing, SEM, and quantification of free (un-crosslinked) amine groups. Samples crosslinked with glutaraldehyde, a common and effective yet cytotoxic crosslinking agent, were used as controls. Improved hAM mechanical properties must not come at the expense of reduced cellular proliferation and induction capabilities. In Chapter 3 are also assessed the viability, proliferation, immunophenotype, and multilineage differentiation ability of human adipose-derived stem cells seeded on riboflavin-UVA crosslinked membranes. This work grew out from results obtained in my Master's thesis, where the mechanical properties of the hAM were reported as insufficient for the development of small diameter tissue engineered blood vessels. Riboflavin-UVA crosslinking of the hAM was developed to improve the mechanical properties of the bare scaffold for potential cardiovascular and tendon tissue engineering applications.

Adipose-derived stem cells represent a reliable adult stem cell source thanks to their abundance, straightforward isolation, and broad differentiation abilities. Consequently, human adipose-derived stem cells (hASCs) have been used *in vitro* for several innovative cellular therapy and regenerative medicine applications. However, the translation of a novel technology from the lab to the clinic requires first to evaluate its safety, feasibility, and potential efficacy through preclinical studies in animals. The anatomy and physiology of pigs and humans are very similar, establishing pigs as an attractive and popular large animal model for preclinical studies. Knowledge of the properties of porcine adipose-derived stem cells (pASCs) used in preclinical studies is critical for their success. While hASCs have been extensively studied this past decade, only a handful of reports relate to pASCs. Chapter 4 summarizes the current findings about the isolation of pASCs, their culture, proliferation, and immunophenotype. The differentiation abilities of pASCs and their applications in porcine preclinical models are also be reported.

Recently, open-source electronics have been used to build hardware/software systems that are yet not commercially available or otherwise too expensive. Among them, the popular Arduino microcontroller has already proven effective in controlling scientific hardware for research purposes while also serving as a practical platform for the training of students. The mechanical properties of soft materials are critically important for a wide range of applications ranging from packaging to biomedical purposes. Chapter 5 describes the construction of a simple mechanical testing apparatus using off-the-shelf materials and open-source software for a total cost of less than $100. The

device consists of a wooden frame supporting a central loading apparatus attached via drawer slides. To perform a mechanical test, a sample was secured within two custom-made 3D-printed clamps affixed to brackets on the base of the frame and the load cell. The extension force was applied by the user pulling on a rope, moving the central loading apparatus up (thereby stretching the sample) while recording the force (measured by a load cell) and the displacement (measured by an ultrasonic sensor). The load cell and ultrasonic sensor were linked to an Arduino microcontroller connected to a laptop through a USB port for data acquisition and analysis.

Chapter 2: The Human Amniotic Membrane: A Versatile Scaffold for Tissue Engineering

Abstract

The human amniotic membrane (hAM) is a collagen-based extracellular matrix derived from the human placenta. It is a readily-available, inexpensive, and naturally biocompatible material. Over the past decade, the development of tissue engineering and regenerative medicine, along with new decellularization protocols, has recast this simple biomaterial as a tunable matrix for cellularized tissue engineered constructs. Thanks to its anti-inflammatory properties and low immunogenicity, the hAM is now commonly used in a broad range of medical fields. New preparation techniques and composite scaffold strategies have also emerged as ways to tune the properties of the hAM. The current state of understanding about the hAM as a biomaterial is summarized in this chapter. We examine the processing techniques available for the hAM, addressing their effect on the mechanical properties, biodegradation, and cellular response of processed scaffolds. The latest *in vitro* applications, *in vivo* studies, clinical trials, and commercially-available products based on the hAM are reported, organized by medical field. We also look at the possible alterations to the hAM to tune its properties, either through composite materials incorporating hAM, chemical crosslinking, or innovative layering and tissue preparation strategies. Overall, this chapter compiles the current literature about the myriad capabilities of the human amniotic membrane, providing a much-needed update on this biomaterial.

Introduction

Anatomy and Components

The human amniotic membrane (hAM), also known as the amnion, is the innermost layer of the fetal membranes. It is loosely attached to the chorionic membrane, or chorion. Together, these fetal membranes form the amniotic sac, which contains the embryo and amniotic fluid during pregnancy. Both membranes are loosely connected via a spongy collagen layer, making them easy to peel and separate from each other.[1]

The hAM is a translucent and avascular biomaterial with a thickness of 20 to 50μm.[1,2] As seen in Figure 01, the hAM consists of an epithelium monolayer in contact with the amniotic fluid, a basement membrane, a compact layer, a fibroblast layer, and then a spongy layer connected to the chorion.[3] In a majority of tissue engineering applications, what is mentioned as the hAM actually refers to the basement membrane, decellularized and isolated from its surrounding layers to produce a thin and homogeneous biomaterial. Collagens type III, IV, and V are the major components of the basement membrane, providing structural integrity and mechanical strength to the tissue.[4,5] Non collagenous glycoproteins such as laminin, fibronectin, and nidogen are also present.[3,6]

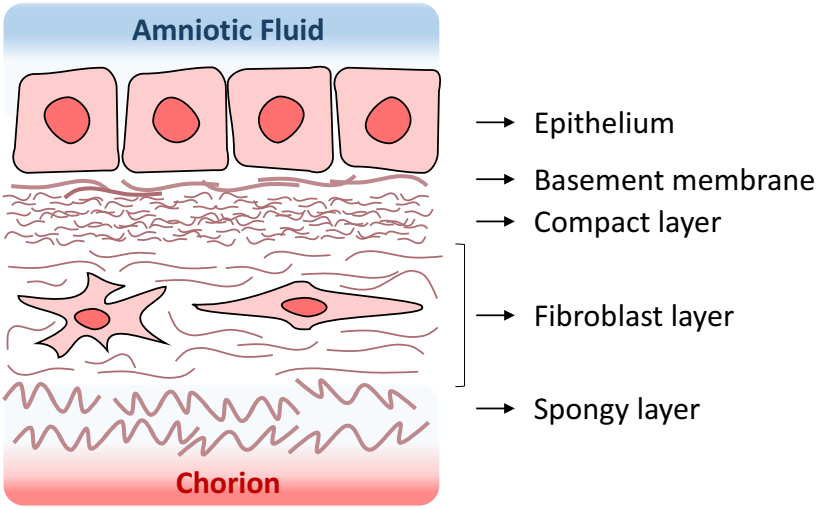

Figure 1: Schematic representation of the structure of the human fetal membranes. The amnion is composed of 5 distinct layers: epithelium, basement membrane, compact layer, fibroblast layer, and spongy layer.

Biological Properties

The hAM possesses anti-microbial, anti-fibrosis, and anti-inflammatory properties.[7,8] When implanted into the human body it effortlessly adheres to the wound surface, reduces scars, decreases pain, promotes wound healing, and has a low risk of immunogenicity.[9,10]

Another critical property of the hAM for tissue engineering applications is its ability to support cell attachment, proliferation, and differentiation.[7] Various cell lines have been reported to adhere and proliferate on decellularized hAM. Figure 02 presents a specific example of the type of results numerous investigators have obtained, demonstrating that the culture of human mesenchymal stem cells on the hAM does not affect their immunophenotype or differentiation abilities.[11] This unique set of biological and biochemical properties combined with its reduced cost and unlimited availability have

shaped the hAM into a biomaterial of choice for clinical and tissue engineering applications.

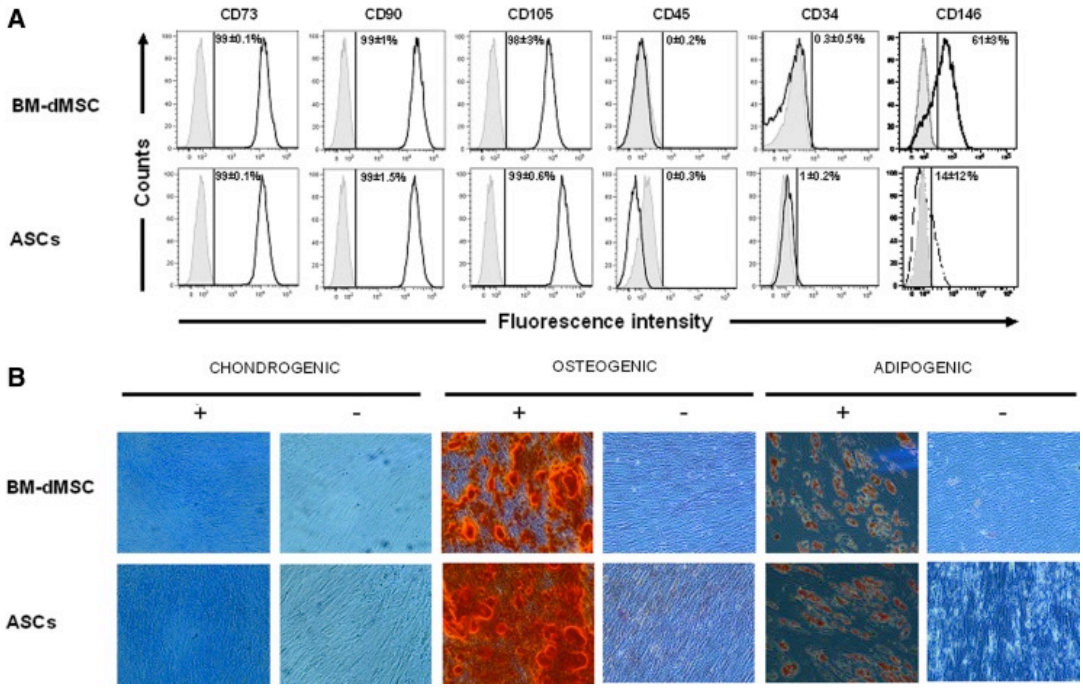

Figure 2: Characterization of human mesenchymal stem cells derived from bone marrow (BM-dMSC) or from adipose tissue (ASCs) previously seeded on hAM scaffolds. A: Immunophenotype of the cells as determined by flow cytometric analysis. B: Chondrogenic (Alcian Blue staining), osteogenic (Alizarin Red staining), and adipogenic (Oil Red O staining) differentiation of the cells. The culture of both BM-dMSC and ASCs on hAM scaffolds did not affect their immunophenotype or differentiation abilities. Adapted from Roux et al.[11]

Amniotic Membrane-Derived Cells

The hAM has also been reported as a source of 2 populations of stem cells: human amniotic epithelial cells (hAECs) and human amniotic mesenchymal stromal cells (hAMSCs).[12,13] hAECs are present on the epithelium monolayer facing the amniotic fluid. hAMSCs are part of the stromal layer found between the basement amniotic membrane and the loose spongy layer connected to the chorion, as depicted in Figure

01. Both of these cell lines can easily be obtained from the hAM after enzymatic digestion, typically with trypsin for hAECs, and collagenase for hAMSCs.[14–16]

Cell isolation from the amniotic membrane has the advantages of being non-invasive and to provide large cell yields. hAECs and hAMSCs express transcription factors and cell surface markers associated with pluripotent stem cells and are able to differentiate into cell lineages from all three germ layers.[14,17,18] Both of these cell lines can also be reprogrammed into induced pluripotent stem cells.[19–21] Amniotic membrane-derived cells have been successfully used in several studies: bone tissue engineering,[22] wound healing management,[23] cartilage repair,[24] and rheumatoid arthritis treatment.[25]

Overall, hAECs and hAMSCs represent valuable sources of multipotent stem cells for tissue engineering and regenerative medicine applications. The possibility of obtaining these cells from the hAM adds even more value to this tissue, which is usually considered to be medical waste. The isolation, characterization, differentiation, and applications of amniotic membrane-derived cells have already been thoroughly reviewed.[14,26–29] Consequently, the present chapter will only focus on the prospects offered by the human amniotic membrane.

Historical Perspective

The hAM was first used for skin reconstruction by Dr. Davis in 1910.[30] Subsequently, the hAM was employed for a broad range of applications: surgical dressings, the treatment of burns and ulcers, the reconstruction of the oral cavity, bladder, and

vagina.[31,32] In the 1940s the first ophthalmic applications of the hAM to treat conjunctival defects and chemical burns were reported.[33–35] The initial interest for this biomaterial then faded away, most likely due to more stringent regulations regarding tissue transplantations, and the hAM almost disappeared from the literature for about 50 years.

The resurgence of the hAM happened in the 1990s when it was reported by Kim et al. as an effective scaffold for ocular surface reconstruction.[36,37] New preparation, preservation, and storage techniques were also developed over the same time period, assisting the hAM to gain significance for ophthalmic and dermatologic applications without the worry of disease transmission from fresh unprocessed tissue. In 2001, processed hAM received approval from the United Stated Food and Drug Administration (FDA) for ocular surface reconstruction, increasing its use even further and triggering the development of several commercial hAM derived products.[38] Nowadays, the hAM has been widely adopted for burn wound dressing and ocular surface reconstruction. New clinical applications are also currently explored such as nerve wrapping,[39–41] reconstruction of the oral cavity,[42] flexor tendon repair,[43] and the treatment of limbal stem cell deficiency.[44]

The development of tissue engineering diversified the potential uses of the hAM as a scaffolding material from traditional fields such as ophthalmology and dermatology to new disciplines. Over the last two decades, novel hAM modifications have been incorporating cells and utilizing the hAM as a scaffold to recreate complex 3D

structures as opposed to last century uses as an acellular dressing.[37] An ideal scaffold for tissue engineering applications is non-immunogenic and supports the attachment and proliferation of cells without affecting their immunophenotype or differentiation abilities. It also has comparable mechanical properties, biodegradation rate permeability, and flexibility to the tissue it intends to replace. Decellularized hAM is a versatile biomaterial that meets these criteria and can be used to engineer several types of tissues from the human body.[7] The hAM is currently being investigated for a broad range of applications such as blood vessel tissue engineering,[45] cartilage regeneration,[46] and urothelium tissue engineering.[47]

Preservation and Decellularization Techniques

Tissue Processing and Preservation

The hAM can be used two ways, either intact with its epithelium layer or decellularized with its epithelium removed. An intact hAM would simply be detached from the chorion, cut to size, and preserved for upcoming applications. The epithelium monolayer and extracellular matrix would remain untouched. Intact membranes are typically used for wound dressing in clinical applications, while decellularized hAM are ideal scaffolds for tissue engineering constructs. Epithelial cells need to be removed from the hAM in order to not interfere with new cells seeded on the scaffold. The goal of the decellularization process is to remove all epithelial cells and obtain a uniform and smooth basement membrane.[16,48,49] Figure 03 illustrates the removal of the epithelium layer after decellularization.[50]

Intact membranes for clinical applications are processed, sterilized, and preserved prior to implantation in humans. Tissue processing simply consists of mechanically separating the amnion from the chorion, cutting it into smaller pieces, and flattening it onto nitrocellulose paper. Tissue preservation helps provide a steady supply of scaffolds for clinical applications. Several protocols have been developed including cryopreservation in glycerol, air-drying, freeze-drying, and incubation in trehalose.[48,51]

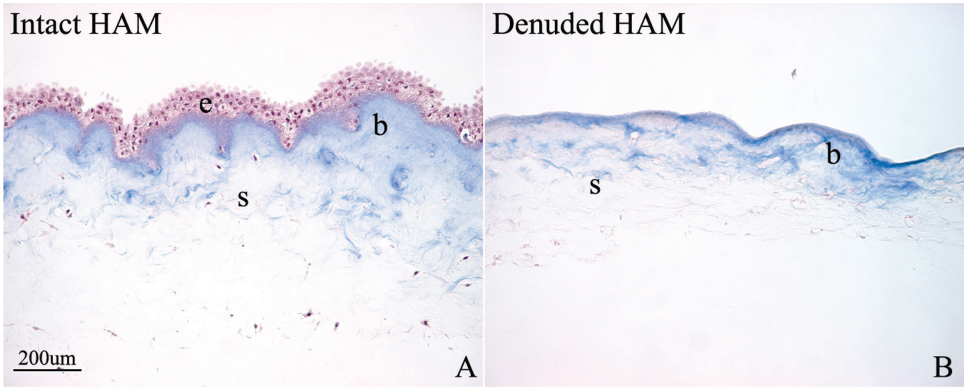

Figure 3: Histological comparison of (A) an intact hAM with (B) a hAM decellularized with 0.1% trypsin-EDTA. The letters, e, b, and s respectively designate the epithelium, basement membrane, and stroma. Adapted from Jin et al.[50]

Decellularization

hAM intended for tissue engineering applications are de-epithelialized. Rapid freezing is often used as a preliminary step to introduce ice crystals into the intracellular space and cause cell lysis.[52] Enzymatic treatments and chemical treatments are then needed to solubilize the remaining cytoplasmic and nuclear cellular membranes.[53]

Enzymatic treatments for decellularization include protease digestion, calcium chelating agents, and nucleases.[54] Most protocols commonly use EDTA, dispase, trypsin, or

thermolysin.[48,53,55] Saghizadeh et al also reported using NaOH to efficiently de-epithelialize the hAM.[56] Nucleases such as DNases and RNases are also advantageous for removing nucleotides after an initial cell lysis.[54] Finally, sodium dodecyl sulfate is one of the most popular and attractive detergents used for treating the hAM since it yields a complete removal of cellular remnants without damaging the collagen from the tissue.[54,57,58]

Gamma irradiation and chemical solutions (peracetic acid and ethanol) are the main techniques used for the sterilization of the hAM.[58] Supercritical carbon dioxide has also been described as a preparation technique to obtain a sterile hAM without affecting its composition.[59]

Commercially Available Products

The advances realized these past decades for the stabilization, preservation, and storage of tissues also lead to the development of several commercially available products derived from the hAM.[46,60] These products have the advantages of being stable, as well as easily transported and stored. A majority of them consist of either cryopreserved or dehydrated intact hAM and have been recommended for the treatment of ophthalmic and dermal wounds. Detailed information about commercially available hAM products can be found in the review written by Gindraux et al.[60]

Tissue Modifications

Despite its attractive biological and biochemical properties, the hAM has been limited by its mechanical properties and biodegradation rate for some tissue engineering or regenerative medicine applications. To overcome these limitations, alterations to the hAM have been made to tune its properties, either through incorporating composite materials, chemical crosslinking, or innovative layering and tissue preparation strategies into the hAM.

Crosslinking

Chemical crosslinking of the hAM has been reported to improve its mechanical properties and biodegradation rate without affecting cellular response.[61–67] Figure 04 presents an innovative technique developed by Hariya et al. for the production of transparent and resilient crosslinked hAM tissue laminates.[68] Carbodiimide was used for crosslinking and up to 8 layers were assembled to produce a tougher and optically clearer graft for corneal transplantation.

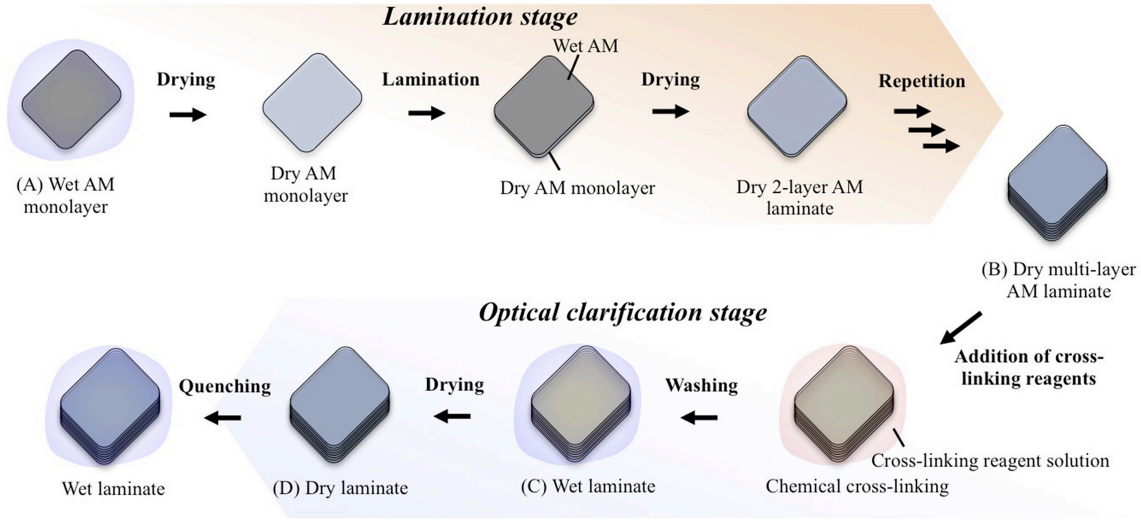

Figure 4: Fabrication of transparent and resilient crosslinked hAM tissue laminates. For the first lamination stage, hAM are repeatedly dried and stacked up to produce a multilayer tissue laminate. Then, tissue constructs are optically clarified after successive carbodiimide crosslinking, washing, drying, and quenching steps. The final laminates contain up to 8 hAM layers and benefit from improved light transmittance and mechanical properties. Adapted from Hariya et al.[68]

Composites

New preparation techniques and composite scaffold strategies have also emerged as ways to tune the properties of the hAM. Recent publications describe applications of the hAM for osteochondral tissue engineering by coating it with poly(lactic-*co*-glycolic acid).[69] The hAM was mixed with fibrin to produce a tissue engineered blood vessel and was combined with collagen-glycosaminoglycan scaffolds for tendon tissue engineering.[70,71] A similar composite material approach was used by Adamowicz et al. who layered denuded hAM with electrospun poly(L-lactide-*co*-ε-caprolactone) (PLCL) for reconstructive urology.[72] These composite scaffolds, presented in Figure 05, were successfully implanted in rats and promoted bladder augmentation.[72]

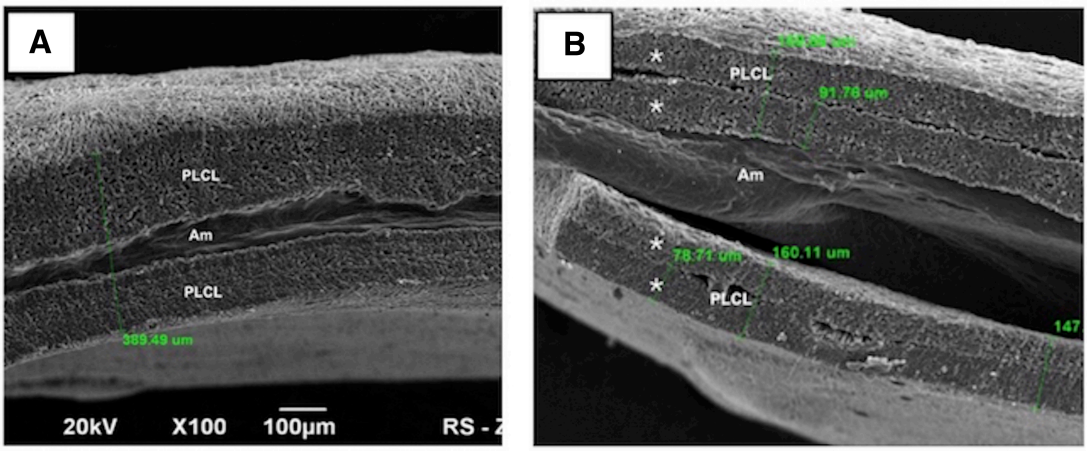

Figure 5: Scanning electron microscopy images of hAM-PLCL composite scaffolds. A: Cross-section image of the composite scaffold. B: Delaminated composite. Frozen hAM was sandwiched and covered on both sides with two layers of electrospun PLCL. Adapted from Adamowicz et al.[72]

Several more composite and preparation techniques have been used to functionally augment the hAM for tissue regeneration purposes.[73] A decellularized hAM was assembled with electrospun silk fibroin to produce a 3D bilayer of artificial skin.[74] Denuded hAM was coated with poly(ester) urethane on both sides to improve its mechanical strength and produce a biocompatible surgical mesh.[75]

Another popular preparation method is the combination of several hAM scaffolds to produce multilayer constructs such as the hAM tissue laminates presented in Figure 04. Multilayer constructs have been reported for the fabrication of tissue engineered blood vessels,[70,76,77] surgical patches,[78] applications in ophthalmology,[68,79,80] and oral and maxillofacial surgery.[81,82] Finally, skin defects have been treated with micronized hAM (300 to 600µm microparticles) and solubilized hAM combined with hyaluronic acid hydrogel.[83,84]

Clinical Applications

Ophthalmology

The hAM is widely used for a variety of ocular surface diseases thanks to its attractive biological properties, transparency, thinness, and composition akin to the one of the conjunctiva.[85] The hAM can be applied on the ocular surface either as a temporary dressing or as a permanent graft.[38] When used as a temporary biological bandage, the hAM acts as barrier to protect the healing epithelium from the movement of the eyelids. A hAM dressing aims to repel inflammation of the host tissue and reduce scarring.[38]

A permanent hAM graft transplanted on the ocular surface is used to promote the proliferation of the epithelial cells present on the ocular surface.[86] The patient's cells will grow over the hAM and the scaffold will be integrated into the patient's tissue. For deep corneal ulcerations or perforations, the hAM can also be stuffed into the defects prior to patching or grafting.[87]

Today the hAM is widely used for the management of several ocular ailments of the cornea or the conjuctiva. Applications of the hAM for corneal surface reconstruction include the treatment of chemical burns, bullous keratopathy, persistent epithelial defects, ulcers, and lesions.[87] The hAM has been adopted for a variety of conjunctival pathologies including symblepharon, pterygium, chemical burns, and scleral thinning, for the covering and reconstruction of conjunctival lesions, and for the management of Stevens-Johnson syndrome.[87–89]

The hAM has also been applied to the treatment of limbal stem cell deficiency. Unlike the ophthalmic applications previously described, this recent method uses the hAM to produce a cellularized graft.[90–92] Limbal stem cells are critical for the constant maintenance and regeneration of the corneal epithelium. Damage to the limbus would lead to the deficiency of these stem cells, epithelial breakdown, chronic inflammation, corneal conjunctivalization, and a loss of corneal clarity.[93] Limbal stem cell deficiency can be treated with the transplantation of limbal epithelial cells expanded *ex vivo*. Cells can be obtained from a small biopsy of the patient's other eye if healthy, or from another living individual or a cadaveric donor if both of the patient's eyes are affected by limbal stem cell deficiency.[93] In the case of donor shortages, oral mucosal epithelial cells and bone marrow mesenchymal stem cells could also be used as replacement cell sources to reconstruct the corneal surface.[94–97] Decellularized hAM have been successfully used as substrates for the *ex vivo* expansion of limbal epithelial cells. Transplantation of these cellularized grafts resulted in the repopulation of the corneal epithelium and integration of the hAM with the corneal tissue.[87,98,99] Figure 06 illustrates the transplantation process of limbal epithelial cells using the hAM as a carrier membrane.

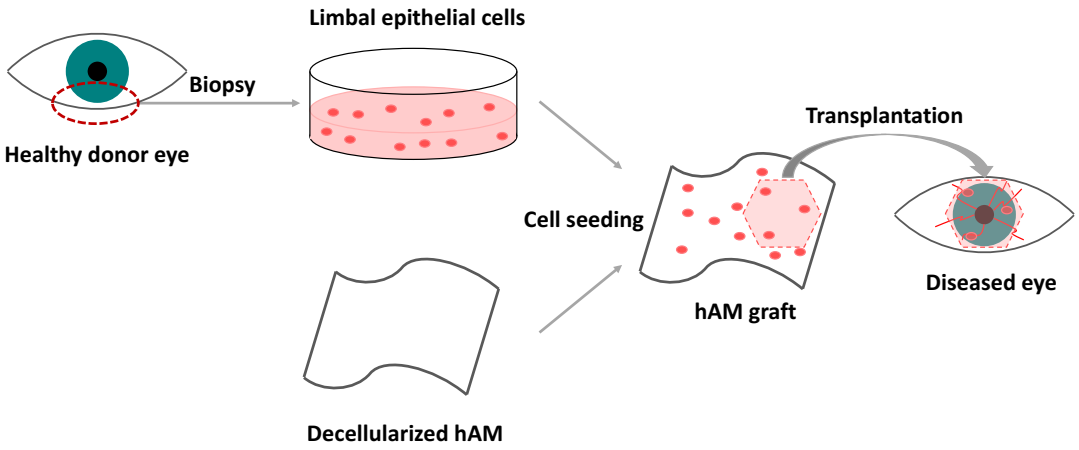

Figure 6: Illustration of the transplantation process of autologous limbal epithelial cells for the treatment of a unilateral limbal stem cell deficiency. A small biopsy (about 2 by 2 mm of tissue) is performed on the patient's healthy donor eye. Limbal epithelial cells are then isolated and seeded onto a sheet of decellularized hAM. After 2 to 3 weeks of culture, the cellularized hAM graft is transplanted onto the patient's diseased corneal surface.

Other recent innovations have been finding new ways to attach the hAM to the ocular surface. The hAM is a thin material that is typically attached to the corneal surface with sutures. However, hAM bandages need to be replaced every week and repeated interventions at the diseased corneal surface is not recommended. Possible side effects of sutures also include conjunctival bleeding or scarring.[100]

The strategies developed for the sutureless fixation of the hAM include the use of fibrin,[101,102] chemically defined bioadhesives,[103,104] light-initiated bonding with Rose Bengal dye[105,106] and medical devices (ProKera and AmnioClip) that use a dual ring system to mount the hAM and apply it like a contact lens.[100,107]

Dermatology

The hAM has been described as an effective therapeutic option for burn wound dressing. Indeed, the hAM presents several advantages for skin applications such as its anti-inflammatory properties, antimicrobial effects, low immunogenicity, and good wound adherence. When used to cover burn wounds, the hAM reduced pain and scars, prevented infections, and promoted re-epithelialization. [108–110]

The hAM has been used to treat both superficial and partial-thickness burns,[110] as an overlay for skin autografts, [111,112] and as a dressing for skin graft donor sites.[113,114] Besides burn wound dressing, the hAM proved effective for the treatment of chronic leg ulcers, pressure sores, and for patients with epidermolysis bullosa.[115–117]

These long-established dermatology applications of the hAM involve using it as an acellular biomaterial, while the most recent studies report using the hAM for the attachment and proliferation of various cell lines. Patients with stable vitiligo were transplanted with autologous melanocytes seeded on a decellularized hAM, resulting in over 90% skin repigmentation.[118,119] Skin equivalents were constructed by combining a hAM seeded with fibroblasts and normal keratinocytes.[65,120,121] Biological wound dressings were designed to promote tissue regeneration for patients with full-thickness skin defects, by combining the hAM with mesenchymal stem cells.[11,83,122]

Oral and Maxillofacial Surgery

After oral surgery, bone surfaces are often exposed to the oral cavity which can lead to possible infections and scar formation. Thanks to its biological properties, the hAM has been described as an effective scaffold for the reconstruction of the oral cavity.[42] Consequently, the hAM has been used for a broad range of applications: treatment of oral mucosa defects after removal or cancerous legions,[123] flap surgery, [124] oronasal fistula reconstruction in cleft palate surgery,[81,82] and temporomandibular joint surgery.[125]

Recent tissue engineering approaches involve the fabrication of a myomucosal flap using oral keratinocytes cultured on hAMs,[126] and the autologous transplantation of oral mucosal epithelial cell sheets cultured on hAMs for intraoral mucosal defects.[127–129] Figure 07 shows that oral mucosal epithelial cells cultured on the hAMs present comparable keratin expression to cells present in the native oral mucosa.[128]

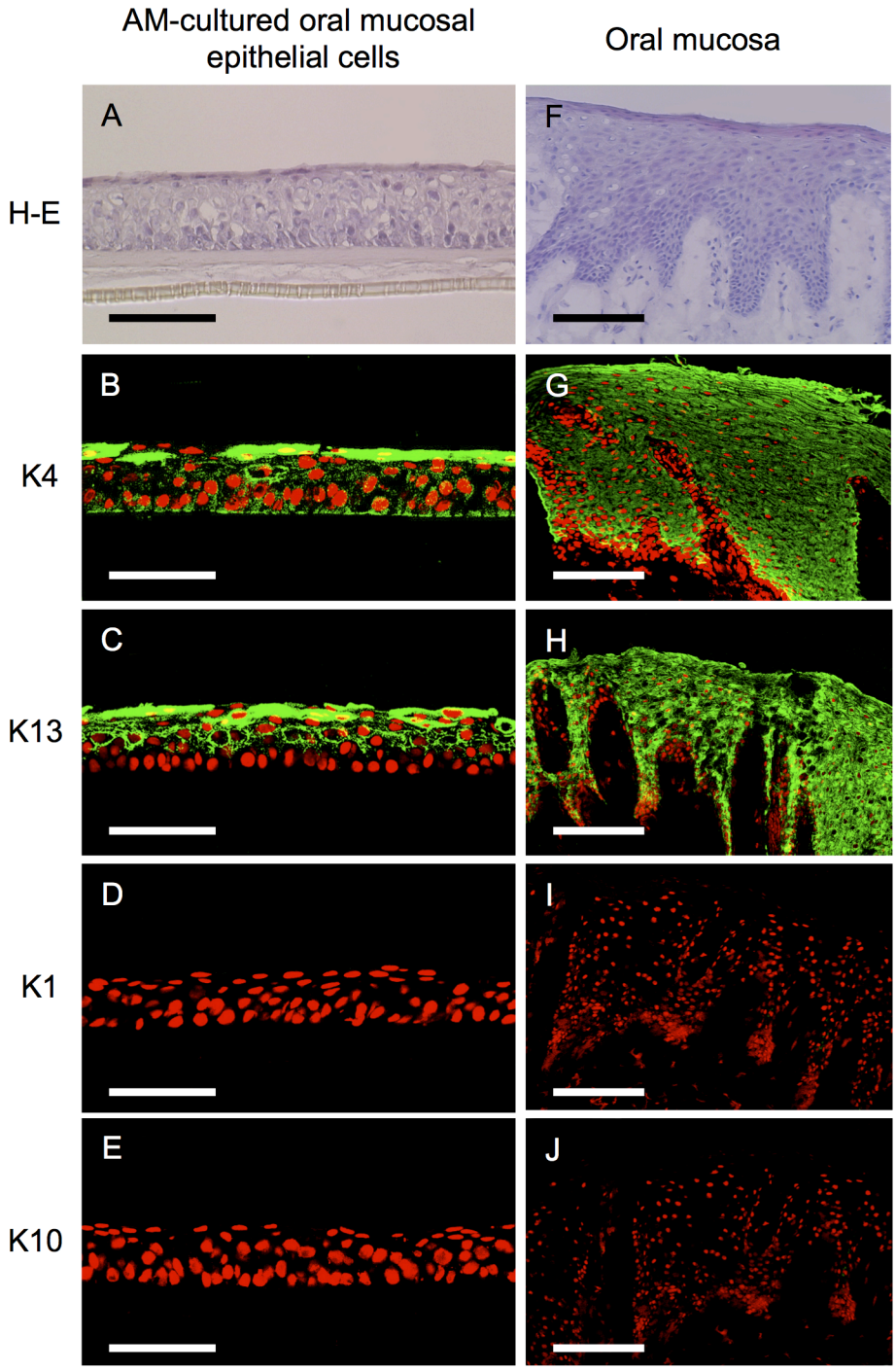

Figure 7: Comparison of hAM-cultured oral mucosal epithelial cells with the oral mucosa. A-F: hematoxylin and eosin staining. B-G, C-H, D-I, E-J: Expression of keratins 4, 13, 1, and 10 in green with the cell nuclei stained in red with propidium iodide. Keratin expression was similar between the hAM cultured oral mucosal epithelial cells and the oral mucosa. Adapted from Amemiya et al.[128]

Otolaryngology

The human amniotic membrane has shown therapeutic promises as a scaffold in otolaryngology. Patches of hyperdry hAM were used as dressing substitutes for fascia grafts of the temporal muscle in canal wall down tympanoplasty.[130,131] The hAM grafts were completely epithelialized faster than the classic fascia grafts.

Tissue Engineering Applications

The hAM has been investigated as a scaffold for tissue engineering and regenerative medicine applications in a broad range of disciplines. Several of these studies were already reported in previous paragraphs dedicated to tissue modifications of the hAM, along with novel cellularized applications of the hAM in ophthalmology, dermatology, and oral and maxillofacial surgery.

Articular cartilage has minimal self-healing capability and often advances to osteoarthritis once damaged.[132,133] The hAM has been described as an ideal substrate for the culture of chondrocytes.[134–137] Consequently, chondrocytes have been seeded on the HAM in order to obtain a delivery vehicle for cell transplantation that could promote cartilage regeneration *in vivo*. For instance, Jin et al. seeded rabbit articular chondrocytes on decellularized hAM and used these constructs *in vivo* to cover rabbit osteochondral defects. After 8 weeks of implantation the defect area was successfully regenerated.[50]

The hAM has been reported as a potential osteoinductive biomaterial for bone regeneration.[138,139] Decellularized hAM helped induce the osteogenic differentiation of human dental apical papilla cells seeded on top of it, opening potential applications for the hAM in bone and tooth tissue engineering.[140] Intact hAM simply exposed to osteogenic media also promoted the differentiation of the stem cells contained in the hAM towards osteogenic pathways.[141]

In the past years, the hAM has been investigated as a scaffold for tissue engineering of the urinary tract system. The hAM was described as a viable scaffold for the culture of urothelial cells and the reconstruction of damaged urothelium tissue.[47,142–144]

The hAM has been characterized as blood compatible and as an adequate cell carrier matrix for endothelial and smooth muscle cells.[76,145,146] Consequently, several studies have reported rolling the hAM to engineer small diameter blood vessels.[45,70,76,77,147]

Finally, the hAM has been used as a scaffold for salivary gland regeneration,[148] for esophageal wall tissue engineering,[149] for the treatment of pelvic floor dysfunction,[150] for liver regeneration, [151,152] and as a support of *in vitro* ovarian follicular culture.[153]

Limitations

Risk of disease transmission

Due to its human origin, the hAM carries a risk of disease transmission from its donor. Consequently, the use of fresh untreated hAM is not recommended. The collection,

processing, and transplantation of the hAM have to follow the proper laws and regulations of the country where they would be performed.[46]

To avoid bacterial contamination, it is recommended to collect hAM tissue after caesarean section under sterile conditions. Typically, serological testing for syphilis, hepatitis, and HIV are performed on the donor at the time of tissue collection.[87] Serological screening is repeated 6 months after birth to confirm that there were no false negatives during the first round of testing. In the meantime, the hAM is quarantined until both results are negative. Then, the hAM needs to be processed under aseptic conditions and stored in a sterile environment.[87,98]

Donor variation

The hAM is a biological human tissue and its composition is affected by intra and inter donor variations.[86,154] The fetal sex, gestational age, donor age, health, and diet are all parameters that affect the properties of the hAM. Between donors, the thickness of the hAM varies from 20 to 50μm.[1,2] From the same donor, the hAM will also be thinner away from the placenta and thicker closer to the umbilical cord.[155] The transparency of the hAM will also change depending on its original location in the amniotic sac.[156] One possibility to overcome these donor variations would be the development of pooling and screening methods to sort out different hAMs according to previously defined characteristics.

Effects of decellularization and storage techniques

The preservation, decellularization, and sterilization protocols used to process the hAM will affect its mechanical properties, transparency, chemical composition, and cell adhesion properties.[48,157–160] Characterizing how a treatment influences the morphology and composition of the hAM helps verify that no undesirable or unwanted property changes were induced. For instance, it is critical to ensure that the cell adhesion properties of the hAM are maintained after processing if the hAM is intended for tissue engineering applications.

Standardization of processing techniques helps reduce variability. Standard protocols developed for commercially available hAM products and for tissue banks help produce consistent hAM allografts for clinical applications.[60,161–163]

Conclusion

The hAM is a readily available and inexpensive biomaterial that can efficiently be processed, preserved, and de-epithelialized. Thanks to its unique set of biological properties, the hAM is now a material of choice for several clinical applications in ophthalmology, dermatology, and oral and maxillofacial surgery. The development of standard processing protocols and tissue banks, along with commercially available hAM derived products, will further expand the clinical applications of the hAM.

Moreover, decellularized hAM has proven worthwhile for a broad range of tissue engineering applications due to its ability to support cell attachment, proliferation, and

differentiation. Modifications of the hAM have been developed to tune its properties, either through composite materials incorporating the hAM, chemical crosslinking, or innovative layering and tissue preparation strategies. Additionally, the hAM has been identified as a source of human amniotic epithelial cells and human amniotic mesenchymal stromal cells. These two multipotent cell lines are valuable for tissue engineering and regenerative medicine applications.

Overall, the hAM is truly a versatile biomaterial and its foreseeable future as a scaffold for tissue engineering applications looks very promising.

Chapter 3: Characterization of Riboflavin-UVA Crosslinking of Amniotic Membranes and its Influence on the Culture of Adipose-Derived Stem Cells

Abstract

The human amniotic membrane (hAM) is a collagen-based extracellular matrix whose applications are restricted by its moderate mechanical properties and rapid biodegradation. In this work, we investigate the use of riboflavin, a water-soluble vitamin, to crosslink and strengthen the human amniotic membrane under UVA light. The effect of riboflavin-UVA crosslinking on hAM properties were determined via infrared spectroscopy, uniaxial tensile testing, proteolytic degradation, permeability testing, SEM, and quantification of free (un-crosslinked) amine groups. Samples crosslinked with glutaraldehyde, a common and effective yet cytotoxic crosslinking agent, were used as controls. Improved hAM mechanical properties must not come at the expense of reduced cellular proliferation and induction capabilities. In this study, we assessed the viability, proliferation, immunophenotype, and multilineage differentiation ability of human adipose-derived stem cells seeded on riboflavin-UVA crosslinked membranes. Overall, hAM crosslinked with riboflavin-UVA benefited from a stable 2.5-fold increase in mechanical properties (comparable to the increase seen with glutaraldehyde crosslinked membranes) and improved biodegradation, all while

retaining their biocompatibility and abilities to support the cultivation and differentiation of adipose-derived stem cells. Together, these results suggest that riboflavin-UVA crosslinking is an effective strategy to enhance the hAM for tissue engineering and regenerative medicine applications establishing it as an attractive and tuneable biomaterial.

Introduction

The human amniotic membrane (hAM) is a collagen-based extracellular matrix derived from the human placenta. It is a readily-available, inexpensive, and naturally biocompatible material [7,27]. Thanks to its anti-inflammatory properties and low immunogenicity [8,164], the hAM is now commonly used in a broad range of medical fields. Recent *in vivo* studies report the successful implantation of hAM to reconstruct the oral mucosa [128], patch skin ulcers [11], wrap transected nerves [165,166], and produce biological meshes [75], tissue engineered urothelium [47], esophageal wall [167], and liver tissue [168]. Furthermore, due to its transparent structure and ability to provide a substrate for the growth of corneal and epithelial cells, the hAM is also an ideal biomaterial for ocular surface reconstruction [87], having proven effective in transplanting *ex vivo* cultivated limbal epithelial stem cells for the treatment of limbal stem cell deficiency in a number of human subjects [169]. For many applications, however, the mechanical properties of the hAM are not consistent with the mechanical properties of the tissue it is attempting to replace.

Chemical crosslinking is a well-documented technique to stabilize extracellular matrix components, improving the mechanical properties of a scaffold and decreasing its biodegradation rate [170,171]. The major components of the hAM are collagens type I and III, and consequently, various crosslinking agents such as glutaraldehyde [61,172,173] and carbodiimide [62,67] have been used to chemically crosslink the hAM. These crosslinking techniques were effective at improving the mechanical properties of the scaffolds. However, the crosslinking agents used were highly cytotoxic, resulting in biocompatibility issues with the resulting scaffolds [171,174].

Riboflavin, or vitamin B_2, is a water-soluble vitamin [175,176] that has been reported as a naturally occurring and non-cytotoxic crosslinking agent when combined with UV light. It has previously been used to crosslink collagen hydrogels [177–179] and corneal collagen [180,181]. Furthermore, after over a decade of successful clinical trials, riboflavin-UVA is now an FDA approved treatment for keratoconus [182], a disease that causes thinning of the corneal stroma [183,184].

In this study, we investigate the potential of using riboflavin-UVA to crosslink the hAM and examine its influence on the cultivation of human adipose-derived stem cells (hASCs). hAM were crosslinked with different concentrations of riboflavin and characterized by FTIR, free amine group quantification, uniaxial tensile testing, proteolytic degradation, and permeability measurements. Membranes crosslinked with glutaraldehyde were also used as a control for all experiments. The influence of crosslinked hAM on the cultivation of mesenchymal stem cells still remains to be

studied since previous studies focused on the cultivation of epithelial cells for ophthalmology applications [62,173,185]. In this work, the effect of riboflavin-UVA crosslinking on the cultivation of human adipose-derived stem cells (hASCs) was examined. Cell viability/cytotoxicity and proliferation assays were conducted to evaluate the effect of riboflavin-UVA crosslinking on cellular adhesion and proliferation. The immunophenotype of hASCs cultivated on crosslinked hAM was determined by flow cytometry analysis of CD29, CD34, CD44, CD45, CD73, CD90, and CD105 cell surface markers. Finally, the adipogenic, osteogenic, and chondrogenic differentiation of hASCs seeded onto crosslinked and noncrosslinked membranes was also examined.

Materials and Methods

De-Epithelialization of the Human Amniotic Membrane

Placentas were collected from the Labor and Delivery unit at Norman Regional Hospital (Norman, OK) five days after birth following procedures that were approved by the Institutional Review Boards of both the hospital and the University of Oklahoma. The hAM was then extracted and processed following established protocols [57,76]. Briefly, the hAM was stripped from the chorion, rinsed with deionized water and cut into smaller pieces to ensure proper exposure to the subsequent de-epithelialization treatments. After two freeze-thaw cycles, the membranes were transferred to a solution of 0.03% (w/v) sodium dodecyl sulfate (J.T. Baker, Center Valley, PA) in deionized water for 12 to 24 hours. Tissues were then incubated in a solution of 50 U/mL of DNase (Sigma-Aldrich,

Saint-Louis, MO) in Tris base for 2 hours at 37°C. Finally, the membranes were sterilized in 0.2% (v/v) peracetic acid (Sigma-Aldrich) and 4% (v/v) ethanol in deionized water for 2 hours and stored in phosphate buffered saline (PBS) at 4°C. Between each treatment, membranes were rinsed five times with deionized water to remove any remaining chemicals. All steps were performed in 500mL bottles on an orbital shaker at 100 rpm to ensure full exposure for each of the membranes.

Chemical crosslinking of membranes

Decellularized amniotic membranes were submerged in solutions of riboflavin (Sigma-Aldrich) at different concentrations and exposed to UV light at 366 nm on a transilluminator (Fotodyne, Hartland, WI) with an intensity of $4mW/cm^2$. Exposure time to the UV light was 60 min and concentrations of riboflavin ranged from 0.001 to 0.1 g/L. As a control, some amniotic membranes were also crosslinked in a 10mM solution of glutaraldehyde for 60 min. All crosslinked samples were thoroughly washed with phosphate buffered saline to remove any residual crosslinking agents before use.

Determination of the crosslinking degree

To evaluate the extent of crosslinking, free amino groups were detected by reaction with ninhydrin [186]. Each tissue sample was boiled in a ninhydrin reagent solution (Sigma-Aldrich) for 20 min. After cooling (to room temperature), the solution was diluted in 95% ethanol and its optical absorbance measured with a Synergy HT microplate reader at 570 nm (BioTek Instruments, Winooski, VT). Standards were prepared using glycine

at different concentrations. The amount of free amines in a sample was proportional to the optical absorbance of its solution. The crosslinking degree was defined as:

$$Crosslinking\ degree\ (\%) = \frac{X_0\text{-}X_1}{X_0} * 100$$

Where X_0 and X_1 represent the amount of free amine groups in a noncrosslinked and crosslinked sample, respectively [62,187].

Fourier Transform Infrared Spectroscopy (FTIR)

IR spectra were recorded on a Shimadzu IRAffinity-1 FTIR spectrometer (Shimadzu, Kyoto, Japan) in the 4000 to 450 cm^{-1} range with 25 scans at a resolution of 4 cm^{-1}. Shimadzu IRsolution version 1.10 was used for data acquisition and Essential FTIR version 3.50 (Operant LLC, Madison, WI) for data processing and analysis.

Mechanical testing

Mechanical properties were assessed using a United Smart Table SSTM-2 uniaxial tensile testing frame (United, Flint, MI) equipped with a 5kg load cell. Sample gauge length was 30 mm and width was 20 mm. Each sample was mounted between two pneumatic grips and preloaded to 5 g of force for 10 seconds before being stretched until failure at a crosshead speed of 5mm/min. Stress-strain curves were acquired using the software Datum 3.0 (United) and subsequently used to determine the Young's modulus and ultimate tensile strength of the tested samples.

In vitro degradation and water content

Membranes were dried, weighed, and then incubated in a solution of PBS at pH 7.4 containing 5 U/mL of collagenase type I (Gibco, Carlsbad, CA) supplemented with 1% (w/v) BSA. This enzymatic digestion was performed at 37°C on an orbital shaker at 100 RPM to ensure full exposure of the membranes to the collagenase. Samples were dried and their weight recorded at different time points for up to 48 hours. The water content of a membrane was determined by measuring its weight after drying and after swelling in deionized water.

Permeability measurement

A custom-made diffusion chamber was used to evaluate the permeability of the membranes.[188,189] Each chamber surrounding the sample had a diameter of 20 mm and a volume of 6.3 mL. 30 x 30 mm square membranes segments were secured between the two chambers. Glucose at a concentration of 1.0 mg/mL was loaded in the first chamber while the second one was filled with nanopure water. 10 μL samples were taken from both chambers every 15 min until equilibrium was reached. Samples were then incubated for 15 min at room temperature with 100 μL of glucose hexokinase assay reagent (Sigma-Aldrich) and their absorbance measured at 340 nm to determine the concentration of the samples. A quasi steady-state was assumed and the hAM was considered as a thin membrane to calculate the coefficient of diffusion D_{eff}. [188,190] The permeability of the hAM to glucose was then obtained by dividing D_{eff} by the thickness of the hAM.[189]

Scanning Electron Microscopy

Amniotic membrane samples were washed in PBS, treated in 1% (v/v) osmium tetroxide (Sigma-Aldrich) in PBS for 2 hours, and then dehydrated in a graded ethanol series. Samples were then critical point dried and sputter-coated with gold before observation. Images were obtained using a Zeiss NEON 40EsB high resolution scanning electron microscope at 5 keV (Carl Zeiss Microscopy, Thornwood, NY, USA).

Stem cell culture

Human adipose-derived stem cells (hASCs) were provided by Dr. Jeffrey Gimble from Tulane University. They were cultured in Dulbecco's Modified Eagle Medium: Nutrient Mixture F-12 media (DMEM/F-12, Gibco) supplemented with 10% fetal bovine serum (Gemini Bio-Products, West Sacramento, CA) and 1% antibiotic-antimycotic (Gemini). Cell culture flasks were kept in a humidified incubator at 37°C with 5% CO_2.

Cell viability and proliferation assays

hASCs at passage 1 were seeded onto the stromal side of hAM at a density of 500 cells/mm^2. 72 hours after, cell viability was assessed using a LIVE/DEAD Viability/Cytotoxicity kit (Invitrogen, Carlsbad, CA) according to the manufacturer's recommendations. Briefly, tissue samples were washed with PBS, and incubated at room temperature for 45 min with a 2 μM calcein AM and 4 μM Ethidium homodimer-1 working solution. Samples were then imaged using a Nikon Eclipse E800

fluorescence microscope (Nikon Instruments Inc., Melville, NY, USA). ImageJ version 1.50i (NIH, Bethesda, MD) was used for image processing.

hASCs at passage 1 were seeded onto the stromal side of hAM at a density of 500 cells/mm^2. On day 1 and day 7 after seeding, 25 by 25 mm hAM samples were digested in collagenase type I (30 U/mL in PBS supplemented with 1% BSA) overnight at 37°C, sonicated, and then submitted to three freeze-thaw cycles to release the DNA content of the cells. A Quant-iT PicoGreen dsDNA assay kit (Invitrogen) was used according to the manufacturer's recommendations to quantify the amount of dsDNA per sample. The total cell number in a sample was then obtained by dividing the amount of dsDNA in a sample by the previously-determined mean dsDNA content per cell (6 pg).

Flow cytometry analysis

All reagents used for flow cytometry analysis were obtained from BD Biosciences, San Jose, CA. hASCs at passage 1 were seeded onto the stromal side of crosslinked and noncrosslinked hAM at a density of 500 cells/mm^2. After 72 hours, cells were harvested from the membranes after incubation with TrypLE Express (Gibco) for 10 min. Aliquots of 10^5 cells were incubated on ice for 20 min with monoclonal antibodies directed against CD29 (phycoerythrin (PE)-conjugated), CD34 (fluorescein isothiocyanate (FITC)-conjugated), CD44 (PE-conjugated), CD45 (PE-conjugated), CD73(PE-conjugated), CD90(FITC-conjugated), and CD105 (FITC-conjugated). The appropriate isotype controls (PE-conjugated Ms IgG_1, κ, and FITC-conjugated Ms IgG_1, κ) and an unstained cell sample were also used to respectively measure non-specific

binding and autofluorescence background. After incubation, cells were washed with PBS supplemented with 1% FBS and 0.1% sodium azide. 10^4 events were recorded for each sample on a BD Accuri C6 flow cytometer (BD Biosciences). Data was analyzed using FCS Express 6 Plus (De Novo Software, Glendale, CA).

Multilineage differentiation

hASCs at passage 1 were seeded on the stromal side of hAM at a density of 500 cells/mm^2. Adipogenic, osteogenic, and chondrogenic differentiation was then performed using commercially available differentiation medium kits (Gibco) and following the manufacturer's recommendations. After 14 days in culture, hASCs exposed to adipocyte differentiation medium were washed in PBS and fixed at 4°C with 10% formalin for an hour. Cells were then washed with DI water and incubated at room temperature for 20 min with a 0.5% Oil Red O solution in isopropanol (Sigma-Aldrich) to stain the cells for lipid accumulation. After a 14-day differentiation period, hASCs exposed to osteogenic differentiation medium were washed in PBS and fixed at 4°C with 70% ethanol for an hour. Cells were then washed with DI water and incubated at room temperature for 10 min with a 2% alizarin red S solution (Sigma-Aldrich) to stain calcium deposits. After 28 days in culture, hASCs exposed to chondrogenic differentiation medium were washed in PBS and fixed at room temperature with 10% formalin for 15 min. Cells were then washed with DI water and incubated at 37°C for 30 min with a 1% alcian blue solution in 3% acetic acid (Sigma-Aldrich) to stain for for glycosaminoglycans. Images were then obtained using an Olympus CKX41 (Olympus, Center Valley, PA) inverted microscope.

Statistical Analysis

All quantitative results are expressed as mean values ± standard error of the mean (SEM). Sample size (n) is indicated in each figure legend. Statistical analysis was performed via one-way analysis of variance (ANOVA) with Tukey's *post hoc* testing, using the software GraphPad Prism version 6.01. Statistical significance was set at $p < 0.05$.

Crosslinking Results

Characterization of the riboflavin-UVA crosslinking reaction

All the hAM used in these experiments were decellularized prior to usage by following previously established protocols [57,76], resulting in 50 μm thick membranes from which the pre-existing monolayer of epithelial cells was completely removed. Five different groups were compared throughout this study: simple noncrosslinked membranes (NON group), membranes crosslinked with 0.001, 0.01, and 0.1 g/L riboflavin which were respectively referred to as the RB Low, RB Med, and RB High groups, and hAM crosslinked with glutaraldehyde at 10 mM, designated as the GLU control group. This glutaraldehyde concentration is in the neighborhood of previously reported crosslinking protocols with glutaraldehyde,[61,172,173] and has the advantage of producing crosslinked hAM with a comparable crosslinking degree than the highest riboflavin concentration used (RB High).

The FTIR spectra of all groups are displayed in Figure 8. FTIR is representative of the entire thickness of a membrane since the light beam is transmitted through the tissue sample. All spectra presented a similar pattern, comparable to previously reported FTIR spectra for the hAM.[59,62] Characteristics absorption bands were observed at 3316 cm^{-1} (N-H stretching), 2923 cm^{-1} (C-H stretching), 1654 cm^{-1} (amide I, C=O stretching), 1552 cm^{-1} (amide II, N-H bending),1239 cm^{-1} (amide III, N-H bending). Lower intensity peaks were present on spectra for crosslinked hAM compared to noncrosslinked hAM, implying that the crosslinking reaction created new chemical bonds.

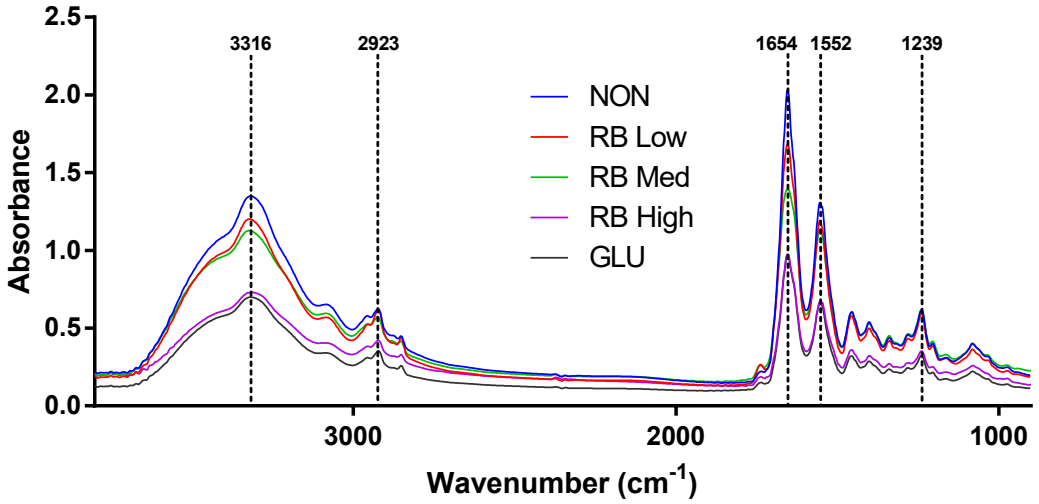

Figure 8: FTIR spectra of noncrosslinked and crosslinked hAM (n=4). Characteristics absorption bands were at 3316 cm^{-1} (N-H stretching), 2923 cm^{-1} (C-H stretching), 1654 cm^{-1} (amide I, C=O stretching), 1552 cm^{-1} (amide II, N-H bending),1239 cm^{-1} (amide III, N-H bending).

Furthermore, ninhydrin was used for the quantification of free amine groups in noncrosslinked and crosslinked membranes. The crosslinking degree for these samples is reported in Figure 9. Crosslinked membranes contained lower concentrations of free amine groups, hence presenting a higher crosslinking degree of up to 42.9±3.6% for hAM crosslinked with a high concentration (0.1% w/v) of riboflavin. The crosslinking degree of the glutaraldehyde crosslinked hAM (46.4±3.3%) was comparable to the one obtained with the highest concentration of riboflavin. The ninhydrin reactivity is not directly proportional to the amount of crosslinking but proportional to the number of free amino groups occupied. It is possible for a low concentration of riboflavin to already react and crosslink all possible reaction sites. Adding more riboflavin with a higher concentration could just bind riboflavin instead of crosslinking it. In this case, the extent of crosslinking would go up because more free amino groups are occupied but this would not directly translate to the amount of free amino groups that could crosslink.

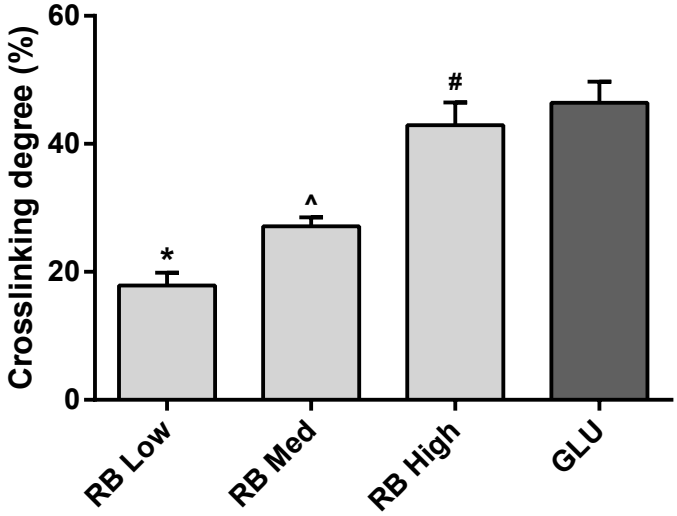

Figure 9: Crosslinking degrees determined by ninhydrin assay of hAM exposed to UVA-riboflavin or glutaraldehyde crosslinking as compared to noncrosslinked hAM (n=6 per group). *Significant differences ($p < 0.05$) when compared to RB Med, RB High, and GLU groups. ^Significant differences ($p < 0.05$) when compared to RB Low, RB High, and GLU groups. #Significant differences ($p < 0.05$) when compared to RB Low, RB Med, and GLU groups.

Results obtained via FTIR and quantification of free amino groups via ninhydrin assay correlate and indicate that exposure of hAM to riboflavin and UVA crosslink the membranes, with amino groups from the hAM collagen participating in the riboflavin-UVA crosslinking reaction.[191]

Evaluation of mechanical properties

The tensile properties of crosslinked and noncrosslinked membranes are reported in Figure 10. A significant increase in Young's Modulus and Ultimate Tensile Strength was observed for all crosslinked groups with up to a 2.5-fold increase compared to noncrosslinked controls.

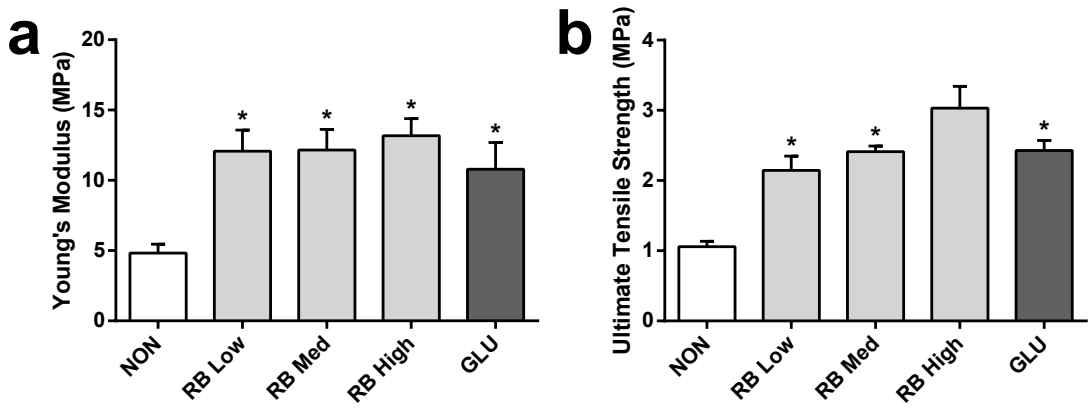

Figure 10: Mechanical properties of noncrosslinked and crosslinked hAM. (a) Young's Modulus. *Significant differences ($p < 0.05$) when compared to NON group. (b) Ultimate Tensile Strength. *Significant differences ($p < 0.05$) when compared to NON and RB High groups.

Proteolytic degradation and water content

To measure the effect of crosslinking on the biodegradation rate, crosslinked and noncrosslinked membranes were exposed to a 5U/mL solution of collagenase type I in PBS on an orbital shaker at 37°C. After 48 hours of collagenase exposure, only 10.0±3.8% of the original weight of the noncrosslinked membrane remained, as opposed to 69.5±4.9% for the hAM crosslinked with glutaraldehyde, as displayed in Figure 11. hAM crosslinked with low, medium, and high concentrations of riboflavin respectively maintained 22.3±3.9%, 35.5±4.4%, and 46.8±3.8% of their original weights. While exhibiting a lower degree of crosslinking than the GLU group, the RB groups still achieved a 2-fold, 3-fold, and 4-fold increase in biodegradation rate when compared to noncrosslinked membranes.

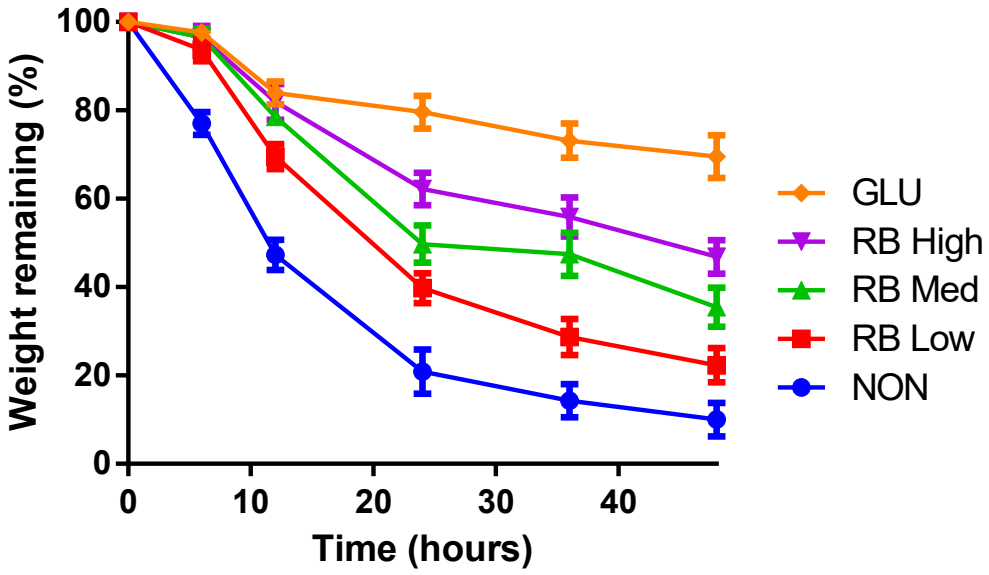

Figure 11: Enzymatic digestion of hAM by collagenase over time (n=6 per group).

Another parameter to characterize the extent of the crosslinking reaction is the water content of membranes. Collagen crosslinking implies changes to the structure of collagen fibers, often bringing them closer together and causing a loss of water. The water content of crosslinked and noncrosslinked hAM is reported in Figure 12. The values obtained are consistent with the crosslinking degrees values shown in Figure 9: the more crosslinked membranes see a larger decrease in water content. However, the maximum loss of water content for a crosslinked hAM compared to a noncrosslinked one was only about 10%, for glutaraldehyde crosslinked samples.

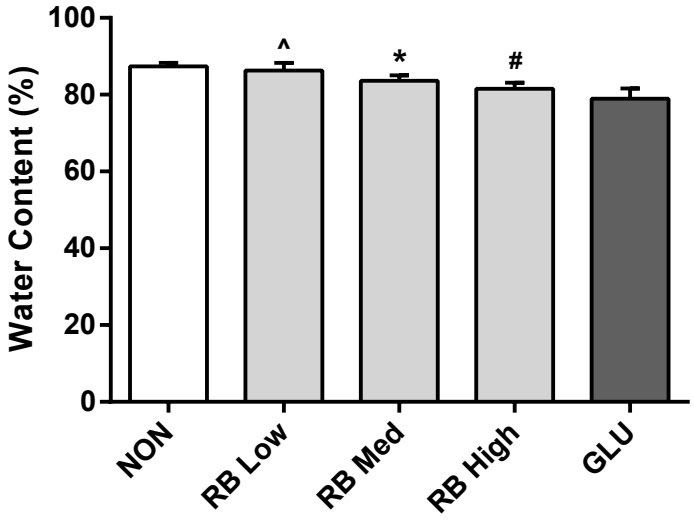

Figure 12: Water content (n=6 per group) of hAM. ^Significant differences ($p < 0.05$) when compared to RB High and GLU groups. *Significant difference ($p < 0.05$) when compared to NON and GLU groups. #Significant differences ($p < 0.05$) when compared to NON and RB Low groups.

Glucose permeability

The effects of riboflavin-UVA and glutaraldehyde crosslinking on the glucose permeability of the hAM are displayed in Figure 13. Glucose is a critical component to ensure cell survival and proliferation and a high permeability is essential to avoid mass transport limitations. The permeability of noncrosslinked membranes was 59.6±3.8 $x10^{-6}$ cm^2/sec, compared to 51.6±4.5 $x10^{-6}$ cm^2/sec, 49.8±3.2 $x10^{-6}$ cm^2/sec, 48.5±5.0 $x10^{-6}$ cm^2/sec, and 52.3±4.2 $x10^{-6}$ cm^2/sec for membranes crosslinked with low, medium, high concentrations of riboflavin, and glutaraldehyde respectively.

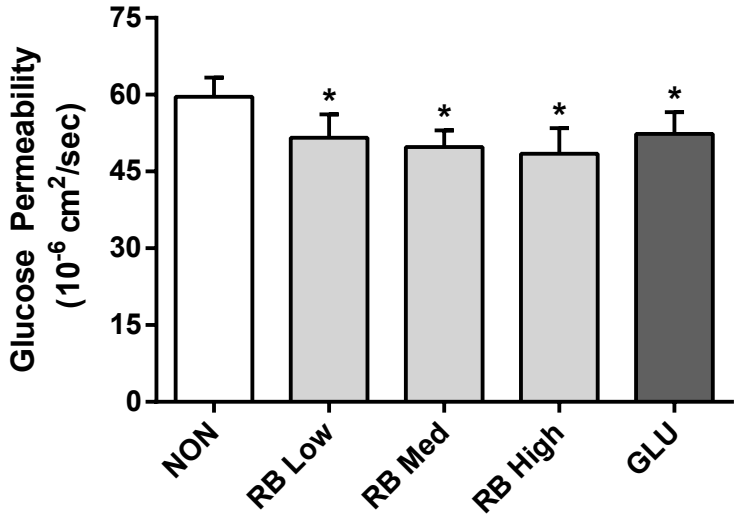

Figure 13: Glucose permeability of noncrosslinked and crosslinked hAM. *Significant difference ($p < 0.05$) when compared to NON group.

Surface morphology of crosslinked hAM

Scanning electron microscopy (SEM) was used to evaluate the effect of crosslinking on the surface morphology of hAM. Representative SEM images are provided in Figure 14. The morphologies of RB Low, RB Med, RB High, and GLU crosslinked samples appear to be different than the NON group. Images of crosslinked samples showed some differences when compared to images of noncrosslinked membranes, but the differences were subtle and difficult to distinguish. Image analysis was not deemed a fruitful approach to quantify differences between the crosslinking groups due to the variability of images for the same group. Variations of collagen fibers volume between the groups would have also been very small and hard to quantify. Slight differences in the chemistry used to crosslink the hAM between the riboflavin-UVA and glutaraldehyde protocols would result in slightly different porosities. These differences

would be consistent with the water content and permeability results reported in Figures 12 and 13.

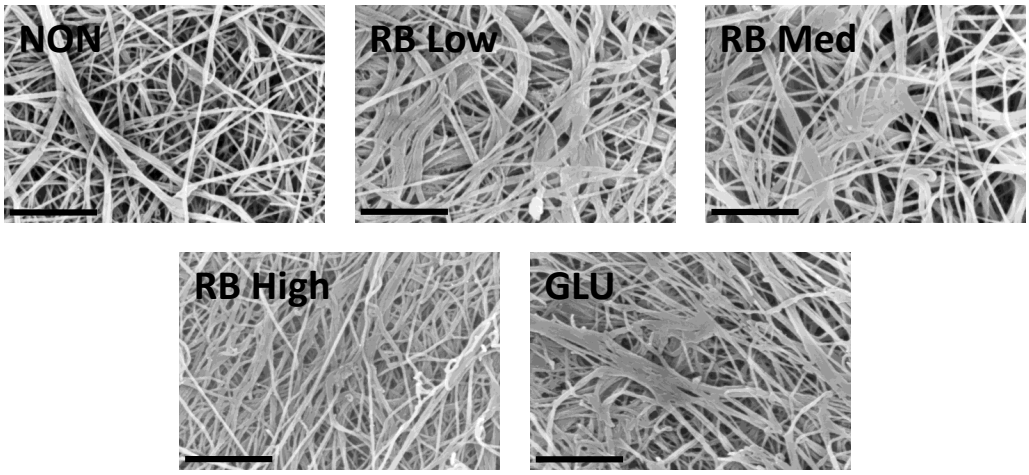

Figure 14: Representative scanning electron microscopy (SEM) images of the stromal side of crosslinked and noncrosslinked hAM membranes. Scale bars represent 1 μm.

hASCs viability and proliferation

hASCs at passage 1 were used to evaluate the cellular compatibility of crosslinked hAM. All cells were seeded on the stromal side up of the membranes, which presents a more favorable arrangement of collagen fibers compared to the epithelial side up.[76] Representative LIVE/DEAD pictures of hASCs cultivated for 72 hours on crosslinked and noncrosslinked hAM are shown in Figure 15. No visible differences were present between the five groups of hAM represented by these fluorescent images.

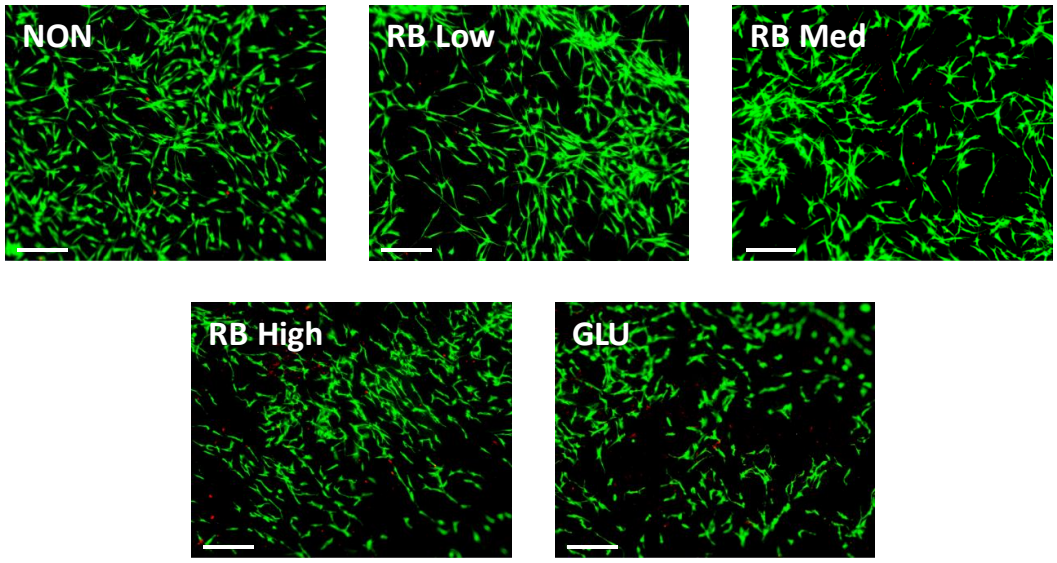

Figure 15: Representative LIVE/DEAD staining of hASCs seeded on hAM scaffolds. Live cells fluoresce in green (stained with calcein AM) while dead cells fluoresce in red (Ethidium homodimer-1 staining). Scale bars represent 100 μm.

Human adipose-derived stem cells (hASCs) adhered and proliferated to the surface of crosslinked and noncrosslinked membranes as demonstrated on Figure 16 by a quantification of cells per scaffold on Day 1 and Day 7 after seeding, as determined via a PicoGreen dsDNA assay. No significant differences in cell growth over time were present between the five types of hAM used to cultivate cells, as supported by the LIVE/DEAD assay.

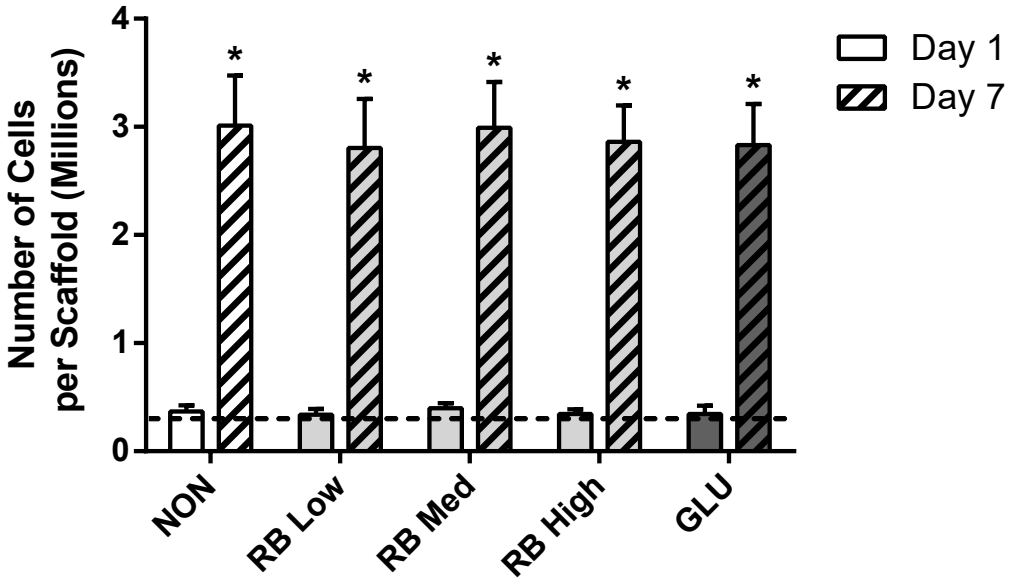

Figure 16: Average number of hASCs on crosslinked and noncrosslinked hAM at Day 1 and Day 7 after initial seeding of 300 000 cells per construct. *Significant difference ($p < 0.05$) when compared to Day 1 number of cells for the same group.

Immunophenotype of hASCs cultivated on membranes

The immunophenotype of hASCs seeded, grown for 72h, and detached from noncrosslinked and crosslinked hAM is reported in Figure 17. Cells were detached using TrypLE Express instead of more stronger dissociation agents (such as Trypsin-EDTA) in order to not interfere with the expression of cell surface markers. All cells analyzed presented a comparable immunophenotype, independent of the type of membrane they were cultivated on. Consequently, for better clarity, only the immunophenotype of cells seeded on noncrosslinked membranes is fully reported in Figure 17.

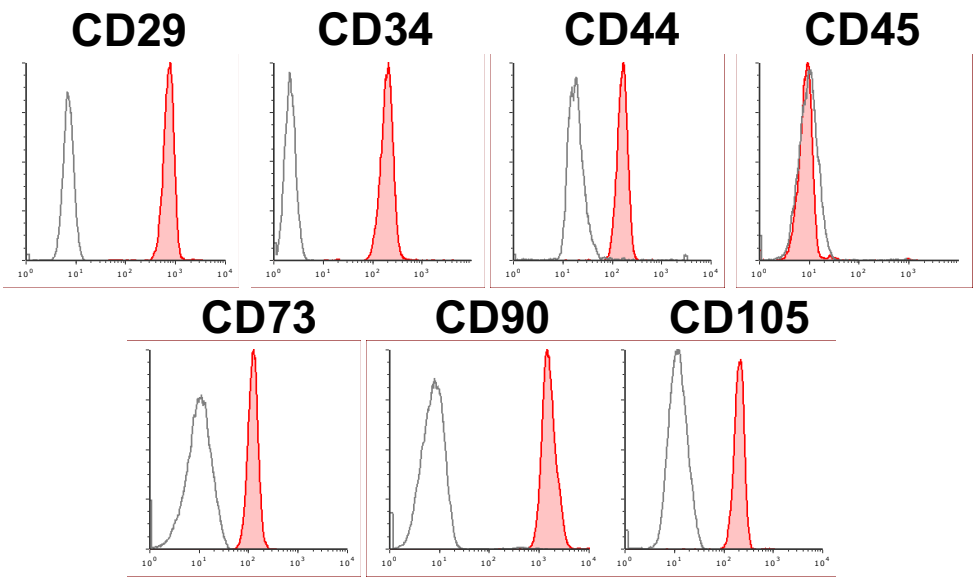

Figure 17: Immunophenotype of hASCs cultivated on noncrosslinked hAM for 72 hours, as determined by flow cytometry analysis. Isotype control antibodies are represented by a grey line and hASCs by a red line. Relative fluorescence on the X axis and counts on the Y axis.

The immunophenotype of hASCs was consistent with previous reports.[192,193] CD29, CD34, CD44, CD73, CD90, and CD105 were positively expressed while CD45 was not expressed. These results demonstrate that the stemness of the hASCs was not influenced by the microstructure changes induced by crosslinking.

Similar gating strategies were applied to each sample in order to obtain comparable data. The median fluorescence intensity (MFI) was determined for each cell surface marker and for each membrane type that hASCs were cultivated on as displayed in Figure 18. When compared to the MFI for cells cultivated on noncrosslinked membranes, comparable results were obtained for cells grown on crosslinked scaffolds. These results are in agreement with the ones displayed in Figure 16 where the type of membrane cells were seeded on did not significantly influence their viability or proliferation.

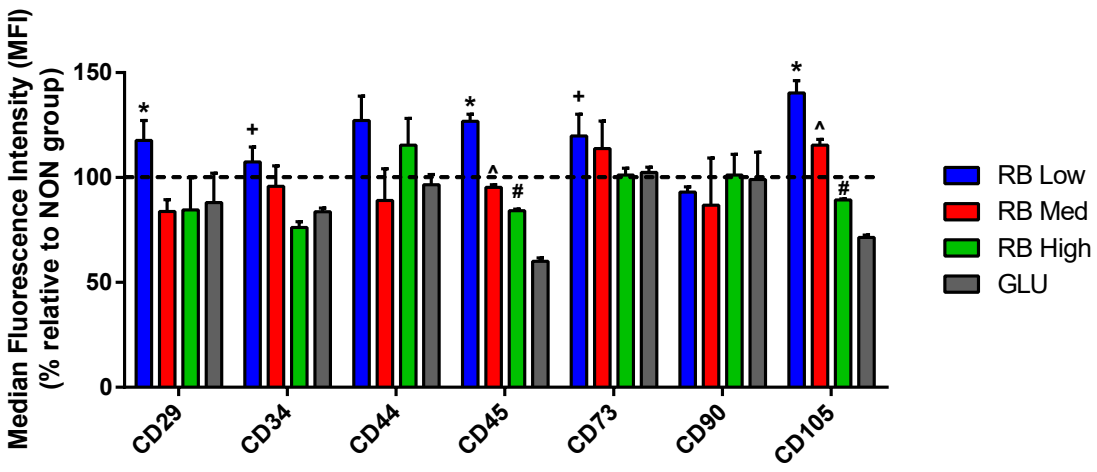

Figure 18: Median Fluorescence Intensity (MFI) of stem cell surface markers for cells cultivated on crosslinked membranes for 72 hours. MFI is relative to the MFI of cells cultivated on noncrosslinked hAM for 72 hours (n=4 per group). *Significant differences ($p < 0.05$) when compared to RB Med, RB High, and GLU groups. ^Significant difference ($p < 0.05$) when compared to RB Low, RB High, and GLU groups. #Significant differences ($p < 0.05$) when compared to RB Low, RB Med, and GLU groups. +Significant differences ($p < 0.05$) when compared to RB High group.

Multilineage differentiation

To evaluate if the differentiation abilities of hASCs were affected by the type of membrane they were cultivated on, hASCs were seeded on both noncrosslinked and crosslinked membranes and exposed to adipogenic, osteogenic, and chondrogenic differentiation media for 14, 14, and 28 days respectively. The type of membrane used for the cultivation of hASCs did not influence their differentiation abilities as displayed in Figure 19. Cells exposed to adipogenic differentiation media stained positive for lipid accumulation with Oil Red O. Calcium deposits were stained positively with alizarin red for cells cultivated with osteogenic differentiation media. Finally, chondrogenic nodules characterized by alcian blue staining were present after 28 days for hASCs exposed to chondrogenic differentiation media.

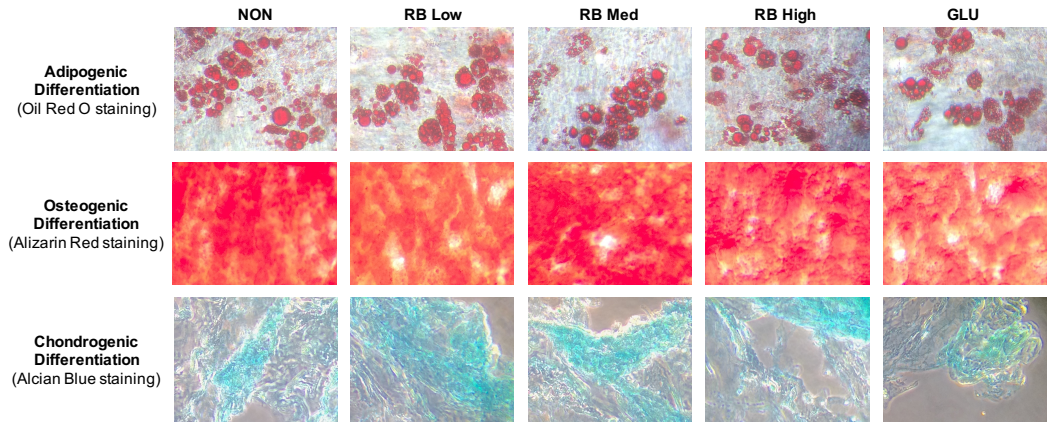

Figure 19: Multilineage differentiation of hASCs seeded on noncrosslinked and crosslinked hAM. Differentiation of hASCs into adipocytes was demonstrated by positive Oil Red O staining. Differentiation into osteoblasts was shown by positive Alizarin red staining. Differentiation into chondrogenic nodules was characterized by alcian blue staining.

Discussion

Naturally occurring materials have been used as scaffolds in a wide range of tissue engineering applications [194,195]. Although they typically provide excellent biocompatibility, the mechanical properties of these materials are often significantly less than that of the tissue they are intended to replace. To overcome this limitation, many investigators have resorted to some form of crosslinking of the natural material which generally improves the mechanical properties. However, *in vivo* studies have suggested that even very small amounts of unreacted residual crosslinking agents in the material can lead to substantial immunological complications [171,196]. Our motivation for this study was that riboflavin-UVA crosslinking has been previously used clinically and did not show biocompatibility issues. Although the hAM is currently being used for a number of surgical procedures and riboflavin-UVA crosslinking of the cornea is FDA approved, there has not previously been a thorough and careful assessment of riboflavin-UVA crosslinked hAM. The goal of this study was to investigate the effect of

riboflavin-UVA crosslinking on the hAM and evaluate its effect on the cultivation of human adipose-derived stem cells.

The extent of crosslinking was characterized in two different ways, by FTIR and by ninhydrin assay which determines the number of free amine groups. Both of these assays demonstrate a dose dependent increase in the extent of crosslinking as the riboflavin concentration is increased. These chemical characterizations of the treated hAM are consistent with the measurements we made of several physical properties of the membranes. As the extent of crosslinking goes up the water content and the permeability of the hAM goes down. This is a less desirable consequence of crosslinking, since these changes have been associated with poorer performance of tissue engineered constructs. On the other hand, crosslinking does significantly improve the mechanical properties of the hAM, essentially to the same strength as glutaraldehyde treated membranes.

Cell attachment and growth can be very sensitive to subtle alterations in the chemical and physical properties of the substrate [197]. To test the suitability of riboflavin-UVA crosslinked hAM for future applications using stem cells, we seeded native and crosslinked membranes with human adipose-derived stem cells. The cells adhered to and retained their stem cell-like character based on the expression of seven specific cell surface markers. While this data showed that stem cells would not be induced to differentiate towards some particular cell type when placed on the crosslinked membranes, we still needed to show that these stem cells retained their ability to

differentiate when exposed to the appropriate conditions. We then examined three well established differentiation protocols, leading cells towards either an adipogenic, osteogenic, or chondrogenic cell lineage. We found no differences in the ability of the cells to differentiate based on the type of membrane they were seeded on. This suggests that although the riboflavin-UVA treatment does change the chemical and physical properties of the hAM, the membrane retains its ability to support stem cell attachment and appropriate cell differentiation.

Taken together, these results show that riboflavin-UVA crosslinked hAM performed similarly to their counterparts crosslinked with glutaraldehyde. However, unlike glutaraldehyde, riboflavin is a non-cytotoxic crosslinking agent that is currently FDA approved for use in humans.[170,176] In contrast, residual levels of most other crosslinking agents, such as glutaraldehyde, are cytotoxic. Lai et al. reported that the crosslinking of hAM with glutaraldehyde impacted their nanofibrous structures and negatively affected the culture of human corneal epithelial cells.[173]

While our results characterize the properties of and demonstrate the potential of riboflavin-UVA crosslinked hAM, we have not yet tested this novel material for use in a particular regenerative medicine application. Each specific application will have a unique set of requirements, both chemical and physical that must be carefully assessed. Thanks to its enhanced mechanical properties and biodegradation rate, riboflavin-UVA crosslinked hAM would be a prime candidate for several clinical and tissue engineering applications. As a consequence of its attractive biological properties, transparency,

thinness, and composition akin to the one of the conjunctiva, the hAM has been widely used in ophthalmology for the treatment of a variety of ocular surface diseases.[85,86] The hAM can be applied on the ocular surface either as a temporary dressing or as a permanent graft.[38] When used as a temporary biological bandage, the hAM acts as barrier to protect the healing epithelium from the movement of the eyelids. However, hAM bandages degrade quickly and need to be replaced every week although repeated interventions at the diseased corneal surface are not recommended.[38] With their increased biodegradation rate, riboflavin-UVA crosslinked hAM could be used as improved dressings for the healing corneal surface.

Similarly, hAM degrade quickly when used as grafts for the transplantation of autologous limbal epithelial cells for the treatment of limbal stem cell deficiency.[93] Various crosslinking agents such as carbodiimide have been used to chemically crosslink the hAM and improve its biodegradation.[62,67] These crosslinking techniques were effective at improving the mechanical properties of the scaffolds. However, the crosslinking agents used were highly cytotoxic, resulting in biocompatibility issues with the resulting scaffolds.[171,174]

Thanks to its enhanced mechanical properties riboflavin-UVA crosslinked hAM would be a prime candidate for blood vessel tissue engineering,[45] cartilage regeneration,[46] urothelium tissue engineering,[47] and tendon repair.[43] For instance, it has been reported in the literature that a native superior infraspinatus tendon has an elastic modulus of 32 ± 13 MPa and an ultimate tensile strength of 16.5 ± 7.1 MPa.[198,199] Single or multilayer

constructs of riboflavin-UVA crosslinked hAM could be potentially used to generate tissue engineered tendons.[43]

Conclusion

In this study, we reported the successful application of riboflavin-UVA crosslinking to the hAM. Tissue samples exposed to riboflavin-UVA benefited from a 3-fold increase in mechanical properties and a decreased biodegradation rate while only incurring a minor decrease in glucose permeability. Moreover, riboflavin-UVA crosslinked membranes successfully supported the growth and differentiation of hASCs. Together these findings suggest that riboflavin-UVA crosslinking can be used to overcome the limitations of the hAM and broaden its use to new tissue engineering applications.

Acknowledgements

The authors would like to acknowledge Norman Regional Hospital for supplying the placentas used in the current study, Dr. Jeffrey Gimble (Tulane University) for providing human adipose-derived stem cells, Nathan Richbourg and the members of the Samuel Roberts Noble Microscopy Laboratory at the University of Oklahoma for their assistance with scanning electron microscopy. This work was supported by the Vice President for Research of the University of Oklahoma.

Chapter 4: Properties of Porcine Adipose-Derived Stem Cells and Their Applications in Preclinical Models

Abstract

Adipose-derived stem cells represent a reliable adult stem cell source thanks to their abundance, straightforward isolation, and broad differentiation abilities. Consequently, human adipose-derived stem cells (hASCs) have been used in vitro for several innovative cellular therapy and regenerative medicine applications. However, the translation of a novel technology from the lab to the clinic requires first to evaluate its safety, feasibility, and potential efficacy through preclinical studies in animals. The anatomy and physiology of pigs and humans are very similar, establishing pigs as an attractive and popular large animal model for preclinical studies. Knowledge of the properties of porcine adipose-derived stem cells (pASCs) used in preclinical studies is critical for their success. While hASCs have been extensively studied this past decade, only a handful of reports relate to pASCs. The aim of this chapter is to summarize the current findings about the isolation of pASCs, their culture, proliferation, and immunophenotype. The differentiation abilities of pASCs and their applications in porcine preclinical models will also be reported.

Introduction

Adipose-derived stem cells represent a reliable adult stem cell source thanks to their abundance, straightforward isolation, and broad differentiation abilities. Consequently, human adipose-derived stem cells (hASCs) have been used in vitro for several

innovative cellular therapy and regenerative medicine applications. However, the translation of a novel technology from the lab to the clinic requires first to evaluate its safety, feasibility, and potential efficacy through preclinical studies in animals. The anatomy and physiology of pigs and humans are very similar, establishing pigs as an attractive and popular large animal model for preclinical studies. Knowledge of the properties of porcine adipose-derived stem cells (pASCs) used in preclinical studies is critical for their success. While hASCs have been extensively studied this past decade, only a handful of reports relate to pASCs. The aim of this concise review is to summarize the current findings about the isolation of pASCs, their culture, proliferation, and immunophenotype. The differentiation abilities of pASCs and their applications in porcine preclinical models will also be reported.

Isolation and Culture of pASCs

Adult stem cells have been identified in several tissues and organs including peripheral blood, bone marrow, adipose tissue, skin, and skeletal muscle.[200,201] Bone marrow mesenchymal stem cells have been the established standard for adult stem cells, but their harvest from bone marrow is a highly invasive procedure involving pain, morbidity and low cell yield.[201] Adipose tissue has proven to be an attractive alternative cell source to bone marrow. [202,203] It has the advantage of being an abundant and easily attainable cell source, with a straightforward and significant less invasive isolation procedure.

The standard process highlighted in Figure 20 to isolate pASCs from adipose tissue is similar to protocols previously reported for hASCs. [204–206] The goal of this procedure is to isolate the stromal vascular fraction (SVF) containing the pASCs from the adipocytes by using simple physical treatments. The first step consists of obtaining adipose tissue from a pig biopsy. The most common locations for subcutaneous adipose tissue are the dorsal and abdominal areas. Other white adipose tissue sources can also be used to obtain pASCs. Niada *et al.* determined that the buccal fat pad, which is an encapsulated fat mass in the cheek, contains pASCs with comparable properties to cells harvested from the subcutaneous interscapular region[207]. After procurement, the adipose tissue is finely minced then digested (typically via collagenase type I treatment). Centrifugation and filtration with cell strainers separate adipocytes from the SVF containing the pASCs. After separation, adipocytes remain in the supernatant while the SVF pelletizes. The adipocytes are then discarded and the SVF pellet is resuspended in culture medium and seeded into culture flasks. Typical cell seeding densities range from 5000 to 7000 cells/cm^2.[204,208,209] Dulbecco's Modified Eagle Medium (DMEM) mixed 1:1 with Ham's F-12 Nutrient Mixture and supplemented with 10% Fetal Bovine Serum has been reported as ideal for the culture of pASCs.[204,209] After 48/72hrs in culture the non-adherent hematopoietic cells are removed. The remaining adherent cells are pASCs who display an elongated morphology, similar to fibroblasts. These primary pASCs complete a cell cycle in 60 to 80 hours.[204,210,211] Reports suggest that pASCs can reach up to 30-40 population doublings without reaching replicative senescence.[204,210]

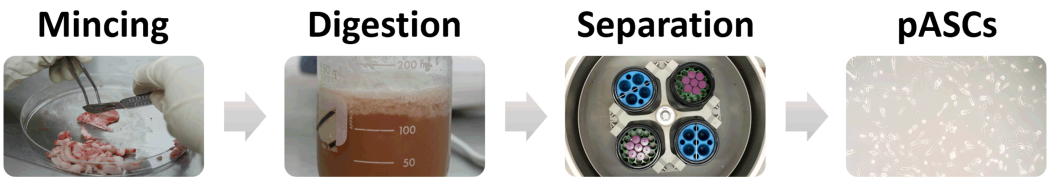

Figure 20: Illustrations of the standard protocol used to isolate pASCs. Subcutaneous porcine adipose tissue is finely minced before being digested in a collagenase type I solution at 37°C. Centrifugation separates the supernatant containing adipocytes from the SVF pellet. Cells are then plated in a tissue culture flask. pASCs are adherent and adopt a fibroblast-like morphology in culture.

On average, 0.5 to 1x10^6 viable and adherent pASCs are obtained per mL of adipose tissue.[204,211] One parameter that has been shown to affect the recovery yield of pASCs is the age of the source animal from whom the cells are extracted.[212,213] However, the abundance and accessibility of subcutaneous adipose tissue in pigs results in the ability to isolate several million cells from a single biopsy. Long term cryopreservation can also be used to store pASCs indefinitely. Cryopreserved pASCs have been shown to display similar proliferative characteristics, expression of cell surface markers, and differentiation abilities to fresh pASCs.[214]

Immunophenotype of pASCs

hASCs have been thoroughly characterized with an extensive literature available detailing their isolation, proliferation, immunophenotype, and differentiation abilities. The International Federation for Adipose Therapeutics and Science (IFATS) and the International Society for Cellular Therapy (ISCT) have defined phenotypic and functional criteria to identify hASCs.[215] Currently, no criteria have been established to facilitate the identification of porcine stem cells, either bone marrow or adipose derived.

Characterization of these animal cells is largely based on morphologic, phenotypic and functional properties, and can still appear rather ambiguous.

Flow cytometry is a convenient and fast method to analyze the immunophenotype of a cell population. It is a powerful tool routinely used to assess the characteristics of a freshly isolated population of cells and verify that they have not been contaminated with endothelial or hematopoietic cells. Indeed, the SVF can include cells other than adipose stem cells such as blood cells, smooth muscle cells, fibroblasts, and endothelial cells. Fluorescence-activated cell sorting (FACS) can be used to purify a cell population by removing undesired subpopulations. Protocols have also been established with hASCs to isolate specific subpopulations of progenitor cells among the hASCs population.[200,202] Similar strategies haven't been implemented on pASCs yet but could prove beneficial for future studies.

Flow cytometry analysis of some pASCs surface markers can prove challenging. Many porcine surface antigens are not cross-reactive with antibodies designed for other species and require porcine-specific antibodies. For instance, among the seven porcine surface antigens reported in Table 1, only CD44, CD90, and CD105 are cross-reacting with anti-human antibodies. A limited number of porcine-specific antibodies are currently commercially available. Consequently, published studies were consistent with one another and reported the use of similar antibodies. The expression of several cell surface markers for pASCs and hASCs are summarized in Table 1.

Surface Antigen	pASCs Expression	Refs	hASCs Expression	Refs
CD14	–	216,217	–	200,203
CD29	+	205,214,216–218	+	200,203
CD31	–	205,214,218	–	200,202,203
CD44	+	205,214,216–218	+	200,202,203
CD45	–	205,216,218	–	200,202,203
CD90	+	205,214,216–218	+	200,202,203
CD105	+	216,218	+	200,202,203

Table 1: Expression of cell surface markers for pASCs and hASCs determined by flow cytometry analysis for cells cultured at low passage numbers and in regular FBS supplemented culture medium. "+" corresponds to a positive expression of the cell surface marker, "–" for a low or non-expressed cell surface antigen.

CD29, CD44, CD90 and CD105 are part of the typical panel of surface markers characteristic of mesenchymal stem cells. These markers are positively expressed by pASCs, demonstrating their stemness. Analysis of stem cell transcription factors (Oct-4, Sox-2, and Nanog) by RT-PCR also reveals that pASCs express these markers of primitive stem cells.[219]

pASCs do not express hematopoietic stem cell markers CD14 and CD45, nor do they express CD31 which is a marker characteristic of endothelial cells. Measuring the

expression of CD14, CD45, and CD31 after isolating a new population of pASCs is a useful technique to verify that the stem cell population is not contaminated with endothelial or hematopoietic cells.

Overall, the cell surface marker expression profile for these typical markers appears similar between pASCs and hASCs. However, the few antibodies available for pASCs only provide a limited representation of the expression of surface antigens by pASCs.

Multilineage differentiation abilities

Besides self-renewal, a high proliferative capacity, and the expression of specific cell surface markers, another defining characteristic of a stem cell is its ability to differentiate into multiple lineages.[200,215] hASCs have demonstrated the ability to differentiate into multiple cell types such as osteoblasts, chondrocytes, adipocytes, epithelial cells, endothelial cells, smooth muscle cells, neural cells, and hepatocytes.[200,201,220] While the differentiation abilities of hASCs have been extensively studied this past decade, only a handful of reports have been related to pASCs. Figure 21 illustrates the differentiation pathways previously reported with pASCs along with the major reagents typically used to promote each cell lineage.

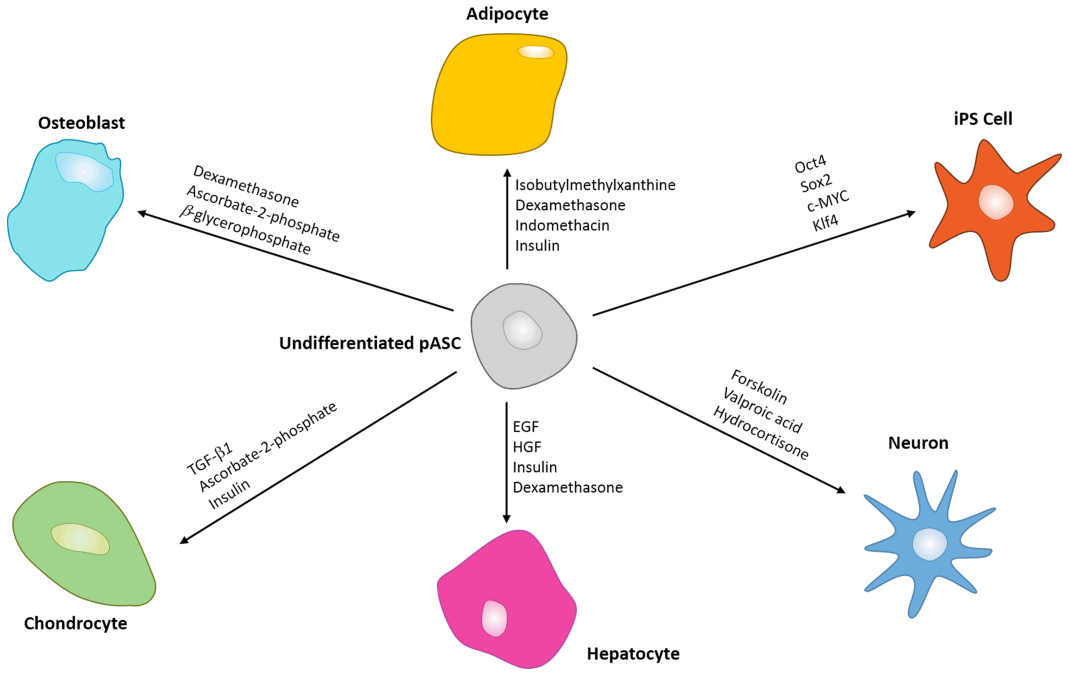

Figure 21: Multilineage differentiation abilities of pASCs. Major typical reagents are specified for each pathway. pASCs have been shown to be able to differentiate into adipocytes, osteoblasts, chondrocytes, hepatocytes, and neurons, as well as being able to be reprogrammed into induced pluripotent stem cells.

The adipogenic, osteogenic and chondrogenic differentiation are classic and easily obtainable mesodermal lineages differentiation pathways. Differentiation protocols for these three lineages are well established, and have been reported with pASCs.[208,221,222] However, studies related to ectodermal or endodermal lineages are scarce. Currently, it has been reported that pASCs can transdifferentiate into hepatocytes,[216,223] neurons,[210,224] and pancreatic islet-like clusters.[225] Using lentivirals carrying reprogramming factors, pASCs have also been reprogrammed into induced pluripotent stem cells (iPSCs).[218,226] Song *et al.* also described that pASCs could also differentiate into oocyte-like cells.[219]

pASCs have been shown to demonstrate similar characteristics to other porcine-derived adult stem cells such as those derived from bone marrow, peripheral blood, adipose

tissue, synovial membrane, and skin.[206,227,228] These include comparable morphology, proliferative capacity, alkaline phosphatase activity, cell surface marker expression, metabolic pathways, biological functions, and transcription factors.[209,222,229] pASCs have often been compared side-by-side with porcine stem cells from these other tissue sources, revealing characteristics and comparable multilineage differentiation abilities as well. [208,222,227]

While knowledge of the differentiation abilities of pASCs is currently limited to a few reports, porcine bone marrow-derived stem cells (pBMSCs) have been differentiated into myocytes,[230] endothelial cells,[231] and epithelial cells.[232] Since pBMSCs and pASCs characteristics are very similar,[233] it can be assumed that these differentiation pathways reported for pBMSCs should also apply to pASCs.

Applications in Preclinical Models

Adult stem cells have proven to be effective for the treatment of several diseases and the repair and regeneration of damaged tissues *in vitro*.[200,202,228] Preclinical animal studies represent a critical step in the translation of a cell transplantation or tissue engineering technology from the lab to the clinic. They are required to evaluate the safety, feasibility and potential efficacy of novel therapies.[201,208] Two criteria need to be addressed in order for an animal study assessing a novel cell-based approach to be beneficial. The animal chosen for the study has to mimic human physiology as closely as possible, and the animal cells that are being used need to be precisely identified and characterized. Some previous clinical trials did not adhere to these guidelines and

concluded with unsatisfactory results. One shortcoming often comes from the use of rodents whose physiology and organ size does not properly match that of humans. [234] Results obtained with small animals, whose anatomy is different to humans, do not typically extrapolate properly to human clinical trials.[208] Large animals such as pigs represent a preferable model. Their organ size along with cell number and distribution more closely mimic human characteristics. Pigs are some of the most attractive and relevant large animal models for preclinical studies since their size, anatomy, genomic organization, and physiology are very similar to humans.[206,208,235] In a porcine preclinical model, the autologous transplantation of pASCs avoids triggering an adverse immune response.

Pigs have been used to investigate innovative pASCs bone regeneration strategies.[235] The osteogenic differentiation of pASCs is a well-known process.[222,236,237] Several studies combined pASCs differentiated into osteocytes with various types of scaffold such as hydroxyapatite,[221] polycaprolactone,[238] or oligo (polyethylene glycol) fumarate (OPF) hydrogel[239] to repair osteochondral defects. pASCs have also been implanted in pigs to evaluate their therapeutic effect in the treatment of osteonecrosis of the femoral head[240] and for the regeneration of osteochondral defects.[241,242] Pigs have also proven a suitable model for oral and maxillofacial studies.[207,243] Wilson *et al.* demonstrated that injections of pASCs enhanced healing of mandibular defects in pigs.[244]

The vascular anatomy and physiology of pigs are quite similar to humans. Pigs have consequently been broadly used to evaluate novel vascular therapies.[245] Recent studies

include the intracoronary administration of pASCs after an acute myocardial infarction model[246–248] and the transplantation of pASCs cell sheets in a porcine model of chronic heart failure.[249]

The structures of porcine and human skin are similar, making pigs a suitable model for dermatologic preclinical studies. Hanson *et al.* harvested pASCs and pBMSCs and injected them in a dermal wound model to study the feasibility of stem cells injections to promote wound healing.[217] pASCs performed similarly to pBMSCs, safely promoting tissue regeneration.

Future Perspectives

pASCs express cell surface markers characteristic of mesenchymal stem cells and are able to differentiate into several lineages. Knowledge about the possible transdifferentiation abilities of pASCs is currently limited but will expand in the foreseeable future. The development of standard protocols for the isolation, culture and differentiation of pASCs would further improve pASC-based preclinical studies.[250]

Pigs represent an excellent animal model for preclinical studies. Besides their similar morphology and physiology to humans, they also have the advantage of providing large quantities of easily obtainable subcutaneous tissue, resulting in a generous supply of pASCs.

Miniature pigs are being developed with the goal to increase the efficiency and translation of preclinical studies in pigs. Minipigs have the advantage of slower growth

curves and a similar weight to an average human male, between 150 to 200lbs.[239,251,252] Such a new advantageous animal model has the potential to become increasingly popular and supplant rodents for relevant preclinical animal studies.

Chapter 5: Fabrication of an Economical Arduino-Based Uniaxial Tensile Tester

Abstract

The mechanical properties of soft materials are critically important for a wide range of applications ranging from packaging to biomedical purposes. We have constructed a simple mechanical testing apparatus using off-the-shelf materials and open-source software for a total cost of less than $100. The device consists of a wooden frame supporting a central loading apparatus attached via drawer slides. To perform a mechanical test, a sample was secured within two custom-made 3D-printed clamps affixed to brackets on the base of the frame and the load cell. The extension force was applied by the user pulling on a rope, moving the central loading apparatus up (thereby stretching the sample) while recording the force (measured by a load cell) and the displacement (measured by an ultrasonic sensor). The load cell and ultrasonic sensor were linked to an Arduino microcontroller connected to a laptop through a USB port for data acquisition and analysis. This instrument was easy to assemble and enabled students to better grasp the meaning of tensile testing while promoting experimentation with electronics, computer programming and mechanical design. Due to its low cost and ease of use, this Arduino-based uniaxial tensile tester can be an ideal device to introduce the concepts of mechanical properties, among other concepts, to students in numerous fields.

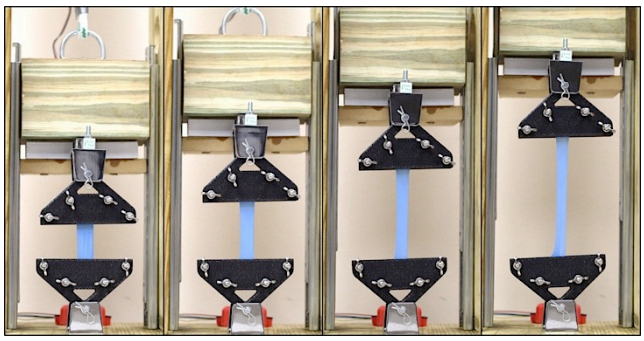

Figure 22: Example of a nitrile glove being tested and stretched in the Arduino-based mechanical tester.

Introduction

The mechanical properties of a material relate to how it responds to mechanical stress. These properties are critical in determining a material's suitability for potential applications. Uniaxial tensile testing is the most common procedure used to measure these mechanical properties, which include the Young's modulus, yield strength, and ultimate tensile strength, among others. Commercial tensile testers are highly accurate but their cost and size make them impractical for hands-on-learning in a classroom setting.[253] Furthermore, they often require costly proprietary software to operate with restrictive software licensing agreements. Recently, open-source electronics have been used to build hardware/software systems that are yet not commercially available or otherwise too expensive.[254] Among them, the popular Arduino microcontroller has already proven effective in controlling scientific hardware for research purposes[255–259] while also serving as a practical platform for the training of students.[260,261] Previous educational applications of the Arduino platform include the fabrication of a photometer[262], an automatic titrator[263], a pH meter[264], a gas sensor[265], an electronic

buret[266], and a potentiostat.[267] Our objective was to develop an inexpensive and portable mechanical tester that could be used for both accurate measuring and educational purposes. Due to its flexibility, low cost, ease-of-use, and wide range of successful applications, we decided to use an Arduino microcontroller to develop our tester, combining it with simple off-the-shelf components.

Materials and Methods

The mechanical tester consists of a wooden frame with a central loading apparatus attached via drawer slides to allow for uniaxial translation, provided by a rope and pulley system (via manual application of force to the rope by the user). The central loading apparatus consists of a wooden block with a rope attachment point on top with a mounting bracket for the load cell on the bottom. Sample holding clamps with symmetric interlocking teeth were designed and 3D printed (STL file available in the supporting information). The clamps were attached to both the frame and the load cell via mounting brackets with clevis pins as shown in Figure 23.

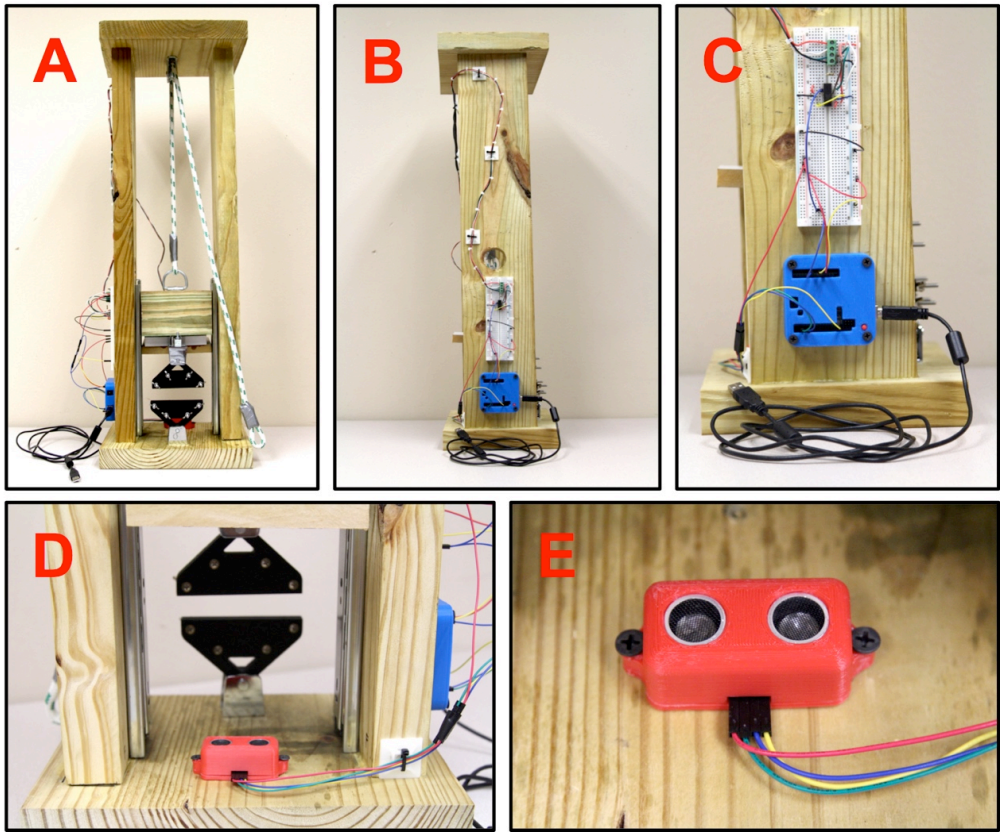

Figure 23: Several different views of the mechanical tester. The front view, A, shows the overall assembly of the tester comprising a wooden frame, a rope-and-pulley system, a central loading apparatus with attached load cell, two sample clamps (black), and the electronics (left). The side views, B and C, reveal the circuitry consisting of a bread board (white), an Arduino Uno (in blue case), and the USB interface for connection to a computer. The back views, D and E, reveal the placement and design of the ultrasonic proximity sensor (in red case), with attached leads. More detail on the circuitry can be seen in Figure 24. More information on the materials is present in the supporting information.

In order to determine the mechanical properties of a sample, two parameters need to be recorded: the load applied to the sample and its extension. In order to measure the load, a 5 kg micro load cell (combined with an INA125P amplifier) was placed in series with the sample (prior to sample runs the load cell circuit was calibrated via a linear 2-point calibration spanning the sampling range). The extension was measured with an HC-SR04 ultrasonic sensor that measured the distance between the frame and the central

loading apparatus to which the load cell (and upper sample clamp) were attached. This sensor works by emitting an ultrasonic pulse which reflects off of the central loading apparatus and is subsequently read by the sensor; the time interval between the signal emission and detection is used to calculate the distance. Both sensors were connected to the Arduino Uno microcontroller as shown in Figure 24.

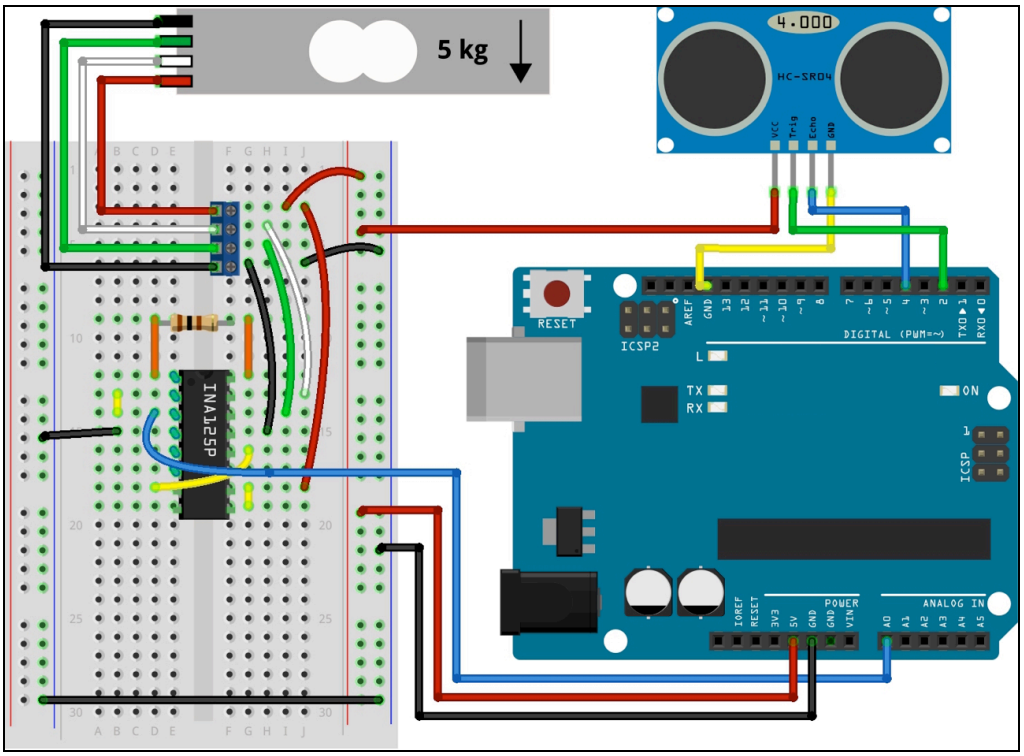

Figure 24: The wiring configuration for the 5 kg load cell (gray, top, silver bracket in Figure 22) and the ultrasonic proximity sensor (blue, top, depicted within red enclosure in Figure 22) connected to the Arduino Uno microcontroller (blue, bottom-right, blue enclosure in Figure 22). A breadboard was used to connect these components with the addition of a 100 Ω resistor and an INA125P signal amplification chip. More information on the wiring is available in the supporting information. Created with Fritzing 0.9.3b.

The Arduino Uno was connected via a USB interface to a laptop running the Arduino Integrated Development Environment (IDE). Values were recorded every 100 ms during a sample run and subsequently exported to Microsoft Excel for processing.

Results and Discussion

The total material cost to build this mechanical tester was under $100 (bill of materials available in the supporting information). This apparatus was lightweight and compact, rendering it readily portable. The inexpensive, off-the-shelf load cell and ultrasonic sensor resulted in accurate and precise measurements. The resulting mechanical properties determined with our Arduino-based mechanical tester were comparable to those obtained with a commercial United SSTM-2 tensile tester as shown in Figure 25 and Table 2.

A stress-strain curve represents the behavior of a material during mechanical testing. Stress is defined as the force applied divided by the area. For a tensile test, the relevant area is that perpendicular to the applied force (in this case the cross-sectional area). Strain describes the elongation with respect to the initial length of the sample. The ultimate tensile strength represents the maximum stress that a material can withstand before breaking. The Young's modulus or elastic modulus of a material is defined as the slope of its stress-strain curve in the region of elastic deformation. Representative stress-strain curves for latex glove samples obtained from both the Arduino-based mechanical tester and the commercial uniaxial tensile tester (United Smart Table SSTM-2, Flint, MI) are provided in Figure 25 as a means of comparison between the two systems.

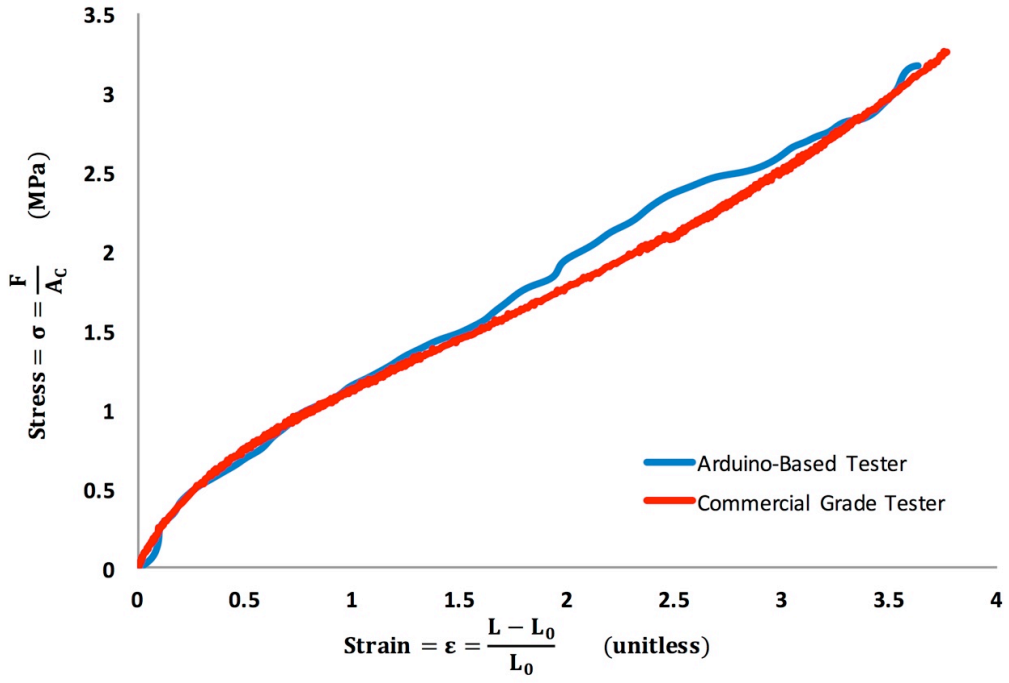

Figure 25: A side-by-side comparison of the Arduino-based tester developed herein (blue curve) and the commercial grade tester (red curve; UNITED SSTM-2) for samples cut from a latex glove. Stress (on the ordinate axis) is the force F (as measured by the load cell) divided by the cross-sectional area A_c of the sample (calculated as the thickness of the sample times its width); strain (on the abscissa) is the amount of elongation with respect to the original length L_0 of the sample. From this graph the Ultimate Tensile Strength (UTS) is the maximum stress obtained prior to failure, and the Young's Modulus is calculated by fitting a straight line to the initial part of the tensile curve (tangent modulus determined in the linear elastic region).

Several household and common laboratory items were used as samples for mechanical testing. Each sample was stretched until failure, and the resulting Young's modulus and ultimate tensile strength values are reported in Table 2. Samples were selected such that they would provide qualitative feedback for students during a sample run; this was accomplished by selecting samples with high strain rates at failure (so the student could witness a large degree of stretching) and fairly high, though obtainable, ultimate tensile strengths (so the student could feel the increasing force required to continue stretching

the sample until failure). All the samples tested were prepared with the same dimensions so that the geometry of the sample did not influence the result of the analysis.

Sample[a]	Thickness[b]	Young's Modulus[c]		Ultimate Tensile Strength[c]	
		Arduino	Commercial	Arduino	Commercial
Latex Glove	110 µm	730 ± 10 kPa	740 ± 10 kPa	3.2 ± 0.1 MPa	3.3 ± 0.1 MPa
Nitrile Glove	70 µm	2.3 ± 0.3 MPa	2.4 ± 0.2 MPa	4.4 ± 0.1 MPa	4.4 ± 0.1 MPa
Parafilm	130 µm	52 ± 5 MPa	57 ± 7 MPa	2.4 ± 0.2 MPa	2.4 ± 0.1 MPa
Biohazard Bag	70 µm	133 ± 6 MPa	135 ± 5 MPa	11.8 ± 0.1 MPa	11.6 ± 0.1 MPa
Trash Bag	40 µm	55 ± 4 MPa	52 ± 3 MPa	8.4 ± 0.1 MPa	8.2 ± 0.2 MPa
Gauze	300 µm	1.2 ± 0.1 MPa	1.4 ± 0.2 MPa	5.9 ± 0.3 MPa	6.1 ± 0.2 MPa

[a]All samples were cut to 20x65 mm rectangles, clamped such that ~30 mm of sample was available for testing (i.e. between the clamps). As is evident, the Arduino-based tester values are in excellent agreement with those for the commercial grade tester. Furthermore, the error in each value is quite low due to the commercial production (and regulation) of each of the materials tested.
[b]Material thickness was measured with a digital caliper.
[c](n=3 for each; values presented as mean ± SD).

Table 2: Mechanical property value comparison for tested samples.

Mechanical testing allowed us to illustrate the differences among mechanical behaviors. After applying some stress to them, nitrile and latex gloves return to their initial dimensions thereby characterizing their deformation as elastic, reversible and non-permanent. For the trash and biohazard bags, however, there was observed a permanent and irreversible plastic deformation. Being able to characterize such deformations distinctly demonstrates the wide applicability of this device to a broad range of materials, and thus a wide range of fields and disciplines.[253,268]

We believe that this mechanical tester is an ideal tool for project-based learning. We tested six different materials in order to determine the differences among them, and validate the device. Many different samples could be tested by students, and their resulting values could be compared with reference values reported in this or other sources (of special interest could be the comparison of material properties with standard specifications such as ISO and ANSI). Students could also be asked to produce a composite material and try to match some target mechanical properties by altering its layers and composition. Having students replicate tests of the same type of sample could also be used as an introduction to some basic statistics concepts.

Furthermore, building this mechanical tester could be defined as a group project for upper-division undergraduate students. The Arduino IDE is downloadable for free online, and the Arduino programming language is simple and intuitive. Other resources are available to automate and visualize the process of data collection, such as the Excel spreadsheet PLX-DAQ .[269] Implementation of such open-source electronics in a curriculum has been shown to develop complementary skills for the students as well as bringing an extra element of interactively engaging students.[270,271]

This mechanical tester could easily be modified for a variety of different tests. The 5kg micro load cell could be replaced to adjust the reading range of the device (from 0.5 kg to 20+ kg) in order to better accommodate various samples. Standards weights or a bucket progressively filled with water would allow to control more precisely the force

applied to the sample. A stepper motor could be used instead of the rope and pulley mechanism, in order to provide a constant strain rate (though this would increase the cost of the device). Finally, this mechanical tester could also be modified for compression testing instead of stretching.

One final advantage of this device is that all the parts and sensors used could easily be reused for other projects. The Arduino microcontroller has already been used for different applications as described earlier. It is possible to imagine that the same Arduino microcontroller could be used for several active learning class activities throughout a semester.

Conclusion

We described the fabrication of an easy-to-use uniaxial tensile tester for a total cost of less than $100. The simplicity and flexibility of the Arduino platform suggests that this is a practical, accurate system for hands-on demonstrations for the determination of the mechanical properties of several different materials. The experiments detailed herein, which can be applied to a wide variety of disciplines, were performed with household and common laboratory items as samples. These revealed the accuracy of the system (as compared with an industrial mechanical tester) and allowed for reliable determination of material properties. Though not intended as a replacement for truly quantitative experimentation, this device serves as an ideal platform for hands-on learning as its construction and use encompasses several disciplines and it lends itself to numerous potential modifications for expansion to further applications.

Chapter 6: Conclusions and Future Directions

The hAM is a readily available and inexpensive biomaterial that can efficiently be processed, preserved, and de-epithelialized. Decellularized hAM has proven worthwhile for a broad range of tissue engineering applications due to its ability to support cell attachment, proliferation, and differentiation. Modifications of the hAM have been developed to tune its properties, either through composite materials incorporating the hAM, chemical crosslinking, or innovative layering and tissue preparation strategies. Overall, the hAM is truly a versatile biomaterial and its foreseeable future as a scaffold for tissue engineering applications looks very promising. The development of standard processing protocols and tissue banks, along with commercially available hAM derived products, will further expand the clinical applications of the hAM.

In Chapter 3 was reported the successful application of riboflavin-UVA crosslinking to the hAM. Tissue samples exposed to riboflavin-UVA benefited from a 2.5-fold increase in mechanical properties and a decreased biodegradation rate while only incurring a minor decrease in glucose permeability. Moreover, riboflavin-UVA crosslinked amniotic membranes successfully supported the growth and differentiation of human adipose-derived stem cells. Together these findings suggest that riboflavin-UVA crosslinking can be used to overcome the limitations of the hAM and broaden its use to new tissue engineering applications. While our results characterize the properties of and demonstrate the potential of riboflavin-UVA crosslinked hAM, we have not yet tested

this novel material for use in a particular regenerative medicine application. Each specific application will have a unique set of requirements, both chemical and physical that must be carefully assessed. Thanks to its enhanced mechanical properties and biodegradation rate, riboflavin-UVA crosslinked hAM would be a prime candidate for blood vessel tissue engineering, cartilage regeneration, urothelium tissue engineering, and tendon repair.

Chapter 4 summarized the current findings about the isolation of porcine adipose-derived stem cells (pASCs), their culture, proliferation, and immunophenotype. The differentiation abilities of pASCs and their applications in porcine preclinical models was also reported. pASCs express cell surface markers characteristic of mesenchymal stem cells and are able to differentiate into several lineages. Knowledge about the possible transdifferentiation abilities of pASCs is currently limited but will expand in the foreseeable future. The development of standard protocols for the isolation, culture and differentiation of pASCs would further improve pASC-based preclinical studies.

In Chapter 5 was described the fabrication of an easy-to-use uniaxial tensile tester for a total cost of less than $100. The simplicity and flexibility of the Arduino platform suggests that this is a practical, accurate system for hands-on demonstrations for the determination of the mechanical properties of several different materials. The experiments detailed herein, which can be applied to a wide variety of disciplines, were performed with household and common laboratory items as samples. These revealed the accuracy of the system (as compared with an industrial mechanical tester) and allowed

for reliable determination of material properties. Though not intended as a replacement for truly quantitative experimentation, this device serves as an ideal platform for hands-on learning as its construction and use encompasses several disciplines and it lends itself to numerous potential modifications for expansion to further applications.

References

1. Bourne, G. L. The microscopic anatomy of the human amnion and chorion. *Am. J. Obstet. Gynecol.* **79,** 1070–1073 (1960).

2. Danforth, D. N. & Hull, R. W. The microscopic anatomy of the fetal membranes with particular reference to the detailed structure of the amnion. *Am. J. Obstet. Gynecol.* **75,** 536–550 (1958).

3. Parry, S. & Strauss, J. F. Premature rupture of the fetal membranes. *N. Engl. J. Med.* **338,** 663–670 (1998).

4. Malak, T. M. *et al.* Confocal immunofluorescence localization of collagen types I, III, IV, V and VI and their ultrastructural organization in term human fetal membranes. *Placenta* **14,** 385–406 (1993).

5. Uchide, N., Ohyama, K., Bessho, T., Takeichi, M. & Toyoda, H. Possible Roles of Proinflammatory and Chemoattractive Cytokines Produced by Human Fetal Membrane Cells in the Pathology of Adverse Pregnancy Outcomes Associated with Influenza Virus Infection. *Mediators of Inflammation* (2012). doi:10.1155/2012/270670

6. Takashima, S. *et al.* Characterization of laminin isoforms in human amnion. *Tissue Cell* **40,** 75–81 (2008).

7. Niknejad, H. *et al.* Properties of the amniotic membrane for potential use in tissue engineering. *Eur Cells Mater* **15,** 88–99 (2008).

8. Hortensius, R. A. & Harley, B. A. Naturally derived biomaterials for addressing inflammation in tissue regeneration. *Exp. Biol. Med.* **241,** 1015 (2016).

9. Inge, E., Talmi, Y. P., Sigler, L., Finkelstein, Y. & Zohar, Y. Antibacterial

properties of human amniotic membranes. *Placenta* **12,** 285–288 (1991).

10. Hao, Y., Ma, D. H.-K., Hwang, D. G., Kim, W.-S. & Zhang, F. Identification of antiangiogenic and antiinflammatory proteins in human amniotic membrane. *Cornea* **19,** 348–352 (2000).

11. Roux, S. *et al.* In Vitro Characterization of Patches of Human Mesenchymal Stromal Cells. *Tissue Eng. Part A* **21,** 417–425 (2015).

12. Toda, A., Okabe, M., Yoshida, T. & Nikaido, T. The Potential of Amniotic Membrane/Amnion-Derived Cells for Regeneration of Various Tissues. *J. Pharmacol. Sci.* **105,** 215–228 (2007).

13. Parolini, O. *et al.* Concise Review: Isolation and Characterization of Cells from Human Term Placenta: Outcome of the First International Workshop on Placenta Derived Stem Cells. *Stem Cells* **26,** 300–311 (2008).

14. Díaz-Prado, S. *et al.* Human amniotic membrane as an alternative source of stem cells for regenerative medicine. *Differentiation* **81,** 162–171 (2011).

15. Díaz-Prado, S. *et al.* Isolation and Characterization of Mesenchymal Stem Cells from Human Amniotic Membrane. *Tissue Eng. Part C Methods* **17,** 49–59 (2010).

16. Niknejad, H., Deihim, T., Peirovi, H. & Abolghasemi, H. Serum-free cryopreservation of human amniotic epithelial cells before and after isolation from their natural scaffold. *Cryobiology* **67,** 56–63 (2013).

17. Parolini, O., Soncini, M., Evangelista, M. & Schmidt, D. Amniotic membrane and amniotic fluid-derived cells: potential tools for regenerative medicine? *Regen. Med.* **4,** 275–291 (2009).

18. Díaz-Prado, S. *et al.* Multilineage differentiation potential of cells isolated from

the human amniotic membrane. *J. Cell. Biochem.* **111,** 846–857 (2010).

19. Nagata, S. *et al.* Efficient reprogramming of human and mouse primary extra-embryonic cells to pluripotent stem cells. *Genes Cells* **14,** 1395–1404 (2009).

20. Cai, J. *et al.* Generation of Human Induced Pluripotent Stem Cells from Umbilical Cord Matrix and Amniotic Membrane Mesenchymal Cells. *J. Biol. Chem.* **285,** 11227–11234 (2010).

21. Zhao, H. *et al.* Rapid and efficient reprogramming of human amnion-derived cells into pluripotency by three factors OCT4/SOX2/NANOG. *Differentiation* **80,** 123–129 (2010).

22. Chen, M. *et al.* A modular approach to the engineering of a centimeter-sized bone tissue construct with human amniotic mesenchymal stem cells-laden microcarriers. *Biomaterials* **32,** 7532–7542 (2011).

23. Datta, S. *et al.* Oleoyl-Chitosan-Based Nanofiber Mats Impregnated with Amniotic Membrane Derived Stem Cells for Accelerated Full-Thickness Excisional Wound Healing. *ACS Biomater. Sci. Eng.* **3,** 1738–1749 (2017).

24. Muiños-López, E. *et al.* Human Amniotic Mesenchymal Stromal Cells as Favorable Source for Cartilage Repair. *Tissue Eng. Part A* **23,** 901–912 (2017).

25. Parolini, O. *et al.* Therapeutic Effect of Human Amniotic Membrane–Derived Cells on Experimental Arthritis and Other Inflammatory Disorders. *Arthritis Rheumatol.* **66,** 327–339 (2014).

26. Miki, T. Amnion-derived stem cells: in quest of clinical applications. *Stem Cell Res. Ther.* **2,** 25 (2011).

27. Mamede, A. C. *et al.* Amniotic membrane: from structure and functions to

clinical applications. *Cell Tissue Res.* **349,** 447–458 (2012).

28. Insausti, C. L., Blanquer, M., García-Hernández, A. M., Castellanos, G. & Moraleda, J. M. Amniotic membrane-derived stem cells: immunomodulatory properties and potential clinical application. *Stem Cells Cloning Adv. Appl.* **7,** 53–63 (2014).

29. Lim, R. Concise Review: Fetal Membranes in Regenerative Medicine: New Tricks from an Old Dog? *STEM CELLS Transl. Med.* **6,** 1767–1776 (2017).

30. Davis, J. W. Skin transplantation with a review of 550 cases at the Johns Hopkins Hospital. *Johns Hopkins Med J* **15,** 307 (1910).

31. Trelford, J. D. & Trelford-Sauder, M. The amnion in surgery, past and present. *Am. J. Obstet. Gynecol.* **134,** 833–845 (1979).

32. Dua, H. S., Gomes, J. A. ., King, A. J. & Maharajan, V. S. The amniotic membrane in ophthalmology. *Surv. Ophthalmol.* **49,** 51–77 (2004).

33. de Rotth, A. Plastic repair of conjunctival defects with fetal membranes. *Arch. Ophthalmol.* **23,** 522–525 (1940).

34. Sorsby, A. & Symons, H. Amniotic Membrane Grafts in Caustic Burns of the Eye - Burns of the 2nd Degree. *Br. J. Ophthalmol.* **30,** 337–345 (1946).

35. Sorsby, A., Haythorne, J. & Reed, H. Further Experience with Amniotic Membrane Grafts in Caustic Burns of the Eye. *Br. J. Ophthalmol.* **31,** 409–418 (1947).

36. Kim, J. C. & Tseng, S. C. Transplantation of preserved human amniotic membrane for surface reconstruction in severely damaged rabbit corneas. *Cornea* **14,** 473–484 (1995).

37. Silini, A. R., Cargnoni, A., Magatti, M., Pianta, S. & Parolini, O. The Long Path of Human Placenta, and Its Derivatives, in Regenerative Medicine. *Front. Bioeng.*

Biotechnol. **3,** (2015).

38. Tseng, S. C. G. *et al.* How Does Amniotic Membrane Work? *Ocul. Surf.* **2,** 177–187 (2004).

39. Mohammad, J., Shenaq, J., Rabinovsky, E. & Shenaq, S. Modulation of peripheral nerve regeneration: a tissue-engineering approach. The role of amnion tube nerve conduit across a 1-centimeter nerve gap. *Plast. Reconstr. Surg.* **105,** 660–666 (2000).

40. Kim, S. S. *et al.* Use of human amniotic membrane wrap in reducing perineural adhesions in a rabbit model of ulnar nerve neurorrhaphy. *J. Hand Surg. Eur. Vol.* **35,** 214–219 (2010).

41. Meng, H., Li, M., You, F., Du, J. & Luo, Z. Assessment of processed human amniotic membrane as a protective barrier in rat model of sciatic nerve injury. *Neurosci. Lett.* **496,** 48–53 (2011).

42. Kesting, M. R., Wolff, K.-D., Nobis, C. P. & Rohleder, N. H. Amniotic membrane in oral and maxillofacial surgery. *Oral Maxillofac. Surg.* **18,** 153–164 (2014).

43. Demirkan, F., Colakoglu, N., Herek, O. & Erkula, G. The use of amniotic membrane in flexor tendon repair: an experimental model. *Arch. Orthop. Trauma Surg.* **122,** 396–399 (2002).

44. Jirsova, K. & Jones, G. L. A. Amniotic membrane in ophthalmology: properties, preparation, storage and indications for grafting—a review. *Cell Tissue Bank.* **18,** 193–204 (2017).

45. Lee, P.-H. *et al.* A prototype tissue engineered blood vessel using amniotic

membrane as scaffold. *Acta Biomater.* **8,** 3342–3348 (2012).

46. Keeley, R., Topoluk, N. & Mercuri, J. Tissues Reborn: Fetal Membrane-Derived Matrices and Stem Cells in Orthopedic Regenerative Medicine. *Crit. Rev. Biomed. Eng.* **42,** 249–270 (2014).

47. Jerman, U. D., Veranič, P. & Kreft, M. E. Amniotic Membrane Scaffolds Enable the Development of Tissue-Engineered Urothelium with Molecular and Ultrastructural Properties Comparable to that of Native Urothelium. *Tissue Eng. Part C Methods* **20,** 317–327 (2014).

48. Riau, A. K., Beuerman, R. W., Lim, L. S. & Mehta, J. S. Preservation, sterilization and de-epithelialization of human amniotic membrane for use in ocular surface reconstruction. *Biomaterials* **31,** 216–225 (2010).

49. Tehrani, F. A., Ahmadiani, A. & Niknejad, H. The effects of preservation procedures on antibacterial property of amniotic membrane. *Cryobiology* **67,** 293–298 (2013).

50. Jin, C. Z. *et al.* Human Amniotic Membrane as a Delivery Matrix for Articular Cartilage Repair. *Tissue Eng.* **13,** 693–702 (2007).

51. Nakamura, T. *et al.* The use of trehalose-treated freeze-dried amniotic membrane for ocular surface reconstruction. *Biomaterials* **29,** 3729–3737 (2008).

52. Gilbert, T. W., Sellaro, T. L. & Badylak, S. F. Decellularization of tissues and organs. *Biomaterials* **27,** 3675–3683 (2006).

53. Keane, T. J., Swinehart, I. T. & Badylak, S. F. Methods of tissue decellularization used for preparation of biologic scaffolds and in vivo relevance. *Methods* **84,** 25–34 (2015).

54. Crapo, P. M., Gilbert, T. W. & Badylak, S. F. An overview of tissue and whole organ decellularization processes. *Biomaterials* **32,** 3233–3243 (2011).

55. Hopkinson, A. *et al.* Optimization of Amniotic Membrane (AM) Denuding for Tissue Engineering. *Tissue Eng. Part C Methods* **14,** 371–381 (2008).

56. Saghizadeh, M. *et al.* A Simple Alkaline Method for Decellularizing Human Amniotic Membrane for Cell Culture. *PLoS ONE* **8,** e79632 (2013).

57. Wilshaw, S.-P., Kearney, J. N., Fisher, J. & Ingham, E. Production of an Acellular Amniotic Membrane Matrix for Use in Tissue Engineering. *Tissue Eng.* **12,** 2117–2129 (2006).

58. Figueiredo, G. S. *et al.* Gamma-irradiated human amniotic membrane decellularised with sodium dodecyl sulfate is a more efficient substrate for the ex vivo expansion of limbal stem cells. *Acta Biomater.* **61,** 124–133 (2017).

59. Wehmeyer, J. L., Natesan, S. & Christy, R. J. Development of a Sterile Amniotic Membrane Tissue Graft Using Supercritical Carbon Dioxide. *Tissue Eng. Part C Methods* **21,** 649–659 (2015).

60. Gindraux, F. *et al.* Human amniotic membrane: clinical uses, patents and marketed products. *Recent Pat. Regen. Med.* **3,** 193–214 (2013).

61. Spoerl, E., Wollensak, G., Reber, F. & Pillunat, L. Cross-linking of human amniotic membrane by glutaraldehyde. *Ophthalmic Res.* **36,** 71–77 (2004).

62. Ma, D. H.-K., Lai, J.-Y., Cheng, H.-Y., Tsai, C.-C. & Yeh, L.-K. Carbodiimide cross-linked amniotic membranes for cultivation of limbal epithelial cells. *Biomaterials* **31,** 6647–6658 (2010).

63. Chau, D. Y. S. *et al.* Tissue transglutaminase (TG-2) modified amniotic

membrane: a novel scaffold for biomedical applications. *Biomed. Mater.* **7,** 045011 (2012).

64. Tanaka, Y. *et al.* Optical mechanical refinement of human amniotic membrane by dehydration and cross-linking. *J. Tissue Eng. Regen. Med.* **6,** 731–737 (2012).

65. Huang, G. *et al.* Accelerated Expansion of Epidermal Keratinocyte and Improved Dermal Reconstruction Achieved by Engineered Amniotic Membrane. *Cell Transplant.* **22,** 1831–1844 (2013).

66. Lai, J.-Y. Photo-cross-linking of amniotic membranes for limbal epithelial cell cultivation. *Mater. Sci. Eng. C* **45,** 313–319 (2014).

67. Ma, D. H.-K. *et al.* Preservation of human limbal epithelial progenitor cells on carbodiimide cross-linked amniotic membrane via integrin-linked kinase-mediated Wnt activation. *Acta Biomater.* **31,** 144–155 (2016).

68. Hariya, T., Tanaka, Y., Yokokura, S. & Nakazawa, T. Transparent, resilient human amniotic membrane laminates for corneal transplantation. *Biomaterials* **101,** 76–85 (2016).

69. Nogami, M. *et al.* A Human Amnion-Derived Extracellular Matrix-Coated Cell-Free Scaffold for Cartilage Repair: In Vitro and In Vivo Studies. *Tissue Eng. Part A* **22,** 680–688 (2016).

70. Amensag, S. *et al.* Pilot assessment of a human extracellular matrix-based vascular graft in a rabbit model. *J. Vasc. Surg.* (2016). doi:10.1016/j.jvs.2016.02.046

71. Hortensius, R. A., Ebens, J. H. & Harley, B. A. C. Immunomodulatory effects of amniotic membrane matrix incorporated into collagen scaffolds. *J. Biomed. Mater. Res. A* **104,** 1332–1342 (2016).

72. Adamowicz, J. *et al.* New Amniotic Membrane Based Biocomposite for Future Application in Reconstructive Urology. *PLOS ONE* **11,** e0146012 (2016).

73. Allen, A. B., Priddy, L. B., Li, M.-T. A. & Guldberg, R. E. Functional Augmentation of Naturally-Derived Materials for Tissue Regeneration. *Ann. Biomed. Eng.* **43,** 555–567 (2015).

74. Gholipourmalekabadi, M. *et al.* Silk fibroin/amniotic membrane 3D bi-layered artificial skin. *Biomed. Mater.* (2017). doi:10.1088/1748-605X/aa999b

75. Shi, P. *et al.* Biocompatible surgical meshes based on decellularized human amniotic membrane. *Mater. Sci. Eng. C* **54,** 112–119 (2015).

76. Brennan, J. A., Arrizabalaga, J. H. & Nollert, M. U. Development of a Small Diameter Vascular Graft Using the Human Amniotic Membrane. *Cardiovasc. Eng. Technol.* **5,** 96–109 (2014).

77. Amensag, S. & McFetridge, P. S. Rolling the Human Amnion to Engineer Laminated Vascular Tissues. *Tissue Eng. Part C Methods* **18,** 903–912 (2012).

78. Kesting, M. R. *et al.* A bioartificial surgical patch from multilayered human amniotic membrane—In vivo investigations in a rat model. *J. Biomed. Mater. Res. B Appl. Biomater.* **90B,** 930–938 (2009).

79. Prabhasawat, P., Tesavibul, N. & Komolsuradej, W. Single and multilayer amniotic membrane transplantation for persistent corneal epithelial defect with and without stromal thinning and perforation. *Br. J. Ophthalmol.* **85,** 1455–1463 (2001).

80. Sridhar, M. S., Bansal, A. K. & Rao, G. N. Multilayered amniotic membrane transplantation for partial thickness scleral thinning following pterygium surgery. *Eye* **16,** 639–642 (2002).

81. Kesting, M. R. *et al.* Repair of oronasal fistulas with human amniotic membrane in minipigs. *Br. J. Oral Maxillofac. Surg.* **48,** 131–135 (2010).

82. Rohleder, N. H. *et al.* Repair of Oronasal Fistulae by Interposition of Multilayered Amniotic Membrane Allograft. *Plast. Reconstr. Surg.* **132,** 172–181 (2013).

83. Ji, S. *et al.* An epidermal stem cells niche microenvironment created by engineered human amniotic membrane. *Biomaterials* **32,** 7801–7811 (2011).

84. Murphy, S. V. *et al.* Solubilized Amnion Membrane Hyaluronic Acid Hydrogel Accelerates Full-Thickness Wound Healing. *STEM CELLS Transl. Med.* **6,** 2020–2032 (2017).

85. Fukuda, K., Chikama, T., Nakamura, M. & Nishida, T. Differential distribution of subchains of the basement membrane components type IV collagen and laminin among the amniotic membrane, cornea, and conjunctiva. *Cornea* **18,** 73–79 (1999).

86. Rahman, I., Said, D. G., Maharajan, V. S. & Dua, H. S. Amniotic membrane in ophthalmology: indications and limitations. *Eye* **23,** 1954–1961 (2009).

87. Malhotra, C. & Jain, A. K. Human amniotic membrane transplantation: Different modalities of its use in ophthalmology. *World J. Transplant.* **4,** 111–121 (2014).

88. John, T., Foulks, G. N., John, M. E., Cheng, K. & Hu, D. Amniotic membrane in the surgical management of acute toxic epidermal necrolysis. *Ophthalmology* **109,** 351–360 (2002).

89. Hsu, M., Jayaram, A., Verner, R., Lin, A. & Bouchard, C. Indications and Outcomes of Amniotic Membrane Transplantation in the Management of Acute

Stevens–johnson Syndrome and Toxic Epidermal Necrolysis: A Case–control Study. *Cornea* **31,** 1394–1402 (2012).

90. Schwab, I. R., Reyes, M. & Isseroff, R. R. Successful transplantation of bioengineered tissue replacements in patients with ocular surface disease. *Cornea* **19,** 421–426 (2000).

91. Tsai, R. J., Li, L. M. & Chen, J. K. Reconstruction of damaged corneas by transplantation of autologous limbal epithelial cells. *N. Engl. J. Med.* **343,** 86–93 (2000).

92. Koizumi, N., Inatomi, T., Suzuki, T., Sotozono, C. & Kinoshita, S. Cultivated corneal epithelial stem cell transplantation in ocular surface disorders. *Ophthalmology* **108,** 1569–1574 (2001).

93. Ahmad, S. Concise Review: Limbal Stem Cell Deficiency, Dysfunction, and Distress. *Stem Cells Transl. Med.* **1,** 110–115 (2012).

94. Nakamura, T. *et al.* Transplantation of cultivated autologous oral mucosal epithelial cells in patients with severe ocular surface disorders. *Br. J. Ophthalmol.* **88,** 1280–1284 (2004).

95. Nishida, K. *et al.* Corneal Reconstruction with Tissue-Engineered Cell Sheets Composed of Autologous Oral Mucosal Epithelium. *N. Engl. J. Med.* **351,** 1187–1196 (2004).

96. Ma, Y. *et al.* Reconstruction of Chemically Burned Rat Corneal Surface by Bone Marrow–Derived Human Mesenchymal Stem Cells. *STEM CELLS* **24,** 315–321 (2006).

97. Rohaina, C. M. *et al.* Reconstruction of limbal stem cell deficient corneal

surface with induced human bone marrow mesenchymal stem cells on amniotic membrane. *Transl. Res.* **163,** 200–210 (2014).

98. Fernandes, M., Sridhar, M. S., Sangwan, V. S. & Rao, G. N. Amniotic membrane transplantation for ocular surface reconstruction. *Cornea* **24,** 643–653 (2005).

99. Nakamura, T., Inatomi, T., Sotozono, C., Koizumi, N. & Kinoshita, S. Ocular surface reconstruction using stem cell and tissue engineering. *Prog. Retin. Eye Res.* **51,** 187–207 (2016).

100. Kotomin, I. *et al.* Sutureless fixation of amniotic membrane for therapy of ocular surface disorders. *PloS One* **10,** e0125035 (2015).

101. Duchesne, B., Tahi, H. & Galand, A. Use of Human Fibrin Glue and Amniotic Membrane Transplant in Corneal Perforation. *Cornea* **20,** 230 (2001).

102. Hick, S. *et al.* Amniotic membrane transplantation and fibrin glue in the management of corneal ulcers and perforations: a review of 33 cases. *Cornea* **24,** 369–377 (2005).

103. Takaoka, M. *et al.* Sutureless amniotic membrane transplantation for ocular surface reconstruction with a chemically defined bioadhesive. *Biomaterials* **29,** 2923–2931 (2008).

104. Takaoka, M. *et al.* Novel sutureless keratoplasty with a chemically defined bioadhesive. *Invest. Ophthalmol. Vis. Sci.* **50,** 2679–2685 (2009).

105. Verter, E. E. *et al.* Light-Initiated Bonding of Amniotic Membrane to Cornea. *Invest. Ophthalmol. Vis. Sci.* **52,** 9470–9477 (2011).

106. Soeken, T. A. *et al.* Sealing of Corneal Lacerations Using Photoactivated Rose

Bengal Dye and Amniotic Membrane. *Cornea* (2017). doi:10.1097/ICO.0000000000001389

107. Sheha, H., Liang, L., Li, J. & Tseng, S. C. G. Sutureless Amniotic Membrane Transplantation for Severe Bacterial Keratitis. *Cornea* **28,** 1118–1123 (2009).

108. Kesting, M. R., Wolff, K.-D., Hohlweg-Majert, B. & Steinstraesser, L. The Role of Allogenic Amniotic Membrane in Burn Treatment. *J. Burn Care Res.* **29,** 907–916 (2008).

109. Lo, V. & Pope, E. Amniotic membrane use in dermatology. *Int. J. Dermatol.* **48,** 935–940 (2009).

110. Fairbairn, N. G., Randolph, M. A. & Redmond, R. W. The clinical applications of human amnion in plastic surgery. *J. Plast. Reconstr. Aesthet. Surg.* **67,** 662–675 (2014).

111. Mohammadi, A. A. *et al.* Effect of fresh human amniotic membrane dressing on graft take in patients with chronic burn wounds compared with conventional methods. *Burns* **39,** 349–353 (2013).

112. Mohammadi, A. A., Johari, H. G. & Eskandari, S. Effect of amniotic membrane on graft take in extremity burns. *Burns* **39,** 1137–1141 (2013).

113. Singh, R., Kumar, A., Singh, D. & Malviya, A. Use of gamma-irradiated amniotic membrane for the healing of split skin graft donor site. *Tissue Eng. Regen. Med.* **10,** 110–114 (2013).

114. Loeffelbein, D. J. *et al.* Evaluation of Human Amniotic Membrane as a Wound Dressing for Split-Thickness Skin-Graft Donor Sites. *BioMed Research International* (2014). doi:10.1155/2014/572183

115. Lo, V., Lara-Corrales, I., Stuparich, A. & Pope, E. Amniotic membrane grafting in patients with epidermolysis bullosa with chronic wounds. *J. Am. Acad. Dermatol.* **62,** 1038–1044 (2010).

116. Serena, T. E. *et al.* A multicenter, randomized, controlled clinical trial evaluating the use of dehydrated human amnion/chorion membrane allografts and multilayer compression therapy vs. multilayer compression therapy alone in the treatment of venous leg ulcers. *Wound Repair Regen.* **22,** 688–693 (2014).

117. Song, M. *et al.* The repairing of full-thickness skin deficiency and its biological mechanism using decellularized human amniotic membrane as the wound dressing. *Mater. Sci. Eng. C* **77,** 739–747 (2017).

118. Redondo, P., Del Olmo, J., García-Guzman, M., Guembe, L. & Prósper, F. Repigmentation of vitiligo by transplantation of autologous melanocyte cells cultured on amniotic membrane. *Br. J. Dermatol.* **158,** 1168–1171 (2008).

119. Redondo, P. *et al.* Amniotic Membrane as a Scaffold for Melanocyte Transplantation in Patients with Stable Vitiligo. *Dermatol. Res. Pract.* **2011,** 1–6 (2011).

120. Yang, L. *et al.* New skin-equivalent model from de-epithelialized amnion membrane. *Cell Tissue Res.* **326,** 69–77 (2006).

121. Yang, L. *et al.* Living skin equivalents constructed using human amnions as a matrix. *J. Dermatol. Sci.* **56,** 188–195 (2009).

122. Sánchez-Sánchez, R. *et al.* Generation of Two Biological Wound Dressings as a Potential Delivery System of Human Adipose-Derived Mesenchymal Stem Cells: *ASAIO J.* **61,** 718–725 (2015).

123. Arai, N. *et al.* Clinical Application of a Hyperdry Amniotic Membrane on Surgical Defects of the Oral Mucosa. *J. Oral Maxillofac. Surg.* **70,** 2221–2228 (2012).

124. Mücke, T. *et al.* Intraoral defect coverage with prelaminated epigastric fat flaps with human amniotic membrane in rats. *J. Biomed. Mater. Res. B Appl. Biomater.* **95B,** 466–474 (2010).

125. Tuncel, U. & Ozgenel, G. Y. Use of Human Amniotic Membrane as an Interpositional Material in Treatment of Temporomandibular Joint Ankylosis. *J. Oral Maxillofac. Surg.* **69,** e58–e66 (2011).

126. Ahn, K.-M. *et al.* Fabrication of Myomucosal Flap Using Tissue-engineered Bioartificial Mucosa Constructed With Oral Keratinocytes Cultured on Amniotic Membrane. *Artif. Organs* **30,** 411–423 (2006).

127. Amemiya, T., Nakamura, T., Yamamoto, T., Kinoshita, S. & Kanamura, N. Immunohistochemical study of oral epithelial sheets cultured on amniotic membrane for oral mucosal reconstruction. *Biomed. Mater. Eng.* **20,** 37–45 (2010).

128. Amemiya, T., Nakamura, T., Yamamoto, T., Kinoshita, S. & Kanamura, N. Autologous Transplantation of Oral Mucosal Epithelial Cell Sheets Cultured on an Amniotic Membrane Substrate for Intraoral Mucosal Defects. *PLoS ONE* **10,** e0125391 (2015).

129. Hsueh, Y.-J. *et al.* Preservation of epithelial progenitor cells from collagenase-digested oral mucosa during ex vivo cultivation. *Sci. Rep.* **6,** 36266 (2016).

130. Shojaku, H. *et al.* Effect of hyperdry amniotic membrane patches attached over the bony surface of mastoid cavities in canal wall down tympanoplasty. *The Laryngoscope* **121,** 1953–1957 (2011).

131. Kanazawa, Y. *et al.* Application of hyperdry amniotic membrane patches without fibrin glue over the bony surface of mastoid cavities in canal wall down tympanoplasty. *Acta Otolaryngol. (Stockh.)* **132,** 1282–1287 (2012).

132. Zhang, L., Hu, J. & Athanasiou, K. A. The Role of Tissue Engineering in Articular Cartilage Repair and Regeneration. *Crit. Rev. Biomed. Eng.* **37,** 1–57 (2009).

133. Yan, L.-P., Oliveira, J. M., Oliveira, A. L. & Reis, R. L. Current Concepts and Challenges in Osteochondral Tissue Engineering and Regenerative Medicine. *ACS Biomater. Sci. Eng.* **1,** 183–200 (2015).

134. Díaz-Prado, S. *et al.* Potential use of the human amniotic membrane as a scaffold in human articular cartilage repair. *Cell Tissue Bank.* **11,** 183–195 (2010).

135. Krishnamurithy, G. *et al.* Human amniotic membrane as a chondrocyte carrier vehicle/substrate: In vitro study. *J. Biomed. Mater. Res. A* **99A,** 500–506 (2011).

136. Tan, S.-L. *et al.* Human amnion as a novel cell delivery vehicle for chondrogenic mesenchymal stem cells. *Cell Tissue Bank.* **12,** 59–70 (2011).

137. Garcia, D. *et al.* Amniotic Membrane Transplant for Articular Cartilage Repair: An Experimental Study in Sheep. *Curr. Stem Cell Res. Ther.* **10,** 77–83 (2015).

138. Li, W. *et al.* Investigating the Potential of Amnion-Based Scaffolds as a Barrier Membrane for Guided Bone Regeneration. *Langmuir* **31,** 8642–8653 (2015).

139. Tang, K. *et al.* Human acellular amniotic membrane: A potential osteoinductive biomaterial for bone regeneration. *J. Biomater. Appl.* 0885328217739753 (2017). doi:10.1177/0885328217739753

140. Chen, Y.-J. *et al.* The effects of acellular amniotic membrane matrix on osteogenic differentiation and ERK1/2 signaling in human dental apical papilla cells.

Biomaterials **33,** 455–463 (2012).

141. Lindenmair, A. *et al.* Osteogenic differentiation of intact human amniotic membrane. *Biomaterials* **31,** 8659–8665 (2010).

142. Wang, F. *et al.* Urethral Reconstruction with Tissue-Engineered Human Amniotic Scaffold in Rabbit Urethral Injury Models. *Med. Sci. Monit. Int. Med. J. Exp. Clin. Res.* **20,** 2430–2438 (2014).

143. Sharifiaghdas, F., Hamzehiesfahani, N., Moghadasali, R., Ghaemimanesh, F. & Baharvand, H. Human amniotic membrane as a suitable matrix for growth of mouse urothelial cells in comparison with human peritoneal and omentum membranes. *Urol. J.* **4,** 71–78 (2009).

144. Sharifiaghdas, F., Moghadasali, R., Baharvand, H., Hosseini-Moghaddam, S. M. & Mahmoudnejad, N. Special characteristics of culturing mature human bladder smooth muscle cells on human amniotic membrane as a suitable matrix. *Urol. J.* **6,** 283–288 (2009).

145. Tsai, S.-H. *et al.* Characterization of porcine arterial endothelial cells cultured on amniotic membrane, a potential matrix for vascular tissue engineering. *Biochem. Biophys. Res. Commun.* **357,** 984–990 (2007).

146. Kakavand, M., Yazdanpanah, G., Ahmadiani, A. & Niknejad, H. Blood compatibility of human amniotic membrane compared with heparin-coated ePTFE for vascular tissue engineering. *J. Tissue Eng. Regen. Med.* **11,** 1701–1709 (2017).

147. Peirovi, H., Rezvani, N., Hajinasrollah, M., Mohammadi, S. S. & Niknejad, H. Implantation of amniotic membrane as a vascular substitute in the external jugular vein of juvenile sheep. *J. Vasc. Surg.* **56,** 1098–1104 (2012).

148. Hsiao, Y.-C., Lee, H.-W., Chen, Y.-T., Young, T.-H. & Yang, T.-L. The impact of compositional topography of amniotic membrane scaffold on tissue morphogenesis of salivary gland. *Biomaterials* **32,** 4424–4432 (2011).

149. Poghosyan, T. *et al.* In Vitro Development and Characterization of a Tissue-Engineered Conduit Resembling Esophageal Wall Using Human and Pig Skeletal Myoblast, Oral Epithelial Cells, and Biologic Scaffolds. *Tissue Eng. Part A* **19,** 2242–2252 (2013).

150. Zhao, B. *et al.* The effect of a human acellular amniotic membrane loaded with mechanical stretch-stimulated bone marrow mesenchymal stem cells for the treatment of pelvic floor dysfunction. *RSC Adv.* **7,** 37086–37094 (2017).

151. Despeyroux, A. *et al.* Mesenchymal stem cells seeded on a human amniotic membrane improve liver regeneration and mouse survival after extended hepatectomy. *J. Tissue Eng. Regen. Med.* doi:10.1002/term.2607

152. Yuan, J. *et al.* Transplantation of human adipose stem cell-derived hepatocyte-like cells with restricted localization to liver using acellular amniotic membrane. *Stem Cell Res. Ther.* **6,** (2015).

153. Motamed, M. *et al.* Tissue Engineered Human Amniotic Membrane Application in Mouse Ovarian Follicular Culture. *Ann. Biomed. Eng.* **45,** 1664–1675 (2017).

154. López-Valladares, M. J. *et al.* Donor age and gestational age influence on growth factor levels in human amniotic membrane. *Acta Ophthalmol. (Copenh.)* **88,** e211–e216 (2010).

155. Hopkinson, A., McIntosh, R. S., Tighe, P. J., James, D. K. & Dua, H. S. Amniotic membrane for ocular surface reconstruction: donor variations and the effect of

handling on TGF-beta content. *Invest. Ophthalmol. Vis. Sci.* **47,** 4316–4322 (2006).

156. Connon, C. J. *et al.* The variation in transparency of amniotic membrane used in ocular surface regeneration. *Br. J. Ophthalmol.* **94,** 1057–1061 (2010).

157. Shortt, A. J. *et al.* The effect of amniotic membrane preparation method on its ability to serve as a substrate for the ex-vivo expansion of limbal epithelial cells. *Biomaterials* **30,** 1056–1065 (2009).

158. Niknejad, H., Deihim, T., Solati-Hashjin, M. & Peirovi, H. The effects of preservation procedures on amniotic membrane's ability to serve as a substrate for cultivation of endothelial cells. *Cryobiology* **63,** 145–151 (2011).

159. Zhang, T. *et al.* The Effect of Amniotic Membrane De-Epithelialization Method on its Biological Properties and Ability to Promote Limbal Epithelial Cell Culture. *Investig. Opthalmology Vis. Sci.* **54,** 3072 (2013).

160. Wolbank, S. *et al.* Impact of human amniotic membrane preparation on release of angiogenic factors. *J. Tissue Eng. Regen. Med.* **3,** 651–654 (2009).

161. Ravishanker, R., Bath, A. S. & Roy, R. "Amnion Bank"—the use of long term glycerol preserved amniotic membranes in the management of superficial and superficial partial thickness burns. *Burns* **29,** 369–374 (2003).

162. Laurent, R., Nallet, A., Obert, L., Nicod, L. & Gindraux, F. Storage and qualification of viable intact human amniotic graft and technology transfer to a tissue bank. *Cell Tissue Bank.* **15,** 267–275 (2014).

163. Marsit, N. *et al.* Substantiation of 25 kGy radiation sterilization dose for banked air dried amniotic membrane and evaluation of personnel skill in influencing finished product bioburden. *Cell Tissue Bank.* **15,** 603–611 (2014).

164. Koob, T. J., Lim, J. J., Zabek, N. & Massee, M. Cytokines in single layer amnion allografts compared to multilayer amnion/chorion allografts for wound healing. *J. Biomed. Mater. Res. B Appl. Biomater.* **103,** 1133–1140 (2015).

165. Fesli, A., Sari, A., Yilmaz, N., Comelekoglu, U. & Tasdelen, B. Enhancement of nerve healing with the combined use of amniotic membrane and granulocyte-colony-stimulating factor. *J. Plast. Reconstr. Aesthet. Surg.* **67,** 837–843 (2014).

166. Patel, V. R. *et al.* Dehydrated Human Amnion/Chorion Membrane Allograft Nerve Wrap Around the Prostatic Neurovascular Bundle Accelerates Early Return to Continence and Potency Following Robot-assisted Radical Prostatectomy: Propensity Score–matched Analysis. *Eur. Urol.* **67,** 977–980 (2015).

167. Barret, M. *et al.* Amniotic membrane grafts for the prevention of esophageal stricture after circumferential endoscopic submucosal dissection. *PloS One* **9,** e100236 (2014).

168. Yuan, J. *et al.* Transplantation of human adipose stem cell-derived hepatocyte-like cells with restricted localization to liver using acellular amniotic membrane. *Stem Cell Res. Ther.* **6,** (2015).

169. Zhao, Y. & Ma, L. Systematic review and meta-analysis on transplantation of ex vivo cultivated limbal epithelial stem cell on amniotic membrane in limbal stem cell deficiency. *Cornea* **34,** 592–600 (2015).

170. Reddy, N., Reddy, R. & Jiang, Q. Crosslinking biopolymers for biomedical applications. *Trends Biotechnol.* **33,** 362–369 (2015).

171. Delgado, L. M., Bayon, Y., Pandit, A. & Zeugolis, D. I. To Cross-Link or Not to Cross-Link? Cross-Linking Associated Foreign Body Response of Collagen-Based

Devices. *Tissue Eng. Part B Rev.* **21,** 298–313 (2015).

172. Fujisato, T. *et al.* Cross-linking of amniotic membranes. *J. Biomater. Sci. Polym. Ed.* **10,** 1171–1181 (1999).

173. Lai, J.-Y. & Ma, D. H.-K. Glutaraldehyde cross-linking of amniotic membranes affects their nanofibrous structures and limbal epithelial cell culture characteristics. *Int. J. Nanomedicine* **8,** 4157–4168 (2013).

174. Bax, D. V. *et al.* Fundamental insight into the effect of carbodiimide crosslinking on cellular recognition of collagen-based scaffolds. *Acta Biomater.* **49,** 218–234 (2017).

175. Tirella, A., Liberto, T. & Ahluwalia, A. Riboflavin and collagen: New crosslinking methods to tailor the stiffness of hydrogels. *Mater. Lett.* **74,** 58–61 (2012).

176. Beztsinna, N., Solé, M., Taib, N. & Bestel, I. Bioengineered riboflavin in nanotechnology. *Biomaterials* **80,** 121–133 (2016).

177. Ahearne, M., Yang, Y., Then, K. Y. & Liu, K.-K. Non-destructive mechanical characterisation of UVA/riboflavin crosslinked collagen hydrogels. *Br. J. Ophthalmol.* **92,** 268–271 (2008).

178. Grunert, P. *et al.* Riboflavin crosslinked high-density collagen gel for the repair of annular defects in intervertebral discs: An in vivo study. *Acta Biomater.* **26,** 215–224 (2015).

179. Ahearne, M. & Coyle, A. Application of UVA-riboflavin crosslinking to enhance the mechanical properties of extracellular matrix derived hydrogels. *J. Mech. Behav. Biomed. Mater.* **54,** 259–267 (2016).

180. Raiskup, F. & Spoerl, E. Corneal Crosslinking with Riboflavin and Ultraviolet

A. I. Principles. *Ocul. Surf.* **11,** 65–74 (2013).

181. Mastropasqua, L. Collagen cross-linking: when and how? A review of the state of the art of the technique and new perspectives. *Eye Vis.* **2,** 19 (2015).

182. Taron, A. FDA Approves CXL For Keratoconus. *Rev. Optom.* **153,** 4–4 (2016).

183. Wollensak, G., Spoerl, E. & Seiler, T. Riboflavin/ultraviolet-a-induced collagen crosslinking for the treatment of keratoconus. *Am. J. Ophthalmol.* **135,** 620–627 (2003).

184. Raiskup, F. & Spoerl, E. Corneal Crosslinking with Riboflavin and Ultraviolet A. Part II. Clinical Indications and Results. *Ocul. Surf.* **11,** 93–108 (2013).

185. Lai, J.-Y. Interrelationship between cross-linking structure, molecular stability, and cytocompatibility of amniotic membranes cross-linked with glutaraldehyde of varying concentrations. *RSC Adv.* **4,** 18871 (2014).

186. Friedman, M. Applications of the Ninhydrin Reaction for Analysis of Amino Acids, Peptides, and Proteins to Agricultural and Biomedical Sciences. *J. Agric. Food Chem.* **52,** 385–406 (2004).

187. Hartrianti, P. *et al.* Fabrication and characterization of a novel crosslinked human keratin-alginate sponge: Crosslinked keratin-alginate sponge. *J. Tissue Eng. Regen. Med.* (2016). doi:10.1002/term.2159

188. Mondalek, F. G. *et al.* The incorporation of poly(lactic-co-glycolic) acid nanoparticles into porcine small intestinal submucosa biomaterials. *Biomaterials* **29,** 1159–1166 (2008).

189. Issa, R. I., Engebretson, B., Rustom, L., McFetridge, P. S. & Sikavitsas, V. I. The Effect of Cell Seeding Density on the Cellular and Mechanical Properties of a Mechanostimulated Tissue-Engineered Tendon. *Tissue Eng. Part A* **17,** 1479–1487

(2011).

190. Truskey, G. A., Yuan, F. & Katz, D. F. *Transport Phenomena in Biological Systems*. (Pearson Prentice Hall, 2004).

191. McCall, A. S. *et al.* Mechanisms of Corneal Tissue Cross-linking in Response to Treatment with Topical Riboflavin and Long-Wavelength Ultraviolet Radiation (UVA). *Investig. Opthalmology Vis. Sci.* **51,** 129 (2010).

192. Yu, G. *et al.* Yield and characterization of subcutaneous human adipose-derived stem cells by flow cytometric and adipogenic mRNA analyzes. *Cytotherapy* **12,** 538–546 (2010).

193. De Francesco, F., Ricci, G., D'Andrea, F., Nicoletti, G. F. & Ferraro, G. A. Human Adipose Stem Cells: From Bench to Bedside. *Tissue Eng. Part B Rev.* **21,** 572–584 (2015).

194. Badylak, S. F. The extracellular matrix as a biologic scaffold material. *Biomaterials* **28,** 3587–3593 (2007).

195. Aamodt, J. M. & Grainger, D. W. Extracellular matrix-based biomaterial scaffolds and the host response. *Biomaterials* **86,** 68–82 (2016).

196. Tam, H. *et al.* A novel crosslinking method for improved tear resistance and biocompatibility of tissue based biomaterials. *Biomaterials* **66,** 83–91 (2015).

197. Murphy, W. L., McDevitt, T. C. & Engler, A. J. Materials as stem cell regulators. *Nat. Mater.* **13,** 547–557 (2014).

198. Gimbel, J. A. *et al.* Supraspinatus tendon organizational and mechanical properties in a chronic rotator cuff tear animal model. *J. Biomech.* **37,** 739–749 (2004).

199. Itoi, E. *et al.* Tensile properties of the supraspinatus tendon. *J. Orthop. Res. Off.*

Publ. Orthop. Res. Soc. **13,** 578–584 (1995).

200. De Francesco, F., Ricci, G., D'Andrea, F., Nicoletti, G. F. & Ferraro, G. A. Human Adipose Stem Cells: From Bench to Bed-Side. *Tissue Eng. Part B Rev.* **21,** 572–584 (2015).

201. Kokai, L. E., Marra, K. & Rubin, J. P. Adipose stem cells: biology and clinical applications for tissue repair and regeneration. *Transl. Res.* **163,** 399–408 (2014).

202. Feisst, V., Meidinger, S. & Locke, M. B. From bench to bedside: use of human adipose-derived stem cells. *Stem Cells Cloning Adv. Appl.* **8,** 149–162 (2015).

203. Lindroos, B., Suuronen, R. & Miettinen, S. The Potential of Adipose Stem Cells in Regenerative Medicine. *Stem Cell Rev. Rep.* **7,** 269–291 (2011).

204. Williams, K. J. *et al.* Isolation and Characterization of Porcine Adipose Tissue-Derived Adult Stem Cells. *Cells Tissues Organs* **188,** 251–258 (2008).

205. Chen, Y.-J. *et al.* Isolation and Differentiation of Adipose-Derived Stem Cells from Porcine Subcutaneous Adipose Tissues. *Jove-J. Vis. Exp.* e53886 (2016). doi:10.3791/53886

206. Rho, G. J., Kumar, B. M. & Balasubramanian, S. S. Porcine mesenchymal stem cells--current technological status and future perspective. *Front. Biosci. Landmark Ed.* **14,** 3942–3961 (2009).

207. Niada, S. *et al.* Porcine adipose-derived stem cells from buccal fat pad and subcutaneous adipose tissue for future preclinical studies in oral surgery. *Stem Cell Res. Ther.* **4,** 1–11 (2013).

208. Casado, J. G. *et al.* Comparative phenotypic and molecular characterization of porcine mesenchymal stem cells from different sources for translational studies in a

large animal model. *Vet. Immunol. Immunopathol.* **147,** 104–112 (2012).

209. Lee, A.-Y. *et al.* Comparative studies on proliferation, molecular markers and differentiation potential of mesenchymal stem cells from various tissues (adipose, bone marrow, ear skin, abdominal skin, and lung) and maintenance of multipotency during serial passages in miniature pig. *Res. Vet. Sci.* **100,** 115–124 (2015).

210. Wang, K.-H. *et al.* Optimizing proliferation and characterization of multipotent stem cells from porcine adipose tissue. *Biotechnol. Appl. Biochem.* **51,** 159–166 (2008).

211. Schwarz, C. *et al.* Effects of different media on proliferation and differentiation capacity of canine, equine and porcine adipose derived stem cells. *Res. Vet. Sci.* **93,** 457–462 (2012).

212. Perruchot, M.-H., Lefaucheur, L., Barreau, C., Casteilla, L. & Louveau, I. Age-related changes in the features of porcine adult stem cells isolated from adipose tissue and skeletal muscle. *AJP Cell Physiol.* **305,** C728–C738 (2013).

213. Ock, S.-A. *et al.* Evaluation of phenotypic, functional and molecular characteristics of porcine mesenchymal stromal/stem cells depending on donor age, gender and tissue source. *J. Vet. Med. Sci. Jpn. Soc. Vet. Sci.* **78,** 987–995 (2016).

214. Dariolli, R. *et al.* Porcine Adipose Tissue-Derived Mesenchymal Stem Cells Retain Their Proliferative Characteristics, Senescence, Karyotype and Plasticity after Long-Term Cryopreservation. *PLoS ONE* **8,** e67939 (2013).

215. Bourin, P. *et al.* Stromal cells from the adipose tissue-derived stromal vascular fraction and culture expanded adipose tissue-derived stromal/stem cells: a joint statement of the International Federation for Adipose Therapeutics and Science (IFATS) and the International Society for Cellular Therapy (ISCT). *Cytotherapy* **15,**

641–648 (2013).

216. Brückner, S. *et al.* A fat option for the pig: Hepatocytic differentiated mesenchymal stem cells for translational research. *Exp. Cell Res.* **321,** 267–275 (2014).

217. Hanson, S. E. *et al.* Local delivery of allogeneic bone marrow and adipose tissue-derived mesenchymal stromal cells for cutaneous wound healing in a porcine model. *J. Tissue Eng. Regen. Med.* **10,** E90–E100 (2016).

218. Zhang, Y. *et al.* Efficient Reprogramming of Naïve-Like Induced Pluripotent Stem Cells from Porcine Adipose-Derived Stem Cells with a Feeder-Independent and Serum-Free System. *PLoS ONE* **9,** e85089 (2014).

219. Song, S.-H. *et al.* Characterization of porcine multipotent stem/stromal cells derived from skin, adipose, and ovarian tissues and their differentiation in vitro into putative oocyte-like cells. *Stem Cells Dev.* **20,** 1359–1370 (2011).

220. Gimble, J. M., Katz, A. J. & Bunnell, B. A. Adipose-derived stem cells for regenerative medicine. *Circ. Res.* **100,** 1249–1260 (2007).

221. Arrigoni, E., Lopa, S., de Girolamo, L., Stanco, D. & Brini, A. T. Isolation, characterization and osteogenic differentiation of adipose-derived stem cells: from small to large animal models. *Cell Tissue Res.* **338,** 401–11 (2009).

222. Bionaz, M., Monaco, E. & Wheeler, M. B. Transcription Adaptation during In Vitro Adipogenesis and Osteogenesis of Porcine Mesenchymal Stem Cells: Dynamics of Pathways, Biological Processes, Up-Stream Regulators, and Gene Networks. *PLOS ONE* **10,** e0137644 (2015).

223. Stock, P. *et al.* The generation of hepatocytes from mesenchymal stem cells and engraftment into murine liver*. *Nat. Protoc.* **5,** 617–627 (2010).

224. Huang, T., He, D., Kleiner, G. & Kuluz, J. Neuron-like Differentiation of Adipose-Derived Stem Cells From Infant Piglets in Vitro. *J. Spinal Cord Med.* **30,** S35–S40 (2007).

225. Liu, H.-Y. *et al.* Chitosan-assisted differentiation of porcine adipose tissue-derived stem cells into glucose-responsive insulin-secreting clusters. *PLoS One* **12,** (2017).

226. Tang, L. *et al.* Proliferative Capacity and Pluripotent Characteristics of Porcine Adult Stem Cells Derived from Adipose Tissue and Bone Marrow. *Cell. Reprogramming* **14,** 342–352 (2012).

227. Ock, S.-A. *et al.* Comparison of Immunomodulation Properties of Porcine Mesenchymal Stromal/Stem Cells Derived from the Bone Marrow, Adipose Tissue, and Dermal Skin Tissue. *Stem Cells Int.* **2016,** e9581350 (2015).

228. Bharti, D., Belame Shivakumar, S., Baregundi Subbarao, R. & Rho, G.-J. Research Advancements in Porcine Derived Mesenchymal Stem Cells. *Curr. Stem Cell Res. Ther.* **11,** 78–93 (2016).

229. Hwang, I.-S., Bae, H.-K. & Cheong, H.-T. Comparison of the characteristics and multipotential and in vivo cartilage formation capabilities between porcine adipose-derived stem cells and porcine skin-derived stem cell–like cells. *Am. J. Vet. Res.* **76,** 814–821 (2015).

230. Du, M. *et al.* Characterization and Differentiation into Adipocytes and Myocytes of Porcine Bone Marrow Mesenchymal Stem Cells. *J. Integr. Agric.* **13,** 837–848 (2014).

231. Pankajakshan, D., Kansal, V. & Agrawal, D. K. In vitro differentiation of bone

marrow derived porcine mesenchymal stem cells to endothelial cells. *J. Tissue Eng. Regen. Med.* **7,** 911–920 (2013).

232. Kokubun, K., Pankajakshan, D., Kim, M.-J. & Agrawal, D. K. Differentiation of porcine mesenchymal stem cells into epithelial cells as a potential therapeutic application to facilitate epithelial regeneration. *J. Tissue Eng. Regen. Med.* **10,** E73-83 (2016).

233. Monaco, E., Bionaz, M., Rodriguez-Zas, S., Hurley, W. L. & Wheeler, M. B. Transcriptomics Comparison between Porcine Adipose and Bone Marrow Mesenchymal Stem Cells during In Vitro Osteogenic and Adipogenic Differentiation. *PLoS ONE* **7,** e32481 (2012).

234. Vatner, S. F. Why So Few New Cardiovascular Drugs Translate to the Clinics. *Circ. Res.* **119,** 714–717 (2016).

235. Rubessa, M. *et al.* Use of Pig as a Model for Mesenchymal Stem Cell Therapies for Bone Regeneration. *Anim. Biotechnol.* 1–13 (2017). doi:10.1080/10495398.2017.1279169

236. Monaco, E., Bionaz, M., Hollister, S. J. & Wheeler, M. B. Strategies for regeneration of the bone using porcine adult adipose-derived mesenchymal stem cells. *Theriogenology* **75,** 1381–1399 (2011).

237. Qu, C., Zhang, G., Zhang, L. & Yang, G. Osteogenic and adipogenic potential of porcine adipose mesenchymal stem cells. *Vitro Cell. Dev. Biol. - Anim.* **43,** 95–100 (2007).

238. Liao, H.-T., Lee, M.-Y., Tsai, W.-W., Wang, H.-C. & Lu, W.-C. Osteogenesis of adipose-derived stem cells on polycaprolactone–β-tricalcium phosphate scaffold

fabricated via selective laser sintering and surface coating with collagen type I. *J. Tissue Eng. Regen. Med.* **10,** E337–E353 (2016).

239. de Girolamo, L. *et al.* Repair of osteochondral defects in the minipig model by OPF hydrogel loaded with adipose-derived mesenchymal stem cells. *Regen. Med.* **10,** 135–151 (2015).

240. Jo, W.-L. *et al.* Co-transplantation of adipose and bone marrow derived stromal cells for treatment of osteonecrosis of femoral head. *Tissue Eng. Regen. Med.* **12,** 410–416 (2015).

241. Cui, L. *et al.* Repair of articular cartilage defect in non-weight bearing areas using adipose derived stem cells loaded polyglycolic acid mesh. *Biomaterials* **30,** 2683–2693 (2009).

242. Murata, D. *et al.* A preliminary study of osteochondral regeneration using a scaffold-free three-dimensional construct of porcine adipose tissue-derived mesenchymal stem cells. *J. Orthop. Surg.* **10,** (2015).

243. Liu, N. *et al.* Animal models for craniofacial reconstruction by stem/stromal cells. *Curr. Stem Cell Res. Ther.* **9,** 174–186 (2014).

244. Wilson, S. M. *et al.* Adipose-Derived Mesenchymal Stem Cells Enhance Healing of Mandibular Defects in the Ramus of Swine. *J. Oral Maxillofac. Surg.* **70,** e193–e203 (2012).

245. Swartz, D. D. & Andreadis, S. T. Animal models for vascular tissue-engineering. *Curr. Opin. Biotechnol.* **24,** 916–925 (2013).

246. Valina, C. *et al.* Intracoronary administration of autologous adipose tissue-derived stem cells improves left ventricular function, perfusion, and remodelling after

acute myocardial infarction. *Eur. Heart J.* **28,** 2667–2677 (2007).

247. Gomez-Mauricio, R. G. *et al.* A preliminary approach to the repair of myocardial infarction using adipose tissue-derived stem cells encapsulated in magnetic resonance-labelled alginate microspheres in a porcine model. *Eur. J. Pharm. Biopharm.* **84,** 29–39 (2013).

248. Vilahur, G. *et al.* Allogenic adipose-derived stem cell therapy overcomes ischemia-induced microvessel rarefaction in the myocardium: systems biology study. *Stem Cell Res. Ther.* **8,** 52 (2017).

249. Ishida, O. *et al.* Adipose-derived stem cell sheet transplantation therapy in a porcine model of chronic heart failure. *Transl. Res.* **165,** 631–639 (2015).

250. Gimble, J. M., Bunnell, B. A., Chiu, E. S. & Guilak, F. Concise Review: Adipose-Derived Stromal Vascular Fraction Cells and Stem Cells: Let's Not Get Lost in Translation. *STEM CELLS* **29,** 749–754 (2011).

251. Schomberg, D. T. *et al.* Miniature Swine for Preclinical Modeling of Complexities of Human Disease for Translational Scientific Discovery and Accelerated Development of Therapies and Medical Devices. *Toxicol. Pathol.* **44,** 299–314 (2016).

252. Stramandinoli-Zanicotti, R. T. *et al.* Brazilian minipig as a large-animal model for basic research and stem cell-based tissue engineering. Characterization and in vitro differentiation of bone marrow-derived mesenchymal stem cells. *J. Appl. Oral Sci.* **22,** 218–227 (2014).

253. Gilmer, T. C. & Williams, M. Polymer mechanical properties via a new laboratory tensile tester. *J. Chem. Educ.* **73,** 1062 (1996).

254. Pearce, J. M. Building Research Equipment with Free, Open-Source Hardware.

Science **337,** 1303–1304 (2012).

255. Mai, T. D. *et al.* Portable Capillary Electrophoresis Instrument with Automated Injector and Contactless Conductivity Detection. *Anal. Chem.* **85,** 2333–2339 (2013).

256. Kadimisetty, K. *et al.* Automated Multiplexed ECL Immunoarrays for Cancer Biomarker Proteins. *Anal. Chem.* **87,** 4472–4478 (2015).

257. Gach, P. C. *et al.* A Droplet Microfluidic Platform for Automating Genetic Engineering. *ACS Synth. Biol.* **5,** 426–433 (2016).

258. Mathupala, S. P., Kiousis, S. & Szerlip, N. J. A Lab Assembled Microcontroller-Based Sensor Module for Continuous Oxygen Measurement in Portable Hypoxia Chambers. *PLOS ONE* **11,** e0148923 (2016).

259. Grinias, J. P., Whitfield, J. T., Guetschow, E. D. & Kennedy, R. T. An Inexpensive, Open-Source USB Arduino Data Acquisition Device for Chemical Instrumentation. *J. Chem. Educ.* **93,** 1316–1319 (2016).

260. Urban, P. L. Open-Source Electronics As a Technological Aid in Chemical Education. *J. Chem. Educ.* **91,** 751–752 (2014).

261. Mabbott, G. A. Teaching Electronics and Laboratory Automation Using Microcontroller Boards. *J. Chem. Educ.* **91,** 1458–1463 (2014).

262. McClain, R. L. Construction of a Photometer as an Instructional Tool for Electronics and Instrumentation. *J. Chem. Educ.* **91,** 747–750 (2014).

263. Famularo, N., Kholod, Y. & Kosenkov, D. Integrating Chemistry Laboratory Instrumentation into the Industrial Internet: Building, Programming, and Experimenting with an Automatic Titrator. *J. Chem. Educ.* **93,** 175–181 (2016).

264. Kubínová, Š. & Šlégr, J. ChemDuino: Adapting Arduino for Low-Cost

Chemical Measurements in Lecture and Laboratory. *J. Chem. Educ.* **92,** 1751–1753 (2015).

265. Stefanov, B. I., Lebrun, D., Mattsson, A., Granqvist, C. G. & Österlund, L. Demonstrating Online Monitoring of Air Pollutant Photodegradation in a 3D Printed Gas-Phase Photocatalysis Reactor. *J. Chem. Educ.* **92,** 678–682 (2015).

266. Cao, T., Zhang, Q. & Thompson, J. E. Designing, Constructing, and Using an Inexpensive Electronic Buret. *J. Chem. Educ.* **92,** 106–109 (2015).

267. Meloni, G. N. Building a Microcontroller Based Potentiostat: A Inexpensive and Versatile Platform for Teaching Electrochemistry and Instrumentation. *J. Chem. Educ.* **93,** 1320–1322 (2016).

268. Erk, K. A., Rhein, M., Krafcik, M. J. & Ydstie, S. Demonstrating the Effects of Processing on the Structure and Physical Properties of Plastic Using Disposable PETE Cups. *J. Chem. Educ.* **92,** 1876–1881 (2015).

269. Walkowiak, M. & Nehring, A. Using ChemDuino, Excel, and PowerPoint as Tools for Real-Time Measurement Representation in Class. *J. Chem. Educ.* **93,** 778–780 (2016).

270. Milner-Bolotin, M. Increasing Interactivity and Authenticity of Chemistry Instruction through Data Acquisition Systems and Other Technologies. *J. Chem. Educ.* **89,** 477–481 (2012).

271. Warner, D. L., Brown, E. C. & Shadle, S. E. Laboratory Instrumentation: An Exploration of the Impact of Instrumentation on Student Learning. *J. Chem. Educ.* **93,** 1223–1231 (2016).

Appendix A: Uniaxial Tensile Testing of Human Amniotic Membranes

This appendix contains supplementary data to Chapter 03 "Characterization of Riboflavin-UVA Crosslinking of Amniotic Membranes and its Influence on the Culture of Adipose-Derived Stem Cells".

A stress-strain curve represents the behavior of a material during mechanical testing. Stress is defined as the force applied divided by the area. For a tensile test, the relevant area is that perpendicular to the applied force (in this case the cross-sectional area). Strain describes the elongation with respect to the initial length of the sample. The ultimate tensile strength represents the maximum stress that a material can withstand before breaking. The Young's modulus or elastic modulus of a material is defined as the slope of its stress-strain curve in the region of elastic deformation.

For the uniaxial tensile testing of human amniotic membranes, sample gauge length was 30 mm and width was 20 mm. The thickness of the human amniotic membrane changes depending on its hydration state and is consequently very hard to measure. For all samples, the thickness of the human amniotic membrane was set constant at 50 μm. After decellularization, all tissue samples possessed a uniform thickness. This value of 50 μm was measured on histological pictures of decellularized human amniotic membranes. For testing, each sample was mounted between two pneumatic grips and preloaded to 5 g of force for 10 seconds before being stretched until failure at a crosshead speed of 5mm/min.

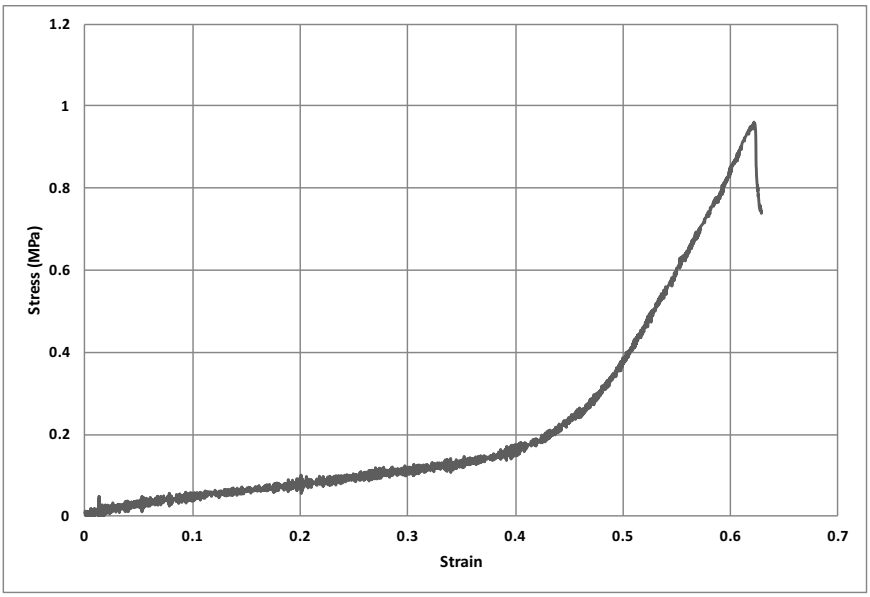

Figure 26: Typical stress-strain curve for a noncrosslinked hAM sample.

Appendix B: Long Term Riboflavin-UVA Exposure for Human Amniotic Membrane Crosslinking

This appendix contains supplementary data to Chapter 03 "Characterization of Riboflavin-UVA Crosslinking of Amniotic Membranes and its Influence on the Culture of Adipose-Derived Stem Cells".

For the experiments reported in Chapter 03, human amniotic membranes were exposed to riboflavin at various concentrations but for a constant 60min reaction time. In this appendix, results are reported for crosslinking of the human amniotic membrane with various concentrations of riboflavin but also exposure times ranging from 30min to 24 hours.

Decellularized amniotic membranes were submerged in solutions of riboflavin (Sigma-Aldrich) at different concentrations and exposed to UV light at 366 nm on a transilluminator (Fotodyne, Hartland, WI) with an intensity of $4mW/cm^2$. Exposure time to the UV light ranged from 30 min to 24 hours and concentrations of riboflavin ranged from 0.001 to 0.1 g/L. As a control, some amniotic membranes were also crosslinked in a 10mM solution of glutaraldehyde for similar exposure times. All crosslinked samples were thoroughly washed with phosphate buffered saline to remove any residual crosslinking agents before use.

Control experiments of UV irradiation without riboflavin of noncrosslinked hAM were performed for exposure times of 30, 60, 120 min. Without any exposure to UV irradiation, noncrosslinked hAM had a Young's modulus of 4.8 ± 0.6 MPa and an ultimate tensile strength of 1.06 ± 0.08 MPa. (see data on Figure 10). Noncrosslinked hAM exposed to UV irradiation without riboflavin for 30, 60, and 120min displayed Young's modulus of 4.6 ± 0.9 MPa, 5.2 ± 0.8 MPa, 4.9 ± 0.5 MPa and ultimate tensile strengths of 1.01 ± 0.05 MPa, 1.11 ± 0.12 MPa, and 1.04 ± 0.08 MPa respectively. It appears that for exposure times under 120min the UV did not degrade the amniotic membrane.

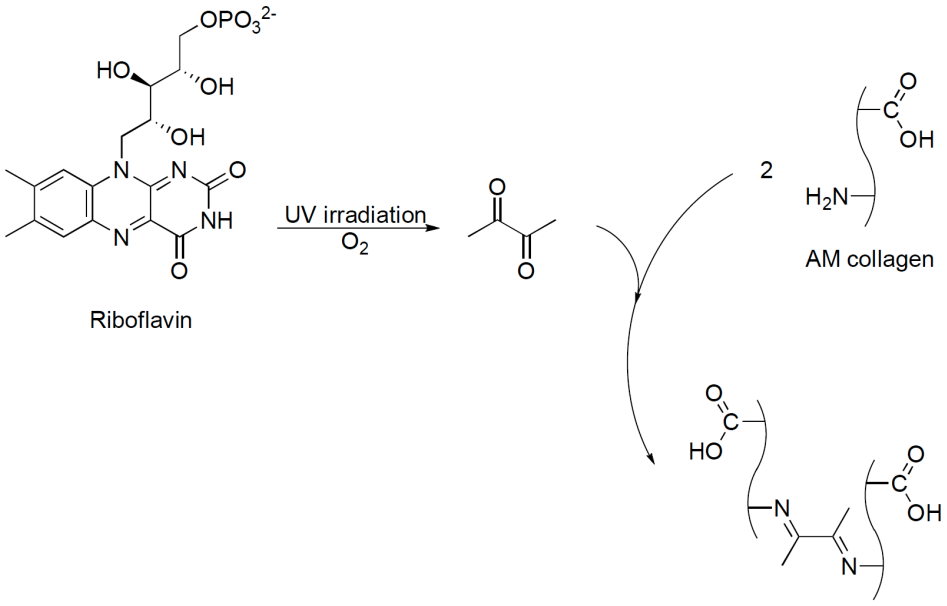

Figure 27: Chemical reaction of riboflavin with the collagen fibers of the human amniotic membrane when exposed to UV light.

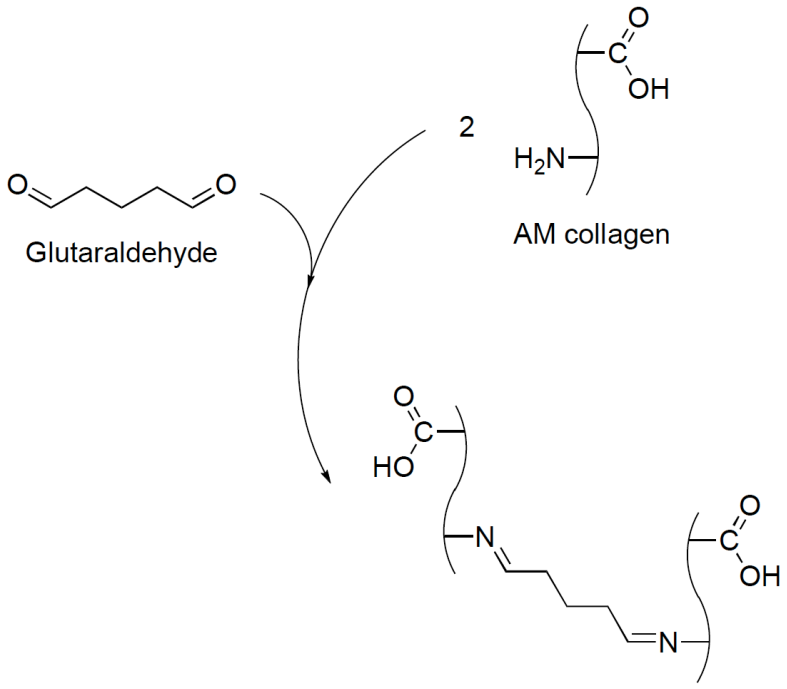

Figure 28: Chemical reaction of glutaraldehyde with the collagen fibers of the human amniotic membrane.

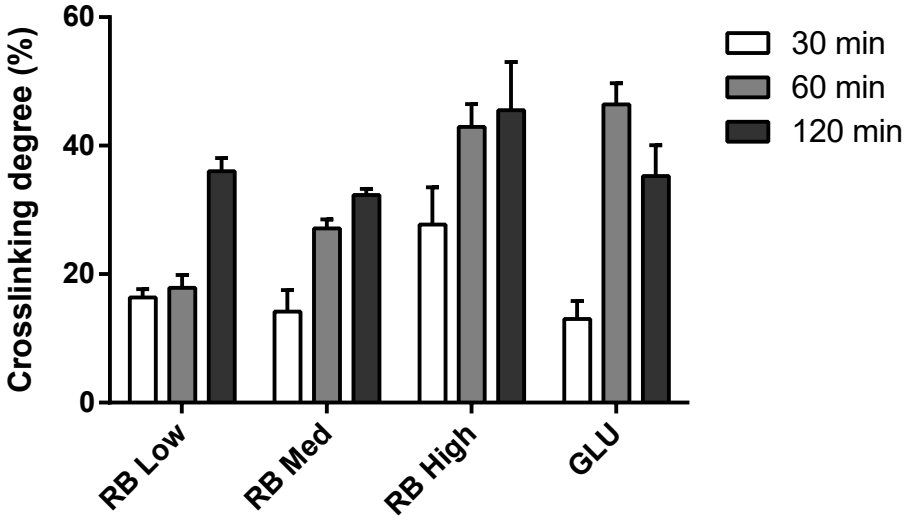

Figure 29: Crosslinking degrees determined by ninhydrin assay of hAM exposed to UVA-riboflavin or glutaraldehyde crosslinking as compared to noncrosslinked hAM for reaction times of 30, 60, and 120min.

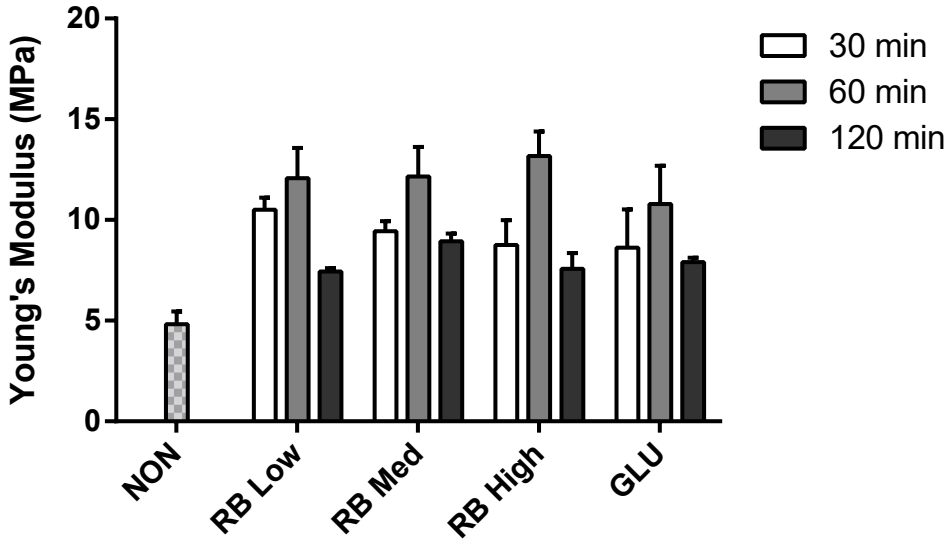

Figure 30: Young's Modulus of noncrosslinked hAM and hAM crosslinked with UVA-riboflavin or glutaraldehyde for reaction times of 30, 60, and 120min.

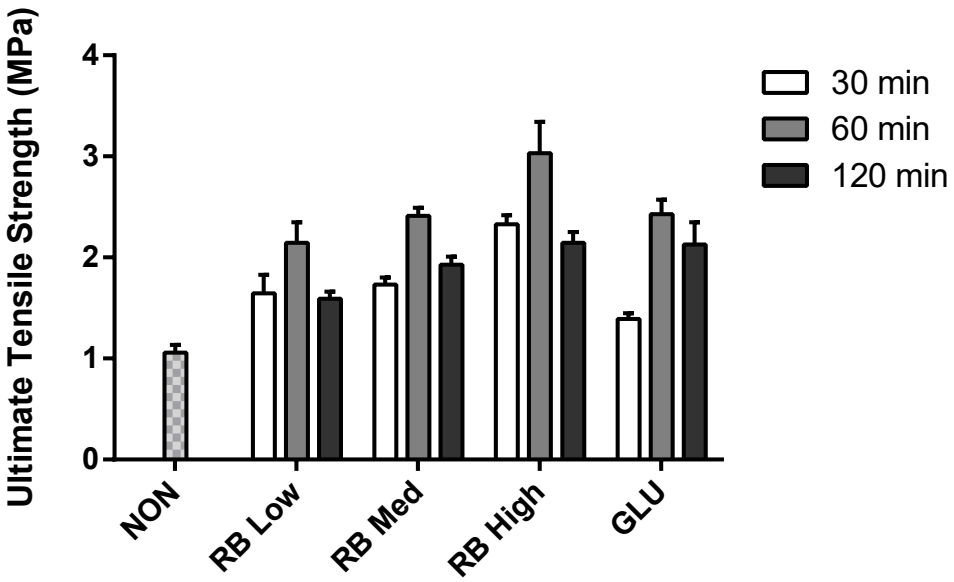

Figure 31: Ultimate Tensile Strength of noncrosslinked hAM and hAM crosslinked with UVA-riboflavin or glutaraldehyde for reaction times of 30, 60, and 120min.

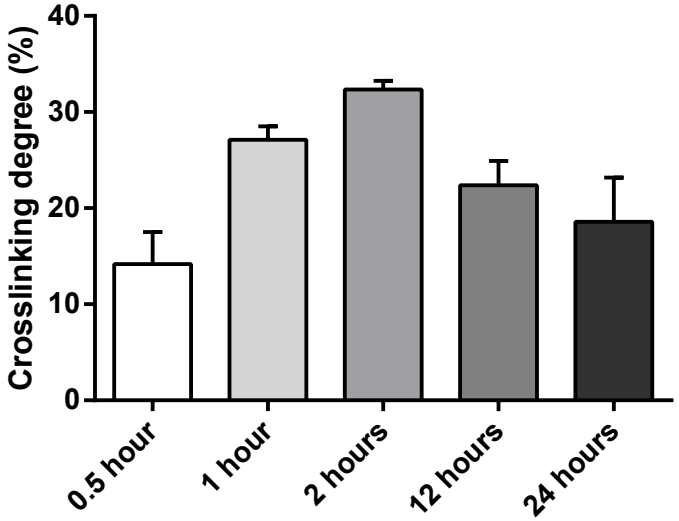

Figure 32: Crosslinking degrees determined by ninhydrin assay of hAM exposed to UVA-riboflavin at a medium concentration of 0.01 g/L as compared to noncrosslinked hAM for reaction times of 0.5, 1, 2, 12, and 24 hours.

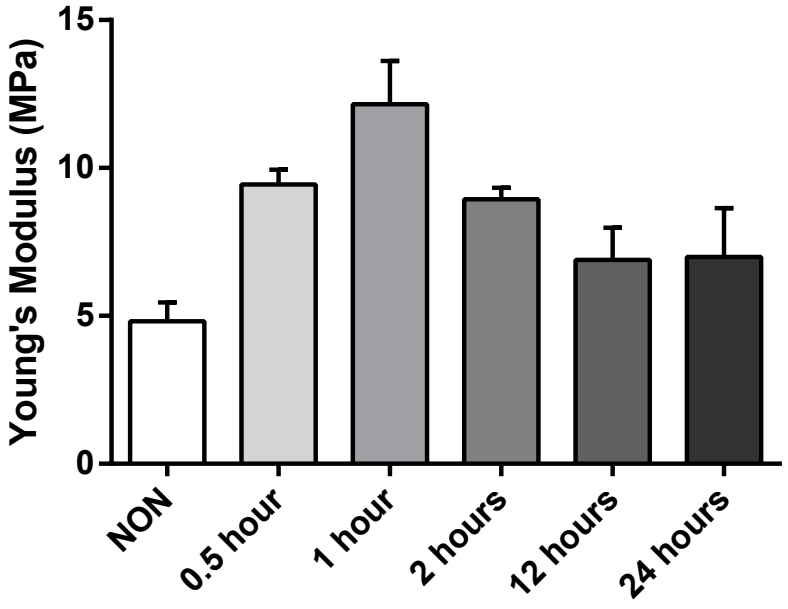

Figure 33: Young's Modulus of noncrosslinked hAM and hAM crosslinked with a medium concentration (0.01g/L) of riboflavin for reaction times of 0.5, 1, 2, 12 and 24 hours.

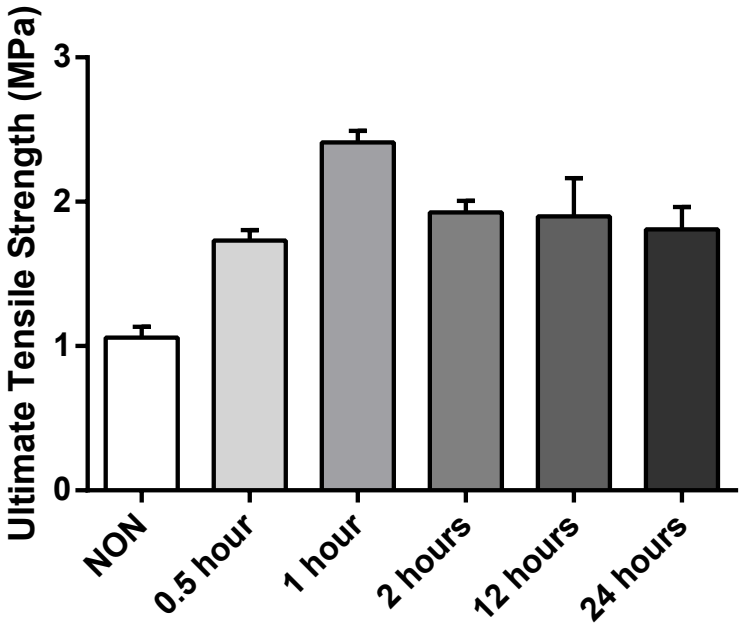

Figure 34: Ultimate Tensile Strength of noncrosslinked hAM and hAM crosslinked with a medium concentration (0.01g/L) of riboflavin for reaction times of 0.5, 1, 2, 12 and 24 hours.

Appendix C: Permeability Measurement

This appendix contains supplementary data to Chapter 03 “Characterization of Riboflavin-UVA Crosslinking of Amniotic Membranes and its Influence on the Culture of Adipose-Derived Stem Cells”.

Experimental setup

A side-by side diffusion chamber was designed to allow the measurement of the effective diffusivity through the human amniotic membrane. The setup consists of two cylindrical chambers having a diameter of 9.5 mm, a length of 3.5 cm, and an individual volume of 2.5 ml. Before being placed in the diffusion chamber, the decellularized hAM was dissected into squares sections having a side length of approximately 1.5 cm.

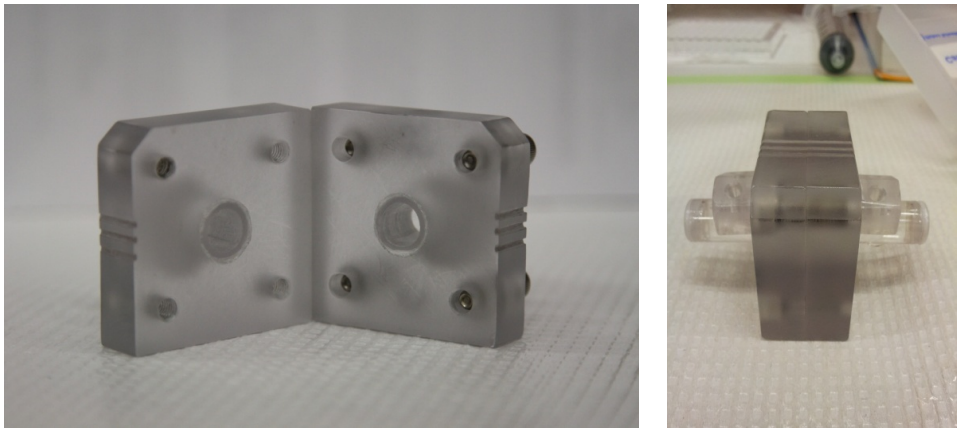

Figure 35: Cross sectional view and side view of the custom-made diffusion chambers.

Glucose was chosen for the diffusion measurements because it is a key component in cell culture media and necessary for cell nutrition and survival. Glucose was loaded on

one side of the chamber at a concentration of 1 mg/mL and DI water was used to fill the second side. 10 μL samples from both sides were taken every 15min during 2 hours.

Glucose Enzymatic Assay

Glucose concentrations were computed using an enzymatic method that results in an increase in the absorbance of the samples which is proportional to the glucose concentration. Standards of known glucose concentrations were prepared (0, 0.2, 0.4, 0.6, 0.8 and 1 mg/ml). Samples and standards were assayed in triplicate to account for sampling error. 10 μl of sample or standard was added to each well. Each occupied well was then supplemented with 100 μl of glucose assay reagent (G3293, Sigma). Blanks were prepared for each sample, in which 100 μl of DI water replaced the glucose assay reagent. The 96-well plate was incubated on a shaker for 20 minutes allowing the glucose assay reagent to react with the samples.

Finally, the absorbance was measured at 340 nm (Bio-Tek, Winooski, VT). Using the data from the standards a linear relationship between the absorbance measured and the glucose concentration was determined. The glucose concentrations in the assayed samples were then determined by linear regression analysis of the standard curve.

Permeability of the Human Amniotic Membrane

Concentrations of glucose at each time point were calculated by measuring the absorbance of the sample as illustrated in the previous section. To calculate its coefficient of diffusion, the human amniotic membrane was considered as a thin

membrane and a quasi-steady state was assumed. The following equation was used to calculate the apparent coefficient of diffusion:

$$ln\left(\frac{2C_1\text{-}C_0}{C_0}\right) = \text{-}\left(\frac{2A_m}{V}\frac{D_{eff}\Phi}{L}\right)t$$

Using this expression, it was possible to plot the value of $ln\left(\frac{2C_1\text{-}C_0}{C_0}\right)$ versus t resulting in a linear fit with a slope of $-\frac{2A_mD_{eff}\Phi}{VL_m}$. Consequently, the apparent diffusion coefficient was calculated as:

$$D_{apparent} = D_{eff}\Phi = \text{-}slope^*\frac{V^*L_m}{2A_m}$$

Where:

- C_0 is the initial solute concentration in chamber 1.
- C_1 is the measured solute concentration in chamber 2 at t time.
- A_m is the cross-sectional area of the amniotic membrane (0.713cm^2).
- Lm is the thickness of the amniotic membrane (50 µm).
- V is the volume of each chamber (2.50 ml).

The permeability P of glucose to the membrane was deduced from the apparent coefficient of diffusion using:

$$P = \frac{D_{apparent}}{L_m}$$

Appendix D: Flow Cytometry Analysis

This appendix contains supplementary data to Chapter 03 "Characterization of Riboflavin-UVA Crosslinking of Amniotic Membranes and its Influence on the Culture of Adipose-Derived Stem Cells".

Description	Fluorochrome	Isotype	Size	Company	Product Number
anti-CD29	PE	Ms IgG_1, κ	25 Tests	BD Biosciences	561795
anti-CD34	FITC	Ms IgG_1, κ	25 Tests	BD Biosciences	560942
anti-CD44	PE	Ms IgG_1, κ	100 Tests	BD Biosciences	550989
anti-CD45	PE	Ms IgG_1, κ	25 Tests	BD Biosciences	560975
anti-CD73	PE	Ms IgG_1, κ	25 Tests	BD Biosciences	561014
anti-CD90	FITC	Ms IgG_1, κ	0.1mg	BD Biosciences	555595
anti-CD105	FITC	Ms IgG_1, κ	100 Tests	BD Biosciences	561443
Ms IgG_1, κ Isotype control	PE	Ms IgG_1, κ	100 Tests	BD Biosciences	555749
Ms IgG_1, κ Isotype control	FITC	Ms IgG_1, κ	100 Tests	BD Biosciences	555748
Stain Buffer FBS			500mL	BD Biosciences	554656

Table 3: List of antibodies used for the characterization of human adipose-derived stem cells.

Appendix E: Supporting Information for the Fabrication of an Economical Arduino-Based Uniaxial Tensile Tester

Bill of materials

Item	Supplier	Product Number	Price
Wood	Home Depot	2x4 / 2x6 / 4x4	$ 10.00
Drawer Slide	McMaster-Carr	11435A12	$ 9.00
Arduino	RobotShop	RB-Ard-34	$ 23.00
Load Cell	RobotShop	RB-Phi-118	$ 7.00
Ultrasonic Sensor	Amazon	HC-SR04	$ 3.00
INA125P	eBay	INA125P	$ 5.00
Breadbord & Jumper Wires	Amazon	Misc.	$ 6.00
Brackets & Clevis Pin	McMaster-Carr	1755A52	$ 7.00
Rope	McMaster-Carr	2222T46	$ 8.00
Miscellaneous hardware (screws, bolts, nuts etc.)	Various	Misc.	$ 10.00
Total			**$ 88.00**

Table 4: Bill of materials for the Arduino-based mechanical tester.

A majority of the parts used to build the mechanical tester prototype were recycled from previous projects, hence the estimated rounded prices for the parts.

Polymer or metal components could also be used instead of wood to build the mechanical tester frame. This would result in a better looking but also heavier and more expensive device. Wood presents the advantages of being inexpensive, structurally very strong, and easy to assemble.

Mechanical Tester Assembly

Two 12x12x2 square pieces of pressured treated wood were used for the base and top parts of the mechanical tester. The sides consisted of two 40x6x2 pieces of wood. These parts were attached together to form the frame of the mechanical tester using wood glue and 3" long wood screws. The drawer slide was attached to the inside of the pillars using the provided hardware. A 10x4x4 piece of wood was connected to the drawer slide and used as the central loading apparatus were the load cell was attached. The rope used was 5ft long, made of high-performance polyester (Vectran) and designed specifically for lifting with low-stretch. It was attached to the central piece through a bracket and traveling through a pulley mounted under the top square piece of the frame. A set of brackets to mount sample clamps were attached to the load cell and the bottom of the frame. Electronics and wires were secured at the back of the mechanical testing in order to not interfere during mechanical testing.

Wiring Details

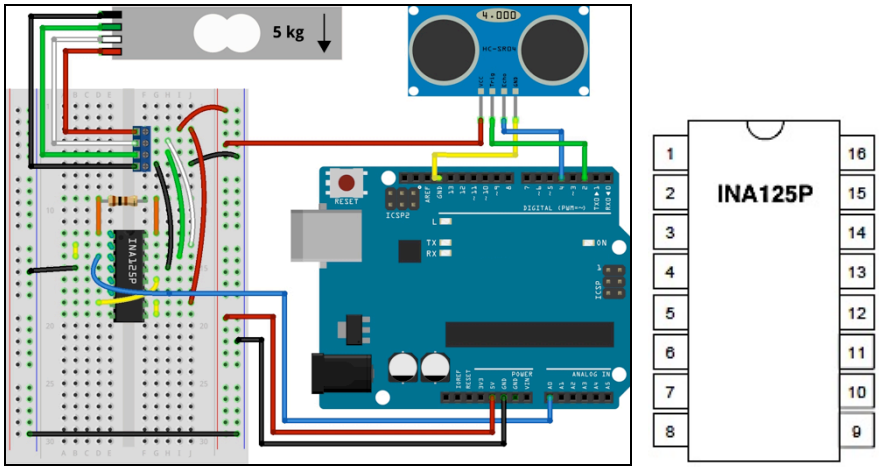

Figure 36: Wiring details for the Arduino-based mechanical tester.

For the 5 kg load cell:

- Black wire: Excitation -
- Green wire: Signal +
- White wire: Signal -
- Red wire: Excitation +

For the INA125P amplifier:

- 100 Ω resistor connected between pins 1 and 16
- Yellow wire between pins 2 and 3
- Blue wire between pin 3 and Arduino Analog Input A0
- Black wire between pin 4 and ground
- Yellow wire between pins 7 and 12
- Yellow wire between pins 9 and 10
- Black wire from load cell on pin 13
- Red wire from load cell on pin 10
- Green wire from load cell on pin 14
- White wire from load cell on pin 15.

For the HC-SR04 ultrasonic sensor:

- Red wire: VCC, to 5V.
- Green wire: Trig, to Arduino digital input 2
- Blue wire: Echo, to Arduino digital input 4
- Yellow wire: GND, to ground.

Sample Holding Clamps

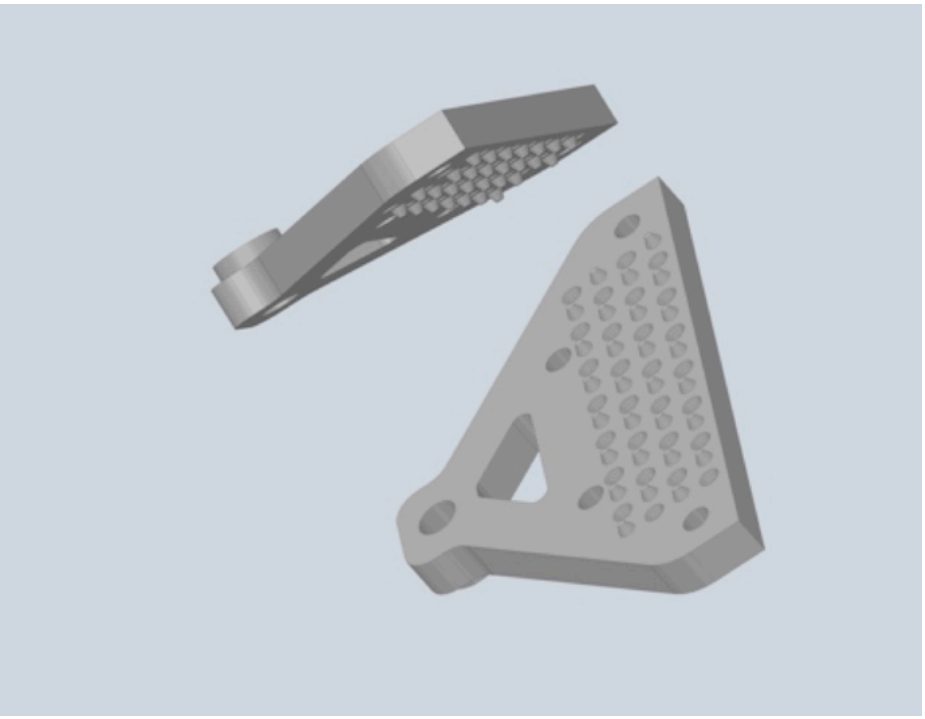

Figure 37: Sample holding clamps for the Arduino-based mechanical tester.

These sample holding clamps have symmetric interlocking teeth and are attached together with bolts and wingnuts. They were 3D printed in polylactic acid (PLA) on a Makerbot Replicator 5th generation. They were 100mm wide by 60mm tall and 5mm thick. The STL file is available separately from this document.

Arduino Code

The Arduino IDE can be downloaded for free at

https://www.arduino.cc/en/Main/Software

```
// 5kg load cell calibration
// Weight of item A in grams
float loadA = 68.83;
// Analog reading taken with item A
int analogvalA = 50;
// Weight of item B in grams
float loadB = 1050.62;
// Analog reading taken with item B
int analogvalB = 183;
float analogValueAverage = 0;
long time = 0;
int timeBetweenReadings = 100;
// Trig Pin of the HC-SR04 on input 02
int trigPin = 2;
// Echo Pin of the HC-SR04 on input 04
int echoPin = 4;
void setup() {
  Serial.begin(9600);
}
void loop() {
// Load cell on Analog input A0
  int analogValue = analogRead(0);
  analogValueAverage = 0.99*analogValueAverage + 0.01*analogValue;
```

```
  if(millis() > time + timeBetweenReadings){
    float load = analogToLoad(analogValueAverage);
    Serial.print("analogValue: ");Serial.println(analogValueAverage);
    Serial.print("            load: ");Serial.println(load,2);
    time = millis();
      long duration;
  float cm;
  pinMode(echoPin, INPUT);
  pinMode(trigPin, OUTPUT);
  digitalWrite(trigPin, LOW);
  delayMicroseconds(2);
  digitalWrite(trigPin, HIGH);
  delayMicroseconds(10);
  digitalWrite(trigPin, LOW);
  duration = pulseIn(echoPin, HIGH);
  cm = microsecondsToCentimeters(duration);
  Serial.print(cm);
  Serial.print("cm");
  Serial.println();
  delay(10);
  }
}
float analogToLoad(float analogval){
```

```
  float load = mapfloat(analogval, analogvalA, analogvalB, loadA, loadB);
  return load;
}
float mapfloat(float x, float in_min, float in_max, float out_min, float out_max)
{
  return (x - in_min) * (out_max - out_min) / (in_max - in_min) + out_min;
}
float microsecondsToCentimeters(long microseconds){
  return (microseconds*0.034029)/2;
}
```